NASA-CR-72027

MATERIALS FOR POTASSIUM LUBRICATED JOURNAL BEARINGS

Quarterly Progress Report No. 10
Quarter Ending October 22, 1965

EDITED BY R. G. FRANK

prepared for
NATIONAL AERONAUTICS AND SPACE ADMINISTRATION
CONTRACT NAS 3-2534

SPACE POWER AND PROPULSION SECTION
MISSILE AND SPACE DIVISION
GENERAL ELECTRIC
CINCINNATI, OHIO 45215

Requests for copies of this report
should be referred to:

National Aeronautics and Space Administration
Scientific and Technical Information Division
Attention: USS-A
Washington, D.C. 20546

NASA-CR-72027

MATERIALS FOR POTASSIUM LUBRICATED JOURNAL BEARINGS

Quarterly Progress Report No. 10

Covering the Period

July 22, 1965 to October 22, 1965

Edited by

R. G. Frank
Program Manager

Approved by

J. W. Semmel, Jr.
Manager, Materials and Processes

Prepared for

NATIONAL AERONAUTICS AND SPACE ADMINISTRATION

Contract NAS 3-2534

Technical Management
NASA - Lewis Research Center
Space Power Systems Division
Mr. R. L. Davies

SPACE POWER AND PROPULSION SECTION
MISSILE AND SPACE DIVISION
GENERAL ELECTRIC COMPANY
CINCINNATI, OHIO 45215

CONTENTS

TABLES

ILLUSTRATIONS

ILLUSTRATIONS (Cont'd)

FOREWORD

The work described herein is being performed by the General Electric Company under the sponsorship of the National Aeronautics and Space Administration under Contract NAS 3-2534. Its purpose, as outlined in the contract, is to evaluate materials suitable for potassium lubricated journal bearing and shaft combinations for use in space system turbogenerators and, ultimately, to recommend those materials most appropriate for such employment.

R. G. Frank, Manager, Physical Metallurgy, Material and Processes, is administering the program for the General Electric Company. L. B. Engel, Jr., T. F. Lyon, W. H. Hendrixson and B. L. Moor are directing the program investigations. The design for the friction and wear testers was executed by H. H. Ernst and B. L. Moor.

I. INTRODUCTION

The program reviewed in this tenth quarterly report, covering activities from July 22, 1965 to October 22, 1965, is performed under the sponsorship of the National Aeronautics and Space Administration. Its purpose is to evaluate materials suitable for potassium lubricated journal bearing and shaft applications in space system turbogenerators operating over a 400° to 1600°F temperature range. The critical role of bearings in such systems demands the maximum reliability attainable within today's state-of-the-art. Achieving this reliability requires an interdisciplinary approach employing the best mechanical designs of journal bearings combined with the selection of the optimum materials to serve as the structural members. Satisfying this latter requirement constitutes the aim of this program.

A number of investigators have conducted studies in this field and their contributions have advanced the state-of-the-art considerably (Section VIII, Ref. 1). Although their work is significant, there are no common criteria for a comparison of the existing data. Therefore, establishing a unified approach to the development and evaluation of materials for potassium lubricated bearing application is deemed essential. The program involves a comprehensive investigation of material properties adjudged requisite to reliable journal bearing operation in the proposed environment. This includes: 1) corrosion testing of individual materials and potential bearing couples in potassium liquid and vapor, 2) determination of hot hardness, hot compressive strength, modulus of elasticity, thermal expansion and dimensional stability characteristics, 3) wetting tests by potassium and 4) friction and wear measurements of selected bearing couples in high vacuum and in liquid potassium.

In cooperation with the cognizant NASA Technical Manager, 14 candidate materials were selected (Table I) from a compilation of existing data on available materials. The materials reviewed fall into four broad categories:

- Superalloys and refractory alloys with and without surface treatment
- Commercial metal bonded carbides
- Refractory compounds such as stable oxides, carbides, borides and nitrides
- Cermets based on the refractory metals and stable carbides

Each material is procured from appropriate suppliers to mutually acceptable specifications and subsequently is subjected to chemical, physical and metallurgical analyses to document its charateristics before utilization in the program. After the documentation of processes and properties, the candidate materials undergo corrosion, dimensional stability, thermal expansion, compression and hot hardness testing. Considering the bearing material requirements and the information obtained

TABLE I. CANDIDATE BEARING MATERIALS

Material Class	Candidate Material	Nominal Composition
A. Nonrefractory Metals and Alloys	Star J	17%W-32%Cr-2.5%Ni-3%Fe-2.5%C-Bal. Co
B. Refractory Metals and Alloys	Mo-TZM (Arc Cast; Stress-Relieved)	0.5%Ti-0.08%Zr-0.02%C-Bal. Mo
	Tungsten (Arc Cast; Stress-Relieved)	99.96%W (Min.)
C. Fe-Ni-Co Bonded Carbides	Carboloy 907	74%WC-20%TaC-6%Co
	Carboloy 999	97%WC-3%Co
	K601	84.5%W-10%Ta-5.5%C
D. Refractory Compounds - Oxides, Carbides, Borides	Lucalox	99.8%Al_2O_3(Min.)-0.1%MgO-0.02%SiO_2-0.02% CaO-0.02%Fe_2O_3
	Zircoa 1027	95.5%ZrO_2-Bal. Proprietary
	Titanium Carbide	94%TiC-4.25%WC-0.9%Ni-0.1%Fe-0.68%Co
	Titanium Diboride	98%TiB_2-0.39%Fe-0.30%C
E. Refractory Metal Bonded Carbided	TiC+5%W	90%TiC-4.79%WC-5%W-0.36%Fe
	TiC+10%Mo	85.4%TiC-10.5%Mo-3.99%WC-0.13%Fe
	TiC+10%Cb	83.6%TiC-9.54%Cb-5.85%WC-0.73%Co-0.33%Fe
	Grade 7178	85.6%W-6.9%Mo-1.8%Cb-0.3%Ti-5.7%C

on the candidate bearing materials which were subject to both potassium and non-potassium testing, seven materials combinations listed below were selected in co-operation with the NASA Technical Manager. Potassium corrosion and wetting tests and friction and wear measurements in high vacuum and liquid potassium will proceed with these combinations.

	Rotating Disc	Stationary Rider
*1.	Grade 7178	Mo-TZM
2.	Mo-TZM	Grade 7178
*3.	Grade 7178	Grade 7178
4.	Carboloy 907	Mo-TZM
5.	Carboloy 907	Carboloy 907
6.	TiC+10%Cb	Mo-TZM
*7.	TiC+10%Cb	TiC+10%Cb

Those materials combinations marked with an asterick (*) were selected for friction and wear testing in both liquid potassium and high vacuum. Where significant differences in hardness exist, the softer material, i.e., Mo-TZM alloy, was selected as the rider material (stationary specimen) to facilitate wear-in during testing in liquid potassium. Couple No. 2 was selected to determine what affect a hard rider material would have on the wear pattern of a soft disc material in comparison with the reverse combination.

The decision to place considerable emphasis on the refractory metal bonded carbides was based on their excellent stability at the higher temperatures. Also, it was elected to test the hard carbide materials against themselves in order to obtain a direct comparison of the friction and wear behavior of hard/hard combinations vs hard/soft combinations where Mo-TZM alloy is one material in a pair. From investigations conducted by Coffin (2,3), it was concluded that generally it is desirable to have one of the materials harder than the other in order to facilitate wear-in of the couple. If both materials are hard and brittle, the surface asperities on the weaker material can fracture and the resultant debris could cause severe surface damage by abrasion. However, recent friction and wear tests and full scale bearing tests conducted elsewhere (4), using liquid potassium as a lubricant, have indicated superior performance of hard/hard combinations over hard/soft combinations because of the tendency of wear debris from the hard material to become imbedded in the soft material of hard/soft combinations and possibly resulting in a cutting action.

The ultimate product of this program will be a recommendation, substantiated with complete documentation, of the material or materials which have the greatest potential for use in alkali metal journal bearings in high speed, high temperature rotating machinery for space applications. Hopefully, the results will indicate the future course of alloy or material development specifically designed for alkali metal lubricated journal bearing and shaft combinations.

II. SUMMARY

During the tenth quarter of the program, the topics abstracted below were covered and the results interpretively presented in this report.

The Cb-1Zr alloy capsules which contained specimens of the Carboloy 907 and Grade 7178 materials and which were isothermally exposed to potassium for 1000 hours at 800° and 1200°F were sectioned and 0.020-inch thick layers from the ID surface of the liquid zones were analyzed for carbon content. The results show that carbon had transferred from both the Carboloy 907 and Grade 7178 materials to the Cb-1Zr alloy capsule wall at 1200°F, i.e., on the order of 40-45 ppm in an 0.020-inch thick section. Essentially no transfer of carbon was observed to have occurred at 800°F. Metallographic examination of the Cb-1Zr alloy containment capsules which had been exposed for 1000 hours at 1600°F revealed a distinct layer of CbC on the ID surface of the capsules containing specimens of Carboloy 999, Star J, and Carboloy 907. Chemical analyses had shown carbon increases in the inner 0.020-inch layer of the Cb-1Zr alloy capsule wall containing the above specimens to be 340, 215 and 145 ppm respectively.

Metallographic examination of the candidate bearing materials which were exposed to potassium for 1000 hours at 800° and 1200°F and x-ray diffraction analyses of the test specimens similarily tested at 1600°F have been completed. No microstructural changes or evidence of attack was observed in any of the candidate bearing material test specimens with the exception of Carboloy 999 and Zircoa 1027. A slight surface roughening was evident in the case of the Carboloy 999 specimens exposed to potassium liquid at 800° and 1200°F and significant corrosion reactions, observed in Zircoa 1027 specimens tested at 1600°F, were still evident in the Zircoa 1027 specimens exposed to both potassium liquid and vapor at 800° and 1200°F. The transfer of carbon from Carboloy 999, Carboloy 907, and Grade 7178 materials to the Cb-1Zr alloy containment capsule during the 1000-hour exposure to potassium at 1200° and 1600°F clearly is substantiated by the results of the x-ray diffraction analyses of the test specimens. The dissociation of WC to form pure tungsten was observed on the surfaces of the three carbide materials listed above as well as for K601. In addition, the formation of the complex carbides Co_2WC_4 and $(Co,W)_xC$ was detected on the surface of the Carboloy 907 specimens exposed to potassium liquid and vapor and the Carboloy 999 specimen exposed to potassium liquid.

The nine corrosion capsules containing candidate bearing material combinations which were tested at 800°, 1200°, and 1600°F for 1000 hours have been opened and the test evaluation of the test specimens has been initiated. Visual examination of the specimens has been completed and metallographic and chemical or x-ray diffraction analyses are in progress. Chemical analyses of the inner 0.020-inch layer in the liquid region of the Cb-1Zr alloy capsule which contained the Carboloy 907/Mo-TZM alloy test specimens and which were exposed to potassium for 1000 hours at 1600°F showed a 210 ppm increase in carbon content. Little or no carbon transfer was observed in similar capsules which contained Grade 7178/Mo-TZM alloy and TiC+10%Cb/Mo-TZM alloy specimens.

Metallographic examination in the liquid zone of the Cb-1Zr alloy containment capsules used in the 1600°F tests revealed CbC on the ID surface of the capsule containing the Carboloy 907/Mo-TZM alloy test specimens.

The potassium reservior of the wetting test facility was filled with approximately 10 grams of potassium and initial wetting tests were conducted on a Mo-TZM alloy specimen. A drop of potassium was formed successfully by distilling potassium over to the Cb-1Zr alloy condenser for 1 1/4 hours at 210°-220°C and subsequently allowing the potassium to melt by passing hot air through the condenser tube. The volume of the solid drop that formed on the specimen was about 0.12 cc and the mass was about 0.10 gram. Three separate trial wetting tests were made with the Mo-TZM alloy. These tests demonstrated that the contact angle of the potassium drop depends on the previous history of the solid surface and, in particular, on whether the surface has been previously wetted by potassium. On a previously wetted surface of Mo-TZM alloy, the contact angle of a potassium drop at a specimen temperature of 115°C at the time the drop was formed was about 10 degrees.

An analysis of the initial tests conducted in the high vacuum friction and wear tester necessitated an investigation of the loading arm design. It was found that the spring rate of the loading arm bellows in the plane of the specimens gave unacceptally high unloading errors if any appreciable wear of the specimens occurred under light loads. A design change was made to reduce the bellows spring rate from 0.020 lb./0.001-inch of wear to 0.002 lb./0.001-inch of specimen wear. Subsequently, all the loading arms were modified to incorporate the design change and three tests were conducted at room temperature, at speeds of 500 and 800 SFM and at pressures of 6.2×10^{-10} to 1.2×10^{-9} torr. Coefficient of friction values of 0.54 were calculated for Grade 7178 vs Grade 7178 carbide at a load of 6.1 lbs. (484,700 psi); a coefficient of friction value of 1.0 was calculated for Mo-TZM alloy vs Grade 7178 at a load of 0.08 lb (94,800 psi).

The test facility for the liquid potassium friction and wear test rig has been completed with the exception of final welding of the potassium fill and drain lines. With the test rig blanked off, the test facility was baked out and evacuated to a pressure of 1×10^{-9} torr by means of a getter-ion pump. Trial friction and wear tests with liquid potassium will be initiated in the next reporting interim.

III. TEST FACILITIES

A. Friction and Wear in High Vacuum

An analysis of the test results of test 200K05A*, in which the coefficient of friction had dropped drastically during the testing interval, necessitated an investigation of the loading arm design--specifically the spring rate of the bellows and the accuracy of the 20-pound load cells in the load range of fractions of a pound.

Loading Arm Redesign

The initial arm design had a calculated bellows spring rate of 0.020 lb./0.001 inch in the plane of the specimens. This spring rate gave unacceptably high unloading errors if any appreciably wear occurred under light loads. A design change was made, as shown in Figure 1 which consisted essentially of lengthening the bellows, attaching the bellows to the arm at the gimbal centerline and moving the gimbal centerline further away from the main shaft centerline. These changes decreased the calculated spring rate to 0.002 lb./0.001 inch of wear. Detailed analyses and calculations used in the redesign of the loading arm are given in Appendix A.

Rework of the loading arms to the design shown in Figure 1 has been completed and the arms reassembled and tested for bellows spring rate with the arms in the testing position. The spring rates in the specimen plane were between 0.00222 and 0.00477 lb./0.001 inch of wear, averaging about 0.0034 lb./0.001 inch. Although these spring rates are higher than the calculated 0.002 lb./0.001 inch they are much lower than the previous calculated spring rates and will produce acceptable unloading errors.

Force Pickup Accuracy

The forces read during the fractional-pound compression load tests, as well as the force pickup calibration curves, indicate that the inherent inaccuracies of the force pickup are unacceptable for the lighter loads. Although it was believed that careful calibration before each run would account for all such errors, this is apparently not true. For the 20-lb. force pickups, the non-linearity of the curve of imposed force vs. output voltage amounts to (or less than) 0.005 (20 lb.) = 0.10 lb. and hysteresis is 0.001 (20 lb.) = 0.02 lb. If not corrected, these errors are unacceptable. With good repeatability of the signal, it should have been possible to establish a calibration immediately prior to testing which would account for both errors. However, the fractional-pound forces were apparently too low to produce proper signal repeatability.

---

* Room temperature test of Grade 7178 vs Mo-TZM alloy at 500 SFM and K load.

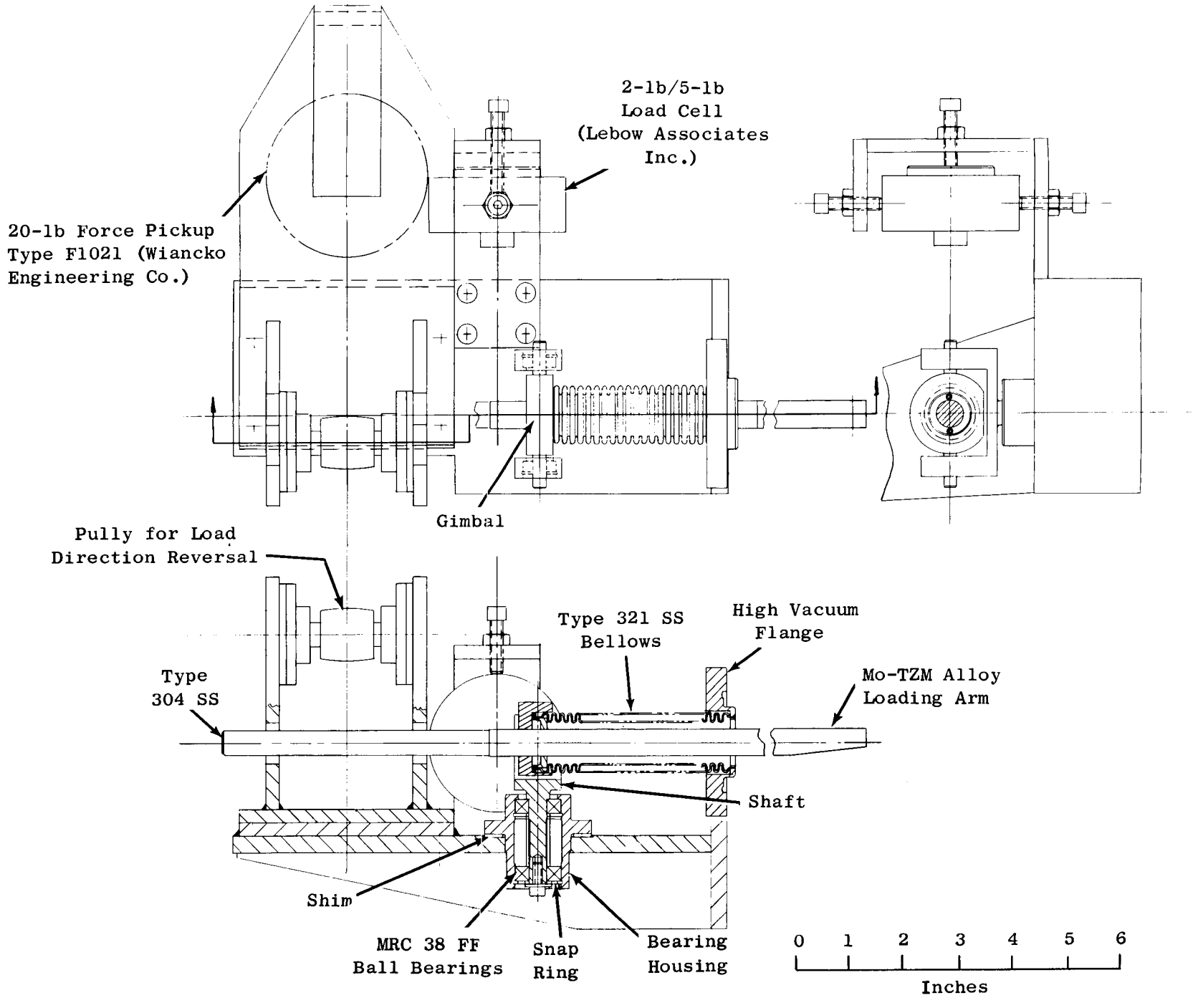

Figure 1. Loading Arm Redesign and Location of Force Cell Assemblies.

An investigation of several types of force pickups led to the conclusion that a LeBow 3108-2 and 3108-5 (2-lb. and 5-lb. capacities) would be the best choices for the lower loads. These are 4-arm bonded strain gauge bridge transducers with non-linearity and hysteresis each about 0.1% (or less) of rated capacity (0.002 lb. and 0.005 lb.). Full load deflection is 0.004 inch. It is stated that dual sensor construction will give a true reading of components parallel to the sensor axis, even though loads may be off center. Excellent linearity allows a small portion of the full range to be expanded for full scale indication of capacities much smaller than rated capacity.

In order to obtain large signals on the Sanborn tape recorder and check force pickup performance, these more accurate force pickups also will be calibrated prior to and after each run. The pre-test calibration will assure that good accuracy will be obtained from the Sanborn tape trace by determining the proper amplification of the signal generated by the pickups at the expected friction loads. Also, it will identify zero-drift, which can occur if the pickup is accidentally loaded beyond its yield point. The post-test calibration will assure that the pickup was not damaged during the test and that the entire tape accurately records friction force.

The 2-pound force pickup will be used for about 80% of the high vacuum tests, about 10% of the tests will require the 5-pound pickup, and the remainder will require the 20-pound pickup.

The 2-lb. capacity force pickup was received and installed on the tester. A typical in-place calibration is shown by Figure 2. The average hysterisis is about $\pm$ 1.4% of the largest calibration load, and is considered satisfactory. Some of this hysterisis undoubtedly is in the calibration load application and signal readout equipment and is not present during actual testing. For comparison, a typical calibration for the 20-lb. capacity load cell is shown in Figure 3 and obviously is not suitable for fractional-pound loads.

Analysis of Loading System Errors Due to Dimensional Inaccuracies

A detailed analysis of the effects of dimensional errors upon the accuracy of the specimen loading system was made, with 96% confidence in the demensions used. The result of the error analysis are given in Appendix B and are summarized below:

A. The loading error is:

$$\sum e = 0.552 + 100 \tan (0.00451 + 0.00081\ T)$$

$$+ \left[\frac{0.26734 + 1.5040P}{10000P}\right] Y_{1.6}N^2 + \left[100 - \left(\frac{2.50}{0.250 \pm b}\right)^2\right]$$

$$+ 50\ Y_{1.6} \pm 801.60\Delta d - 1606.4\ \Delta d^2 + f_f \ldots\ldots\%$$

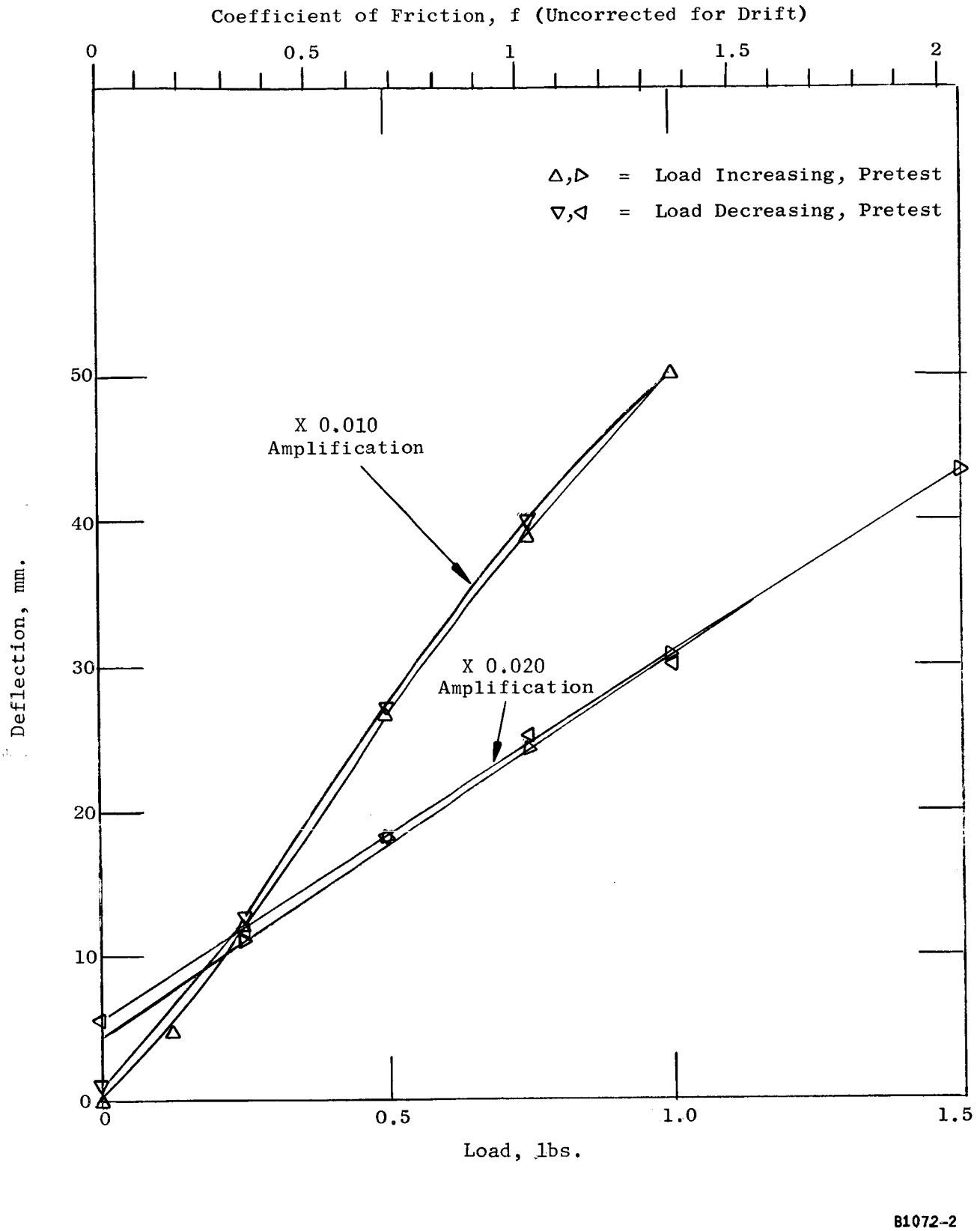

Figure 2. Two-Pound Force Pickup Calibration for Test 100K08A (Assembly VII-2).

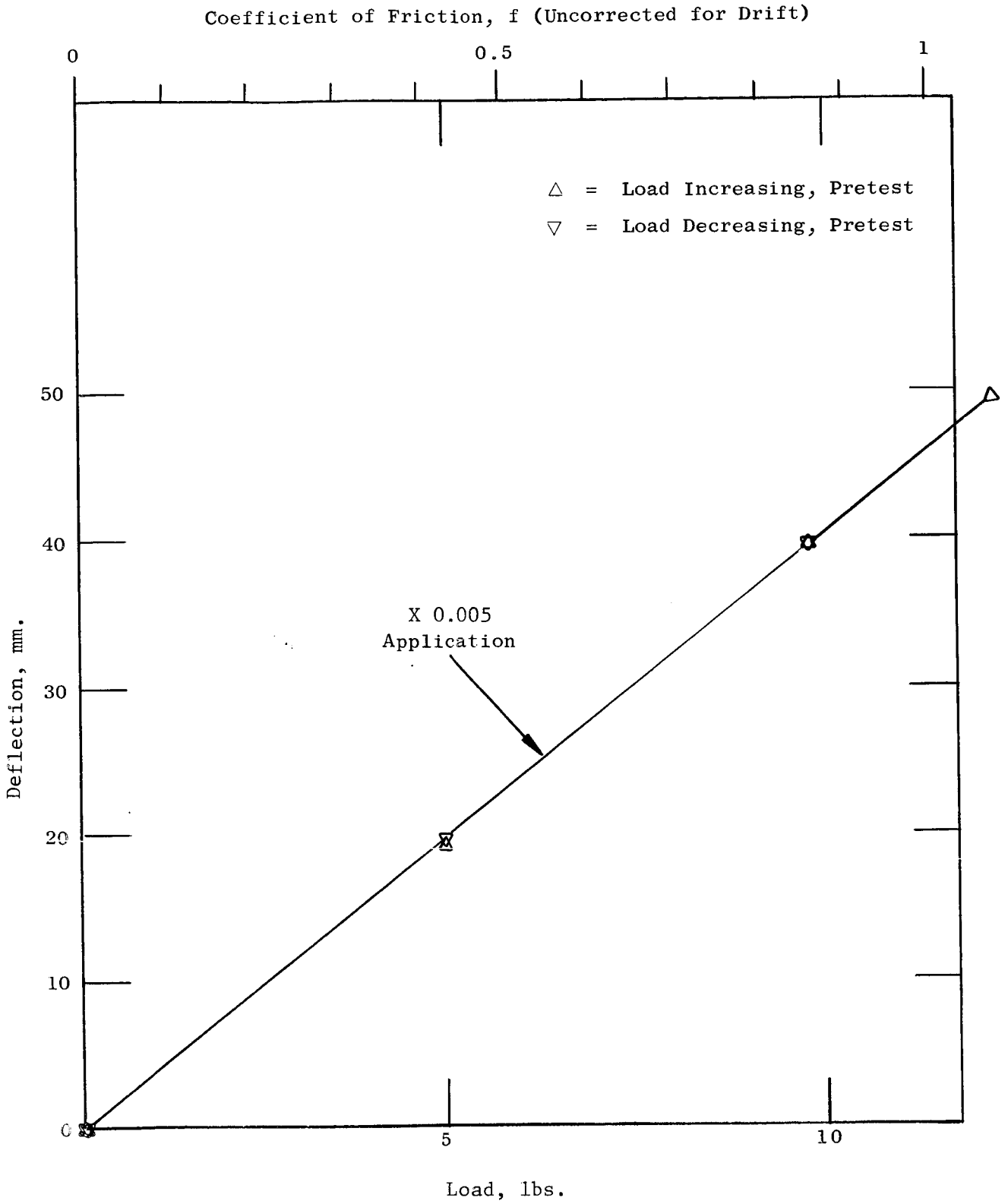

Figure 3. Twenty-Pound Force Pickup Calibration for Test 300705B (Assembly VII-1).

B1072-3

Where:

T = test temperature, °F x 10^2

$Y_{1.6}$ = vertical runout of disc specimen when rotated about main shaft axis, in.

N = rotating speed, RPM

b = out-of-plane deviation of disc specimen surface to be tested, in.

$\triangle d$ = deviation of rider specimen diameter from 0.2495 in., in.

With a test procedure which holds 100 tan (0.00451 + 0.000801T) to 1% and $Y_{1.6}$ to $\pm$ 0.001 in.,

$$\sum e = 101.552 + 0.001 \left(\left[\frac{0.26734 + 1.5040P}{1000P} \right] N^2 + 50 \right)$$

$$- \left(\frac{2.50}{0.250 \pm b} \right)^2 \pm 801.60\triangle d - 1606.3\triangle d^2 + f_f \ldots\ldots\ldots \%$$

At 764 RPM,

$$\sum_8 e = 102.45 + \frac{0.15605}{P} - \left(\frac{2.50}{0.250 \pm b} \right)^2$$

$$\pm 80160 \triangle d - 1606.4 \triangle d^2 + f_f \ldots\ldots\ldots\ldots \%$$

At 4778 RPM,

$$\sum_{50} e = 135.91 + \frac{6.1032}{P} - \left(\frac{2.50}{0.250 \pm b} \right)^2$$

$$\pm 801.60 \triangle d - 1606,4 \triangle d^2 + f_f \ldots\ldots\ldots\ldots \%$$

With no errors due to the variables in the equations, the constant portions of the errors would be:

$\sum_8 e_c = 2.45\%$

$\sum_{50} e_c = 35.91\%$

This emphasizes the strong effect of the $\pm$ 0.001 in. runout in the disc specimen at 4478 RPM.

B. The speed error is:

$$\Sigma_E = 1.336\%$$

C. The force error into the pickup is:

$$\Sigma_f = 0.005 + \frac{0.1}{f_f P} + \frac{0.667}{f_f} = 0.005 + \frac{1}{f_f}\left(\frac{0.1}{P} + 0.667\right) \quad \%$$

D. The pickup calibration force error is:

$$\Sigma_{f1} = 0.015\%$$

The above summaries refer only to those errors from dimensional discrepancies and cannot be considered full system inaccuracies.

B. Friction and Wear in Liquid Potassium

Low Speed Impeller Pump Test

Water flow tests were conducted using the low speed impeller to determine the shaft rotational speed that would achieve equal flow over the top and bottom discs. The cannister, Figure 4, fabricated to supply water to a known level with respect to the impeller and to accurately collect the flow from the upper and lower specimens, was bolted rigidly to the main bearing housing. Water was supplied through the bottom of the cannister at a sufficient rate to maintain a steady drip through the overflow tube during the test. The water, which was pumped through the specimen holders and across the disc specimens, impinged against the walls of the cannister and fell into trays. Subsequently, the water flowed through metal and plastic collector tubes into graduated beakers. To inhibit splashing, a rubberized mat was placed between the specimens and the cannister walls. The collection period was ten minutes.

The flow quantities measured are shown in Figure 5. No measureable flow was achieved at 478 RPM (500 SFM) even at the highest water levels which were considered to be consistently obtainable inside the tester during actual tests. Based upon this curve, it was recommended that the planned lower test speed (for both the liquid potassium and high vacuum friction and wear tests) be changed from 478RPM (500 SFM) to 764 RPM (800 SFM). A speed of 764 RPM will give a balanced flow of approximately 30 cc/min. across the specimens at a medium water supply level.

High Speed Impeller Pump Test

Water flow tests with the high-speed impeller assembly, Figure 6 , were conducted initially in a glass beaker without collection trays to obtain quantitative information on the speed at which flow first occurred across the

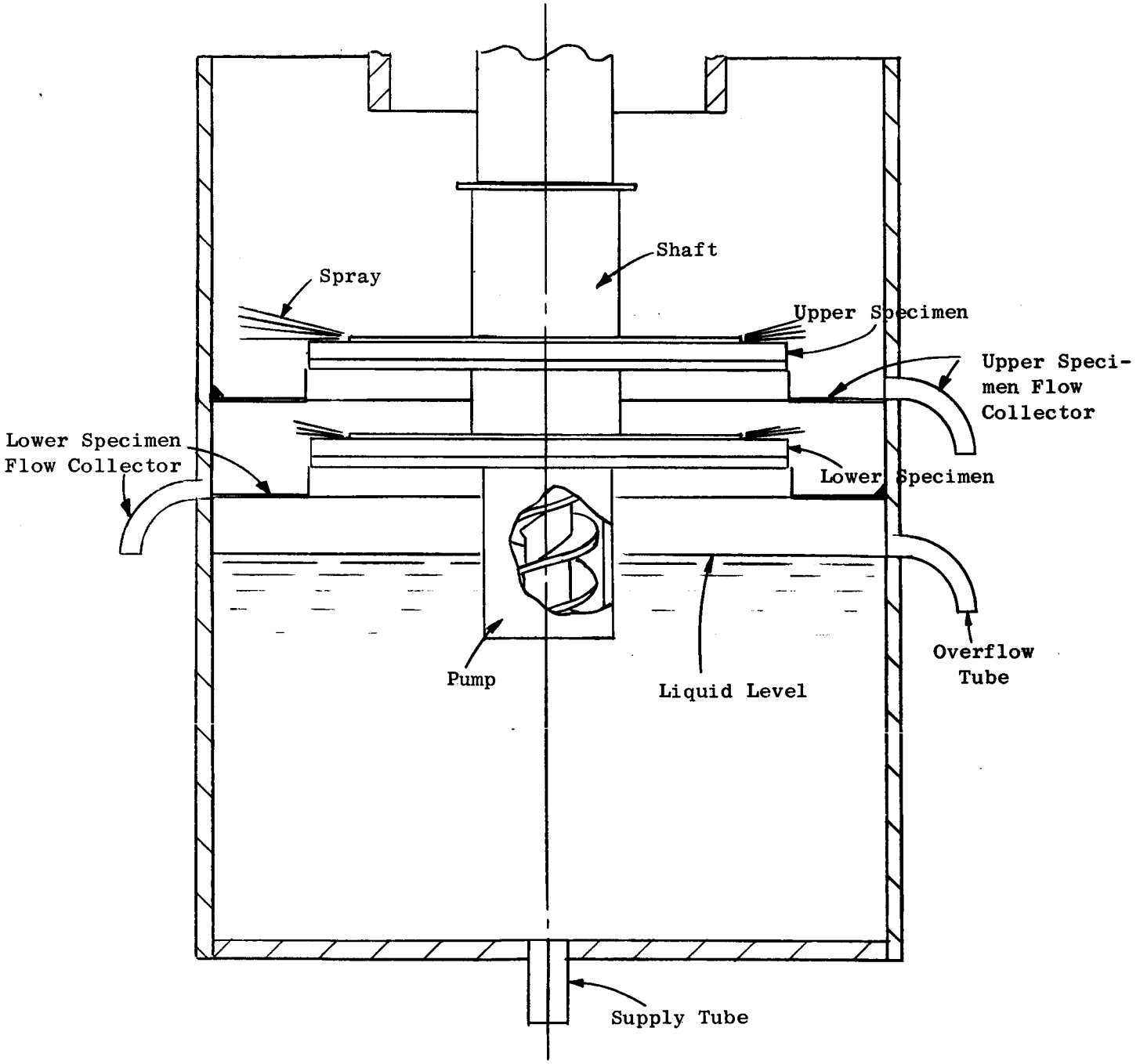

Figure 4. Schematic of Device for Calibrating Potassium Flow Over Friction and Wear Specimens.

B1072-4

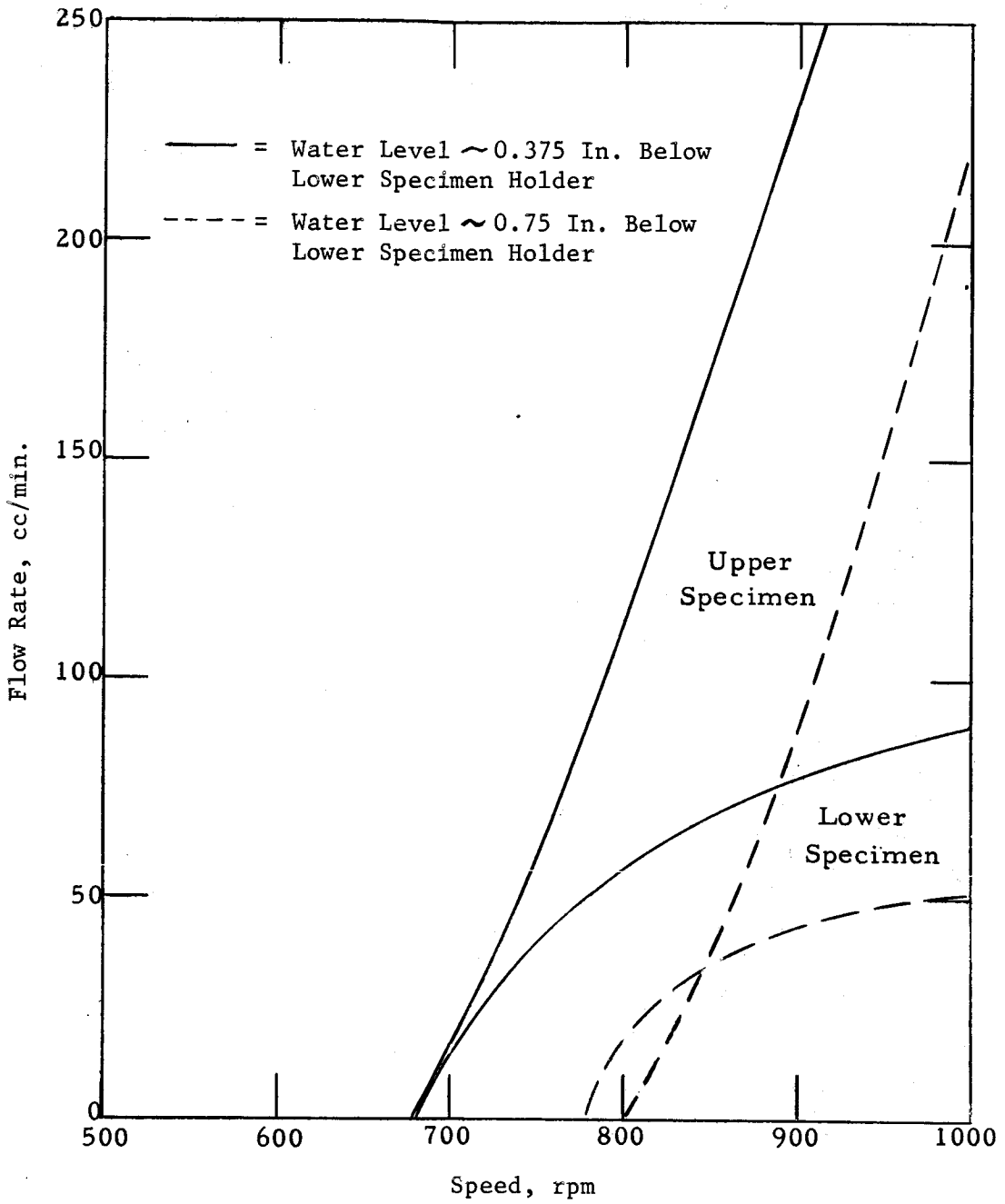

Figure 5. Water Flow Achieved with the Low-Speed Impeller of the Potassium Friction and Wear Tester.

B1072-5

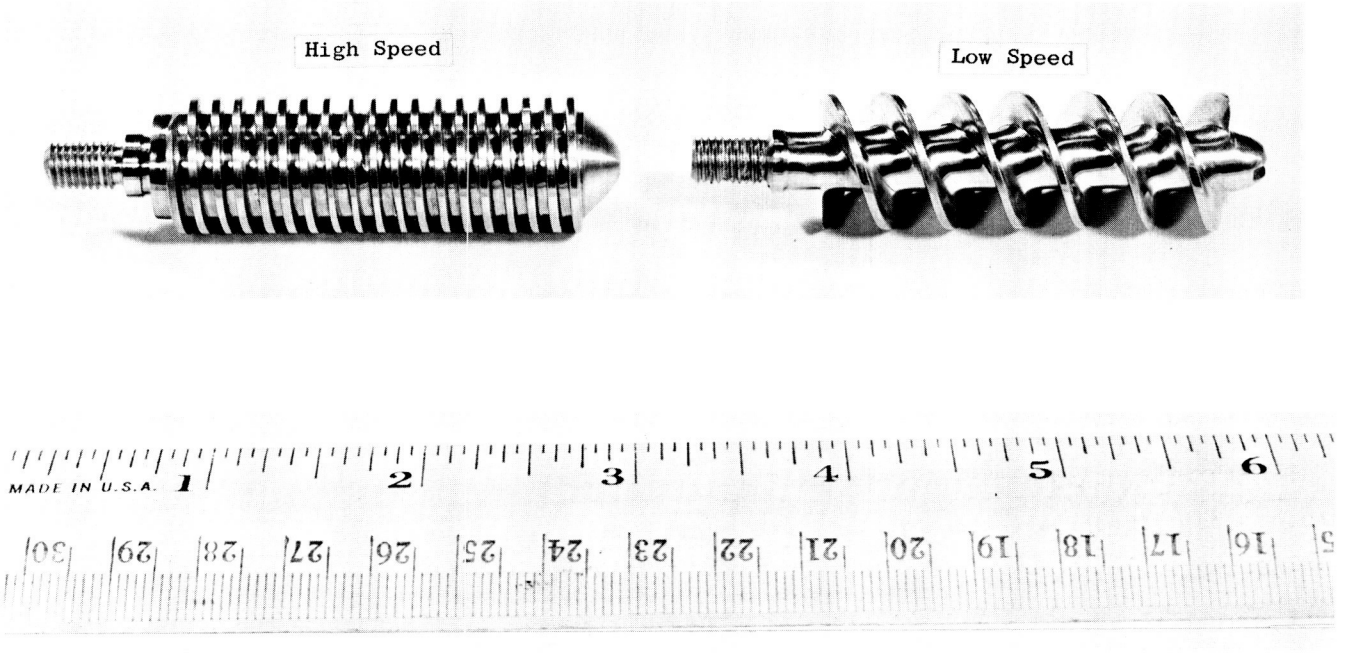

B1072-6

Figure 6. Columbium--1% Zirconium Alloy Pump Impellers for Potassium Friction and Wear Tester. (C65011465)

specimens and on the severity of vortexing. These tests showed that with the liquid level about 0.375 inch below the lower specimen holder, vortexing was observed at speeds of 1250 RPM and was unacceptably severe above 2000 RPM; at a liquid level about 1.250-inch below the lower specimen holder, vortexing was noticed at 1500 RPM and was unacceptably severe above 3300 RPM. Subsequently, a plastic baffle 0.25 inch thick was fabricated to the same pattern as that used to fabricate the Cb-1Zr alloy baffle for the potassium sump and installed in the flow test facility. Tests with the liquid level about 0.375 inch below the lower specimen holder were repeated. Although the liquid surface was quite agitated above 4000 RPM, the full speed requirements of 4775 RPM were reached without impeller inlet starvation. Flow started across the lower specimen at 1500 RPM and across the upper specimen at 2250 RPM. When the tests with the liquid level about 1.250-inch below the lower specimen holder were repeated, the surface was smooth to 4850 RPM. In the latter tests, flow started across the lower specimen at 2000 RPM and across the upper specimen at 3000 RPM. It was concluded that the present baffle design is satisfactory. However, proof of its efficiency in potassium at several different temperature levels will have to be obtained with liquid potassium.

Check tests with the water collectors in place showed that with the lower specimen orifices plugged, the flow over the upper specimen was 48 cc/min at 4770 RPM. Leakage on the lower specimen was 9 cc/min. With both flow orifices open, a flow of 54 cc/min. was measured over the lower specimen and 7 cc/min. over the upper specimen, Figure 7. Subsequent tests will be conducted with the high speed impeller to determine the proper size of the lower orifice in order to achieve a balanced flow of 30 cc/min., the expected flow at 764 RPM across both specimens.

Test Facility

The test facility for the liquid potassium friction and wear tester has been completed with the exception of final welding of the potassium fill and drain lines to the test rig. Heaters, thermocouples, and thermal insulation were installed, and the system was baked out at temperatures up to 750°F to demonstrate heater capability for removing residual potassium from the test assembly by vacuum distillation. The flange connection between the facility and the test rig was blanked off, and the facility was evacuated to a pressure of 1×10^{-9} torr by means of a getter-ion pump. A photograph of the completed assembly is shown in Figure 8.

The following minor modifications were made to the facility to facilitate liquid metal operation.

1. The potassium sampling valves were relocated and an additional argon-vacuum valve added to the system to simplify the potassium sampling procedures during filling and draining operations.

2. A 0.500-inch OD tube well was added to the hot trap tank to provide a means of monitoring the hot trap liquid level with a MSA portable level probe.

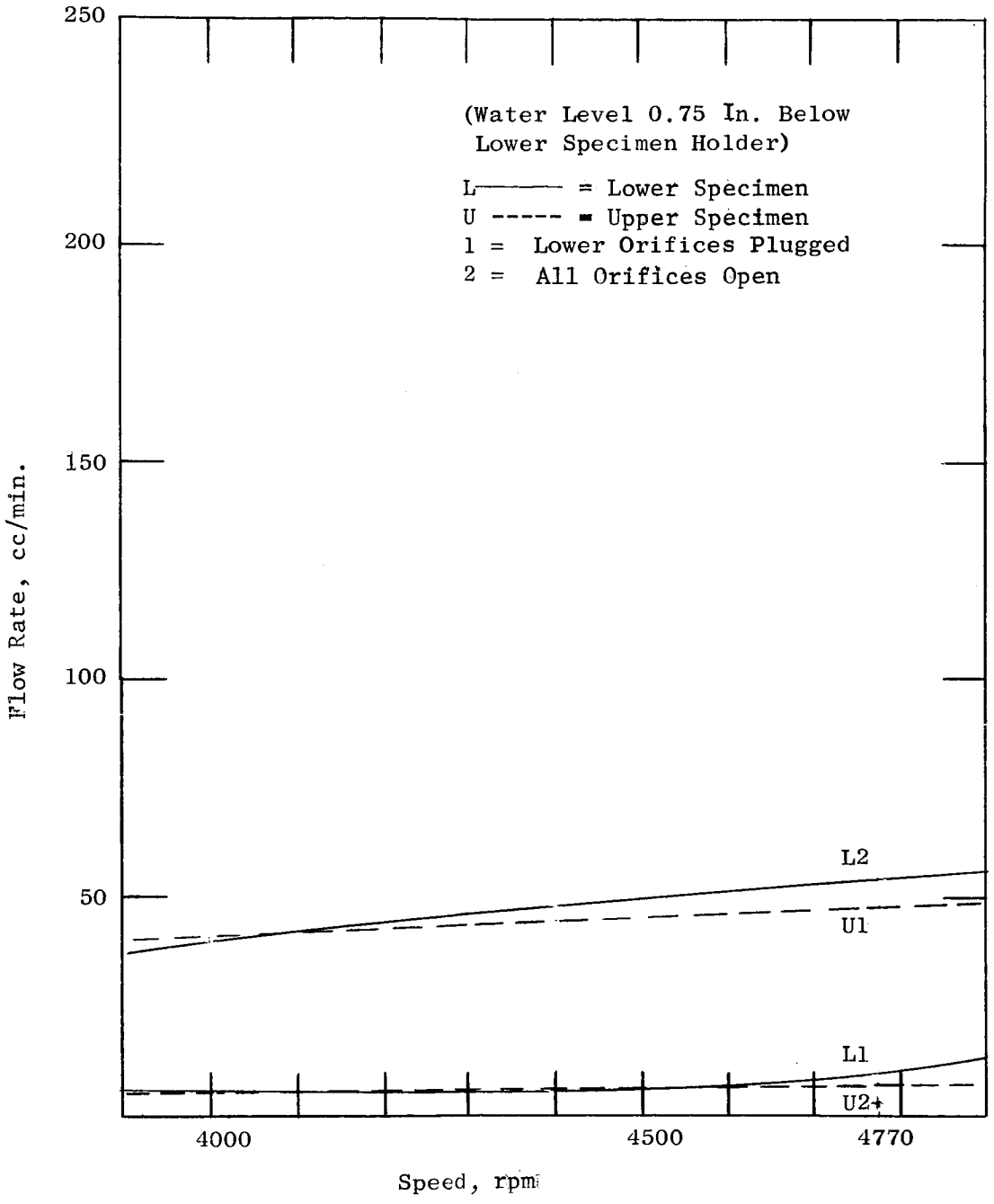

Figure 7. Water Flow Achieved with the High-Speed Impeller of the Potassium Friction and Wear Tester.

B1072-7

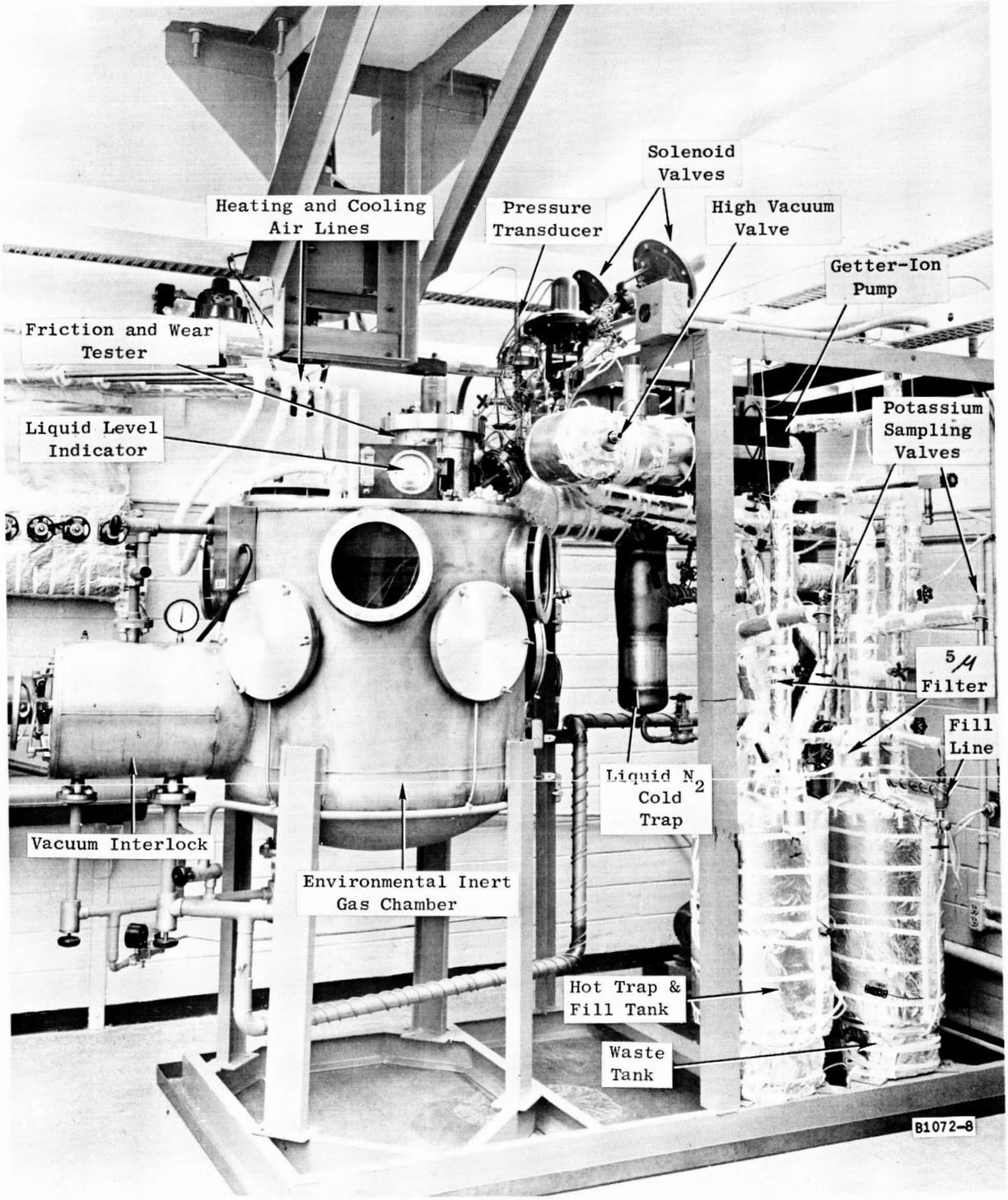

Figure 8. Liquid Potassium Friction and Wear Test Facility.

3. A calibrated volume tank was installed in the fill line to assure that the proper quantity of potassium will be transferred to the test rig.

4. An alternate method of liquid level detection in the test rig was incorporated into the facility. Water flow tests with the impeller pump indicated a faster liquid level monitoring response time is required than what could be achieved with the nuclear liquid level gauge. The alternate system, described below, has been tested with water and has a repeatability of 0.1 inch of water. This is equivalent to a level change of approximately 0.13 inch of potassium at 600°F. The system operated satisfactorily with less than 0.1 SCFM argon flow.

The alternate liquid level system is shown schematically in Figure 9 and is functionally identical to "bubbler" type level measuring devices which have been used successfully in the process industries. The system will measure the vertical distance between a dip tube located in the lower section of the potassium sump and the liquid-gas interface by flowing a small amount of inert gas through the dip tube. A differential pressure measurement is obtained which is proportional to the height of the liquid in the dip tube. The system to be used consists of a differential pressure gauge (0 to 10 inches of water), a variable area gas flowmeter and a fine control needle valve. Argon gas flows through the needle valve and flowmeter into the liquid potassium extraction line (dip tube) which is connected to the high pressure side of the differential pressure gauge. The low pressure side of the differential pressure gauge is connected to the test rig argon-vacuum system.

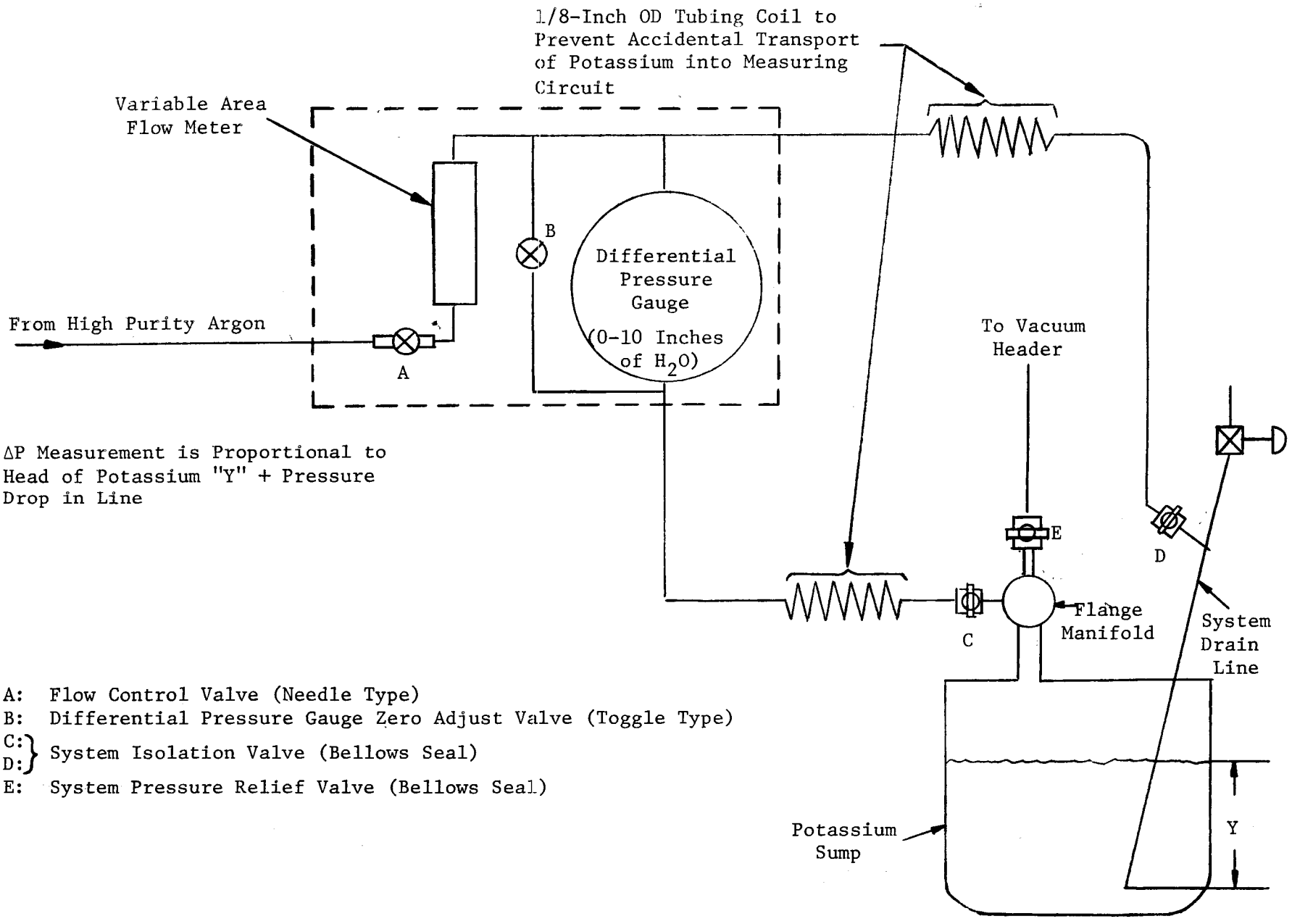

Valve A: Flow Control Valve (Needle Type)
Valve B: Differential Pressure Gauge Zero Adjust Valve (Toggle Type)
Valve C:
Valve D: } System Isolation Valve (Bellows Seal)
Valve E: System Pressure Relief Valve (Bellows Seal)

Figure 9. Schematic of Liquid Level Measuring System for Liquid Potassium Friction and Wear Tester.

B1072-9

IV. TEST PROGRAMS

A. Corrosion

Candidate Bearing Materials

The Cb-1Zr alloy capsules which contained the Carboloy 907 and Grade 7178 specimens and which were used for the 1000-hour, 800° and 1200°F isothermal potassium corrosion tests were sectioned and 0.020-inch layers from the ID of the liquid zones were analyzed for carbon content. The location of the samples and methods of sectioning and analysis were the same as employed for the capsules tested at 1600°F.[5] The data are presented in Table II and summarized in Table III along with the data previously reported for the 1600°F tests. The results show that carbon had transferred from both Carboloy 907 and Grade 7178 to the Cb-1Zr alloy capsule wall at a temperature of 1200°F, i.e., on the order of 40-45 ppm in a 0.020-inch thick section. Essentially no transfer of carbon was observed to have occurred at 800°F.

Metallographic examination of the Cb-1Zr alloy containment capsules used in the 1600°F corrosion testing of candidate bearing materials revealed no significant changes in the microstructure as a result of the 1000-hour exposure except in those capsules that contained Carboloy 999, Carboloy 907, and Star J specimens. Through stain etching techniques,[6] a layer of CbC was identified on the ID surfaces of these capsules, Figure 10. This is in agreement with the relatively large increases in carbon observed in the inner 0.020-inch portion of the wall of the capsules by chemical analyses.

The metallographic examination of the candidate bearing materials test specimens that were exposed to potassium in Cb-1Zr alloy capsules for 1000 hours at 800° and 1200°F has been completed. Results of the metallographic examination of the candidate bearing materials tested at 1600°F were previously reported.[5] No microstructural changes or evidence of surface attack was observed in any of the candidate bearing material test specimens with the exception of the Carboloy 999 specimen exposed to potassium liquid and the Zircoa 1027 specimens exposed to potassium liquid and vapor. In the case of the Carboloy 999, only a slight surface roughening was evident after the 1000-hour exposure to potassium liquid at 800° and 1200°F as compared to an apparent 0.0004-inch deep corrosion reaction observed in a similar specimen tested at 1600°F, Figure 11. Essentially no change was evident in the microstructure of the Carboloy 999 specimens that was exposed to potassium vapor at 800° and 1200°F in contrast to the 0.0002-inch deep corrosion reaction observed in the Carboloy 999 specimen that was tested in potassium vapor at 1600°F. With respect to the Zircoa 1027 material, the corrosion reaction observed in the specimens tested at 1600°F was still evident, although considerably less extensive, in the specimen tested at 1200°F and the outer portion of the specimen tested at 800°F, Figure 12. Similar reactions were observed both in the liquid and vapor zones.

TABLE II. CARBON CONTENT OF Cb-1Zr ALLOY CAPSULES CONTAINING CANDIDATE JOURNAL BEARING MATERIAL TEST SPECIMENS AFTER EXPOSURE TO POTASSIUM FOR 1000 HOURS AT 800° AND 1200°F

Candidate Bearing Materials	Test Temp., °F	Capsule No.	Carbon Content[1] ppm
Carboloy 907	1200	BIC-7	80/100
	800	BIC-25	60/60
Grade 7178	1200	BIC-33	80/100
	800	BIC-32	30/30
Control (1005-7)	--	--	50/30
Control (1005-4)	--	--	50/70
As-Received (Bulk[2])	--	--	40

[1]Analyses of Inner 0.020-Inch Thick Layer of Cb-1Zr Alloy Capsule in Liquid Zone by Combusion Conductometric.

[2]0.080-Inch Thick Wall.

TABLE III. SUMMARY OF CARBON TRANSFER FROM CANDIDATE BEARING MATERIALS TO Cb-1Zr ALLOY IN POTASSIUM

Material	Composition	Carbon Increase (ppm) in Inner 0.020-Inch of Cb-1Zr Alloy Capsule After 1000-Hour Exposure to Potassium		
		1600°F	1200°F	800°F
Carboloy 999	97%WC-3%Co	340	--	--
Star J	17%W-32%Cr-2.5%Ni 3%Fe-2.5%C-Bal Co	215	--	--
Carboloy 907	74%WC-20%TaC-6%Co	145	45	10
Grade 7178	85.6%W-6.9%Mo-1.8%Cb 0.3%Ti-5.7%C	70	40	0
TiC+10%Cb	83.6%TiC-9.5%Cb-5.9%WC	0	--	--
Mo-TZM	Mo-0.5%Ti-0.08%Zr-0.02%C	0	--	--

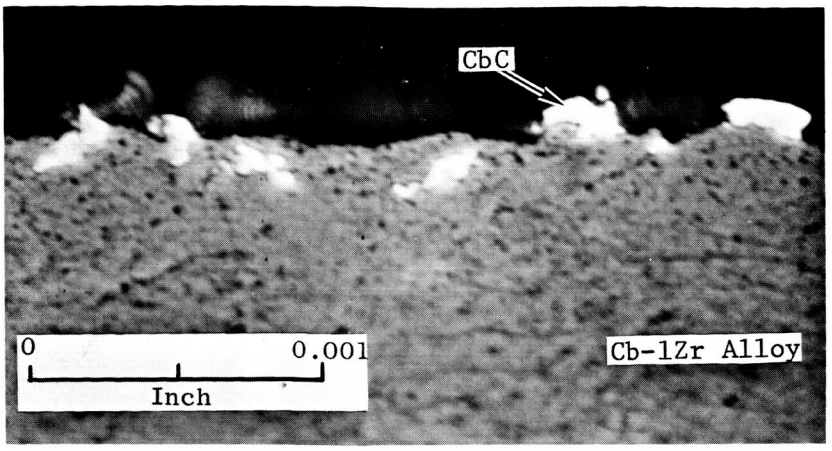

Carboloy 999 Test Specimens (Capsule BIC-10)
(A060412)

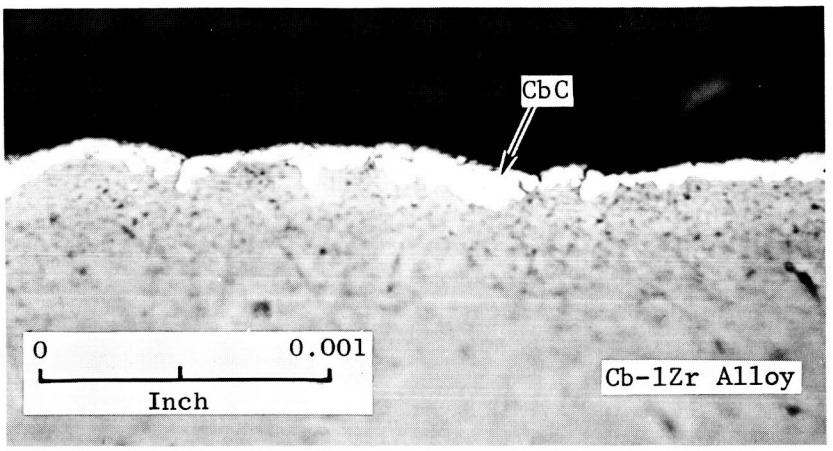

Carboloy 907 Test Specimens (Capsule BIC-9)
(A060212)

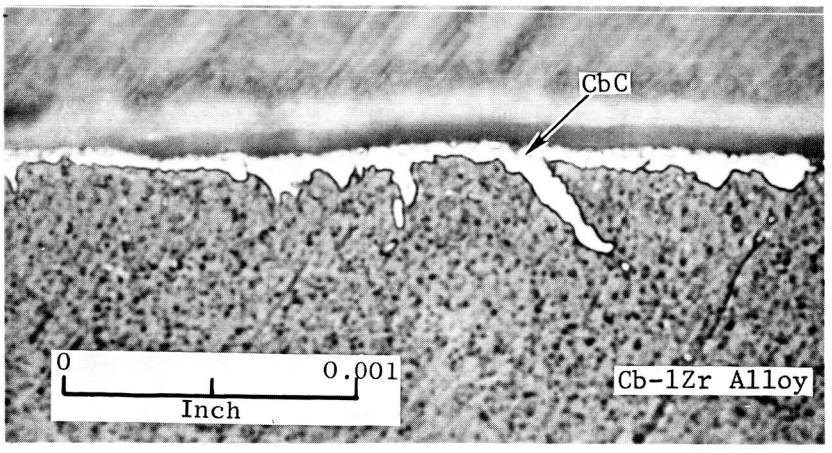

Star J Test Specimens (Capsule BIC-40)
(A062012)

B1072-10

Figure 10. Microstructure of Transverse Sections of Cb-1Zr Alloy Containment Capsules Showing CbC Layers on ID Surfaces in Liquid Zone After Corrosion Testing of Candidate Bearing Materials for 1000 Hours at 1600°F.

Etchant: Stain Etched (Ref. 6)

Magnification: 1500X
N.A.: 0.95

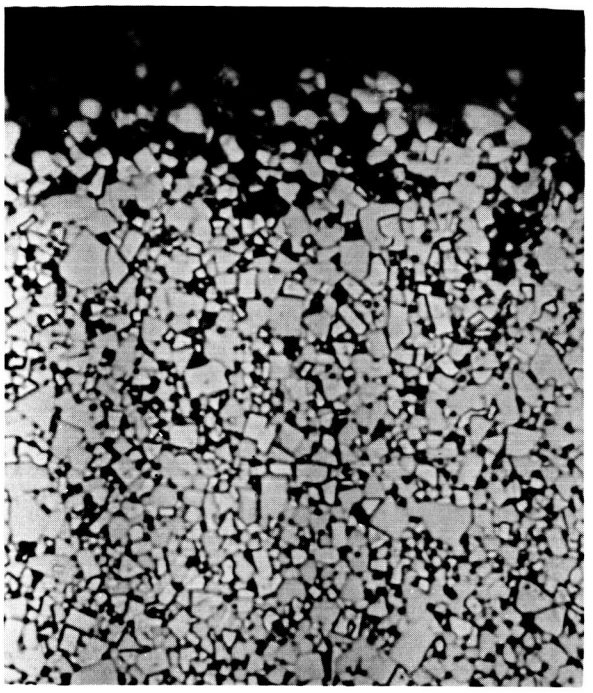

1600°F-Liquid Zone
Post Test (A050323)
Note Apparent Surface Attack
to a Depth of 0.0004 Inch.

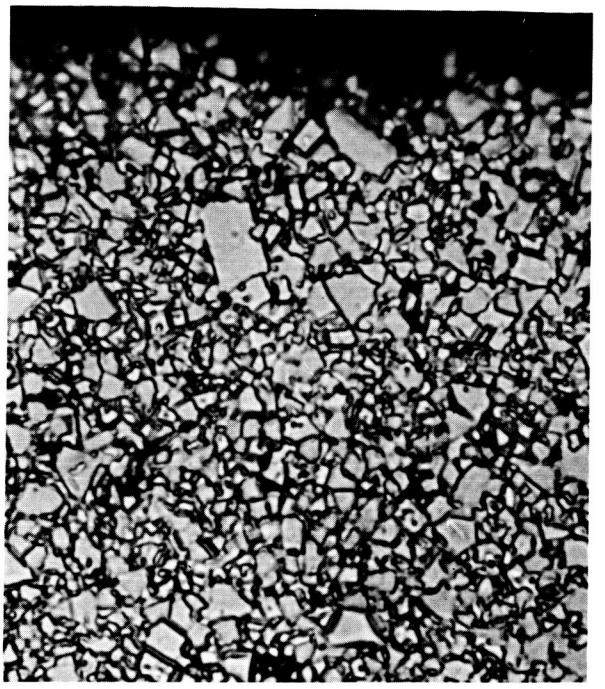

1200°F-Liquid Zone
Post Test (A330112)

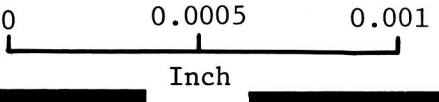

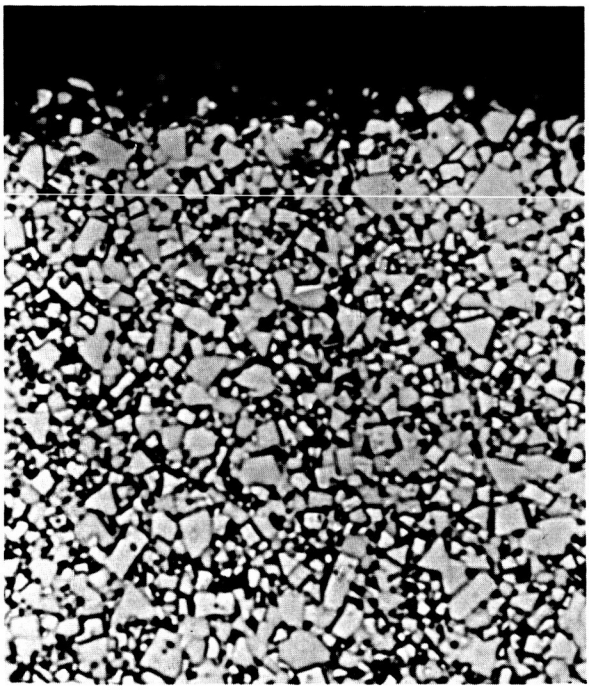

Pre-Test (A050313)

800°F-Liquid Zone
Post Test (A880112)

B1072-11

Figure 11. Microstructure of Transverse Sections of Carboloy Grade 999 Before and After Exposure to Potassium for 1000 Hours at 800°, 1200°, and 1600°F.

Etchant: 10%NaOH, Electrolytic

Magnification: 2000X
N.A.: 1.30

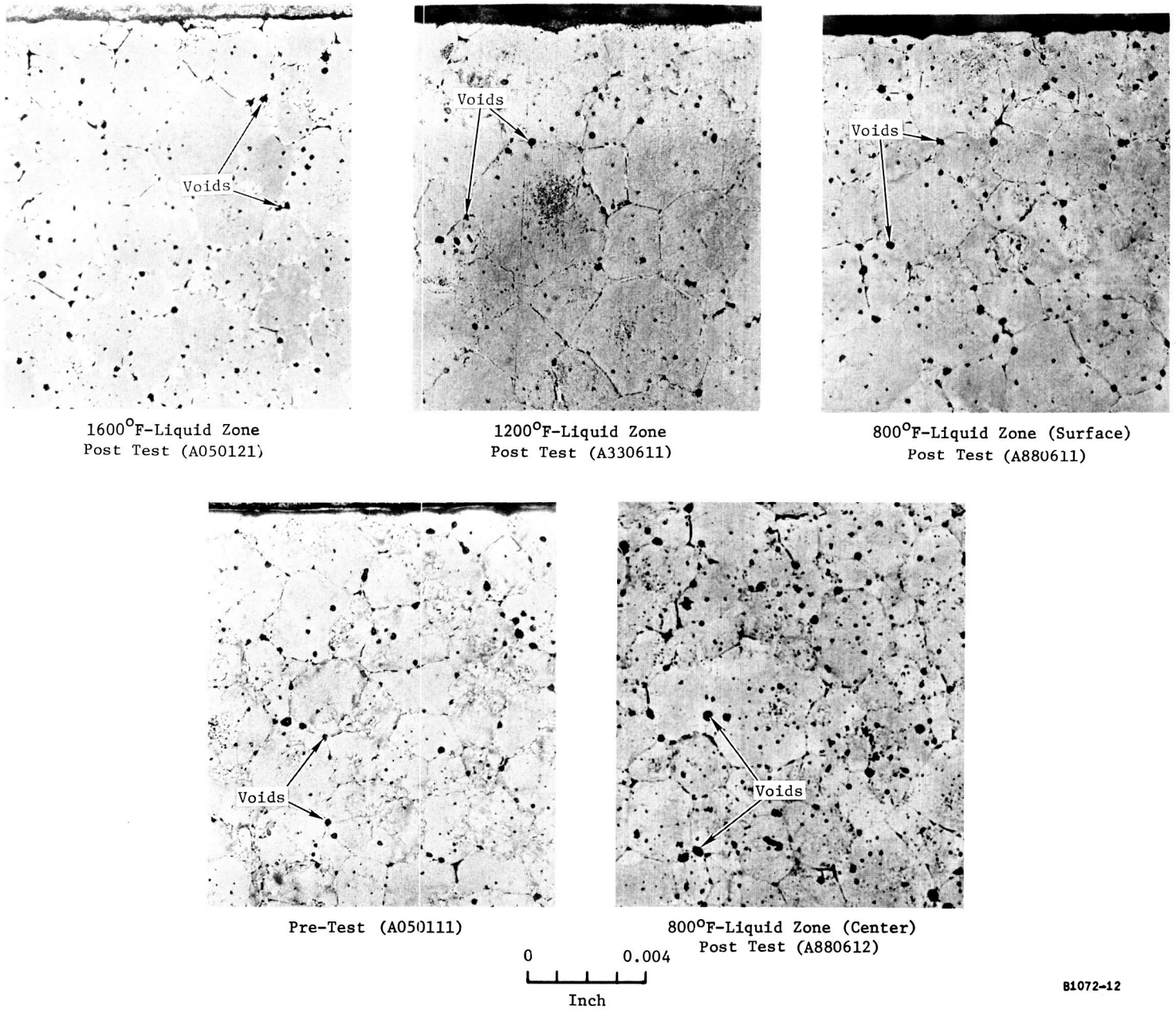

1600°F-Liquid Zone
Post Test (A050121)

1200°F-Liquid Zone
Post Test (A330611)

800°F-Liquid Zone (Surface)
Post Test (A880611)

Pre-Test (A050111)

800°F-Liquid Zone (Center)
Post Test (A880612)

Figure 12. Microstructure of Transverse Sections of Zircoa 1027 Before and After Exposure to Potassium for 1000 Hours at 800°, 1200°, and 1600°F.

Etchant: Boiling H_2SO_4+HF Magnification: 250X

Other candidate bearing materials that exhibited some attack due to exposure to potassium at 1600°F and which showed no attack at 800° or 1200°F are Carboloy 907 (Figure 13), TiC (Figure 14), and TiC+5%W (Figure 15). The Carboloy 907 specimens tested at 1600°F in potassium liquid and vapor showed corrosion reactions on the surface to depths of 0.0007 inch and 0.0001 inch deep, respectively. The TiC and TiC+5%W specimens tested at 1600°F in potassium liquid had exhibited a surface roughening and what appeared to be intergranular attack to depths of 0.0002 inch and 0.0004 inch, respectively; only surface roughening was apparent on the TiC and TiC-5%W specimens tested in potassium vapor at 1600°F.

No changes in phase morphology were observed in the Star J specimens tested at 800° and 1200°F as were observed in the specimens tested at 1600°F (Figure 16). This is in agreement with the dimensional changes that were observed after the 1000-hour exposure.

Although examination of the Grade 7178 specimens tested at 800°F and 1200°F revealed no significant differences from the specimens tested at 1600°F, a greater amount of eutectic phase was retained through improved metallographic procedures (Figure 17). The fact that the structures still appear to be more coarse after the 1000-hour exposure is attributed to inhomogeniety between specimens.

The x-ray diffraction analyses of the candidate bearing material specimens exposed to potassium liquid and vapor at 1600°F for 1000 hours have been completed. The phases detected on the surface of the specimens before and after testing are shown in Table IV. No phase changes were observed after testing the following materials: TiC, TiC+5%W, TiC+10%Mo, TiC+10%Cb, Lucalox (Al_2O_3), and TiB_2.

The transfer of carbon from the tungsten carbide base Carboloy 999, Carboloy 907, and Grade 7178 materials to the Cb-1Zr alloy containment capsule during the 1000-hour exposures to potassium at 1600°F and 1200°F, which was discussed in Quarterly Report No. 8[7] and on page 23 of this report, clearly is substantiated by the results of the x-ray analyses of these materials. All of the specimens of the forementioned materials which were exposed to potassium liquid exhibited a major surface change from WC to tungsten. Although no increase in carbon was observed in the inner 0.020-inch layer of the Cb-1Zr alloy capsule containing the K601 material, pure tungsten also was detected on the surface of the K601 specimens exposed to potassium liquid. A minor amount of tungsten also was detected on the surface of the K601 specimen exposed to potassium vapor; no tungsten was detected on the surfaces of the Carboloy 999, Carboloy 907 and Grade 7178 specimens exposed to potassium vapor. In addition to tungsten, a minor amount of WC was detected on the surfaces of the Carboloy 999, K601, and Grade 7178 specimens after exposure to liquid potassium; no WC was found on the surfaces of the Carboloy 907 after exposure to potassium liquid.

The formation of Co_2W_4C and $(Co,W)_xC$ was detected on the surface of the Carboloy 907 specimens exposed to potassium liquid and vapor and the Carboloy 999 specimen exposed to potassium liquid. These two phases were not detected in the Carboloy 999 specimen exposed to potassium vapor.

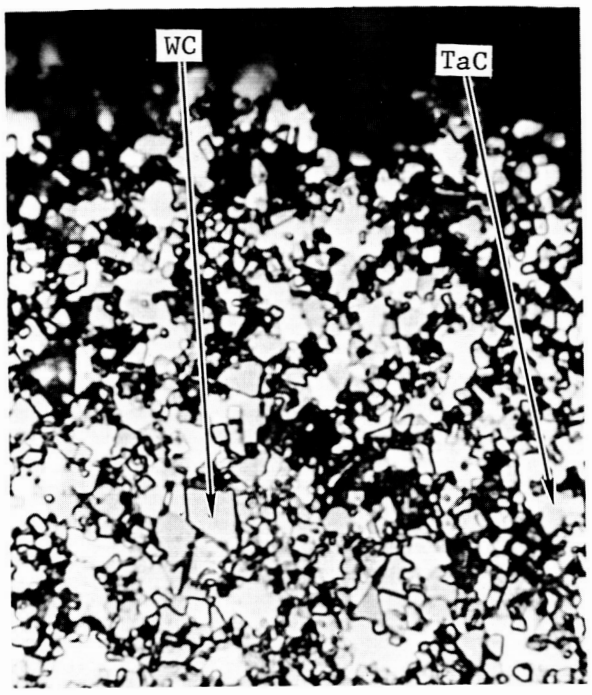

1600°F-Liquid Zone
Post Test (A052323)
Note Apparent Surface Attack
to a Depth of 0.0007 Inch.

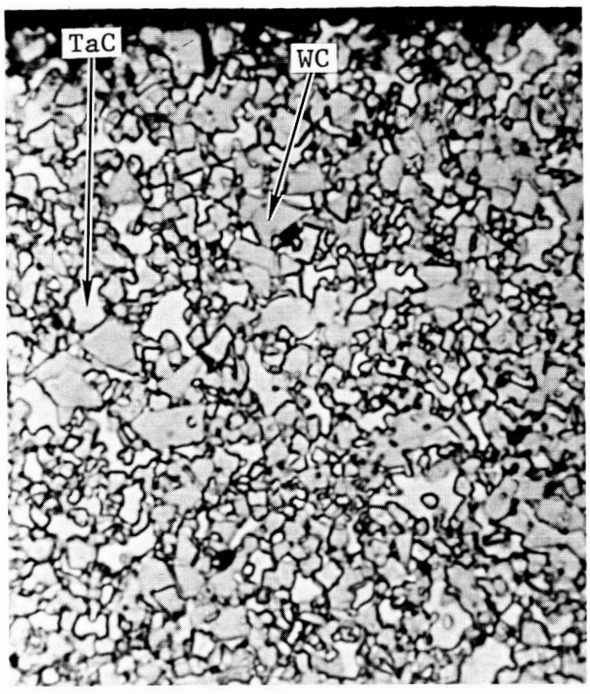

1200°F-Liquid Zone
Post Test (A330212)

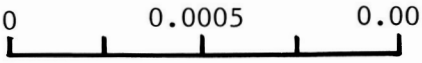

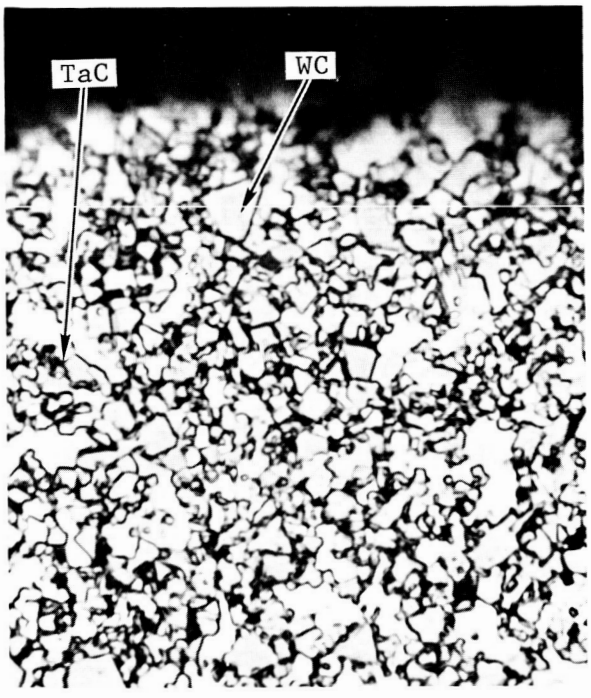

Pre-Test (A052313)

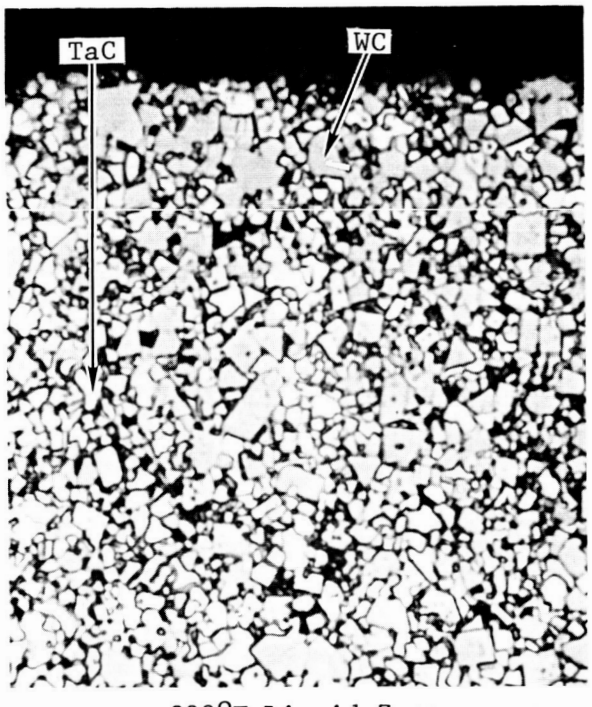

800°F-Liquid Zone
Post Test (A880212)

B1072-13

Figure 13. Microstructure of Transverse Sections of Carboloy Grade 907 Before and After Exposure to Potassium for 1000 Hours at 800°, 1200°, and 1600°F.

Etchant: 10%NaOH, Electrolytic

Magnification: 2000X
N.A.: 1.30

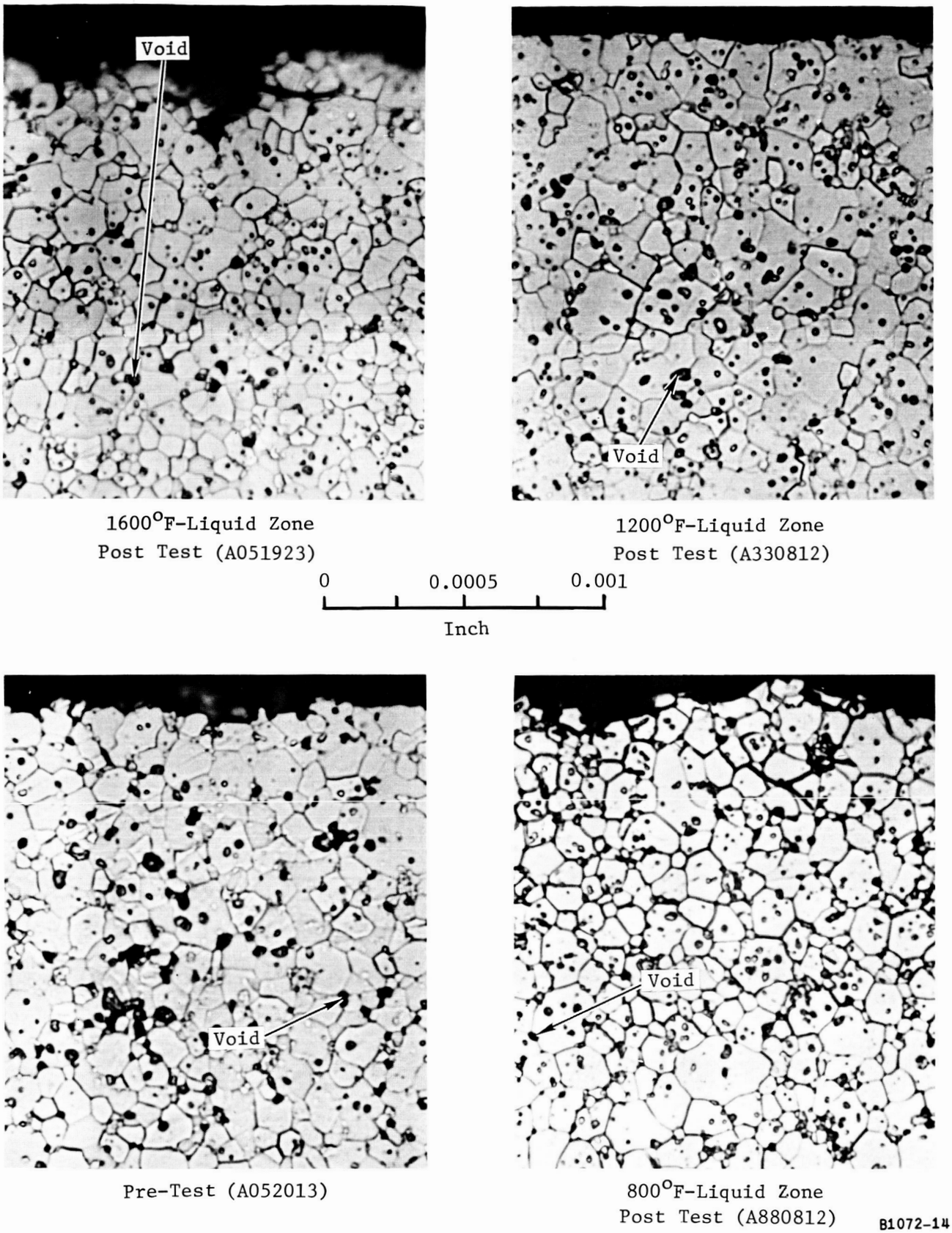

Figure 14. Microstructure of Transverse Sections of TiC Before and After Exposure to Potassium for 1000 Hours at 800°, 1200°, and 1600°F.

Etchant: $80HNO_3+20HF$ Magnification: 2000X
N.A.: 1.30

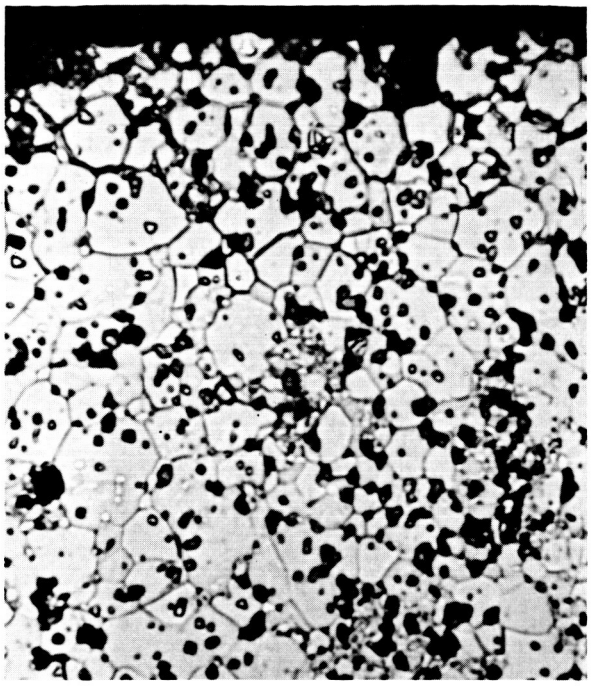

1600°F-Liquid Zone
Post Test (A051523)

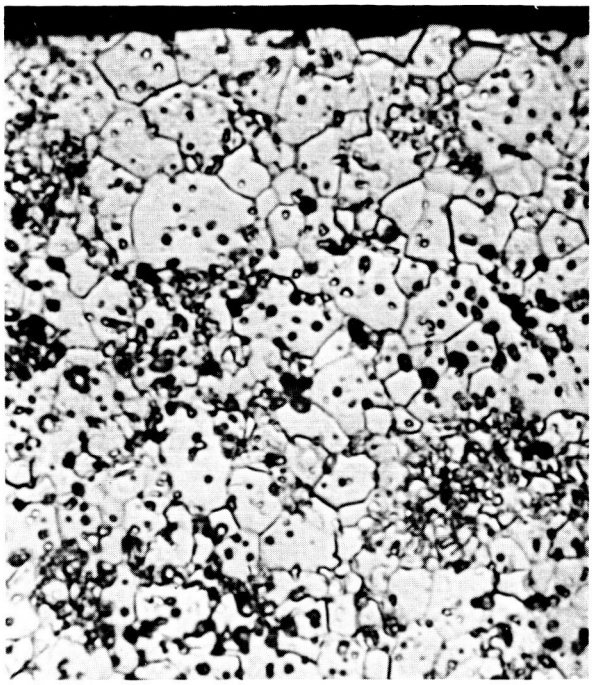

1200°F-Liquid Zone
Post Test (A330912)

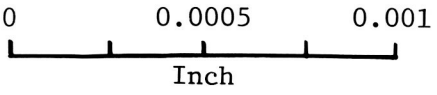

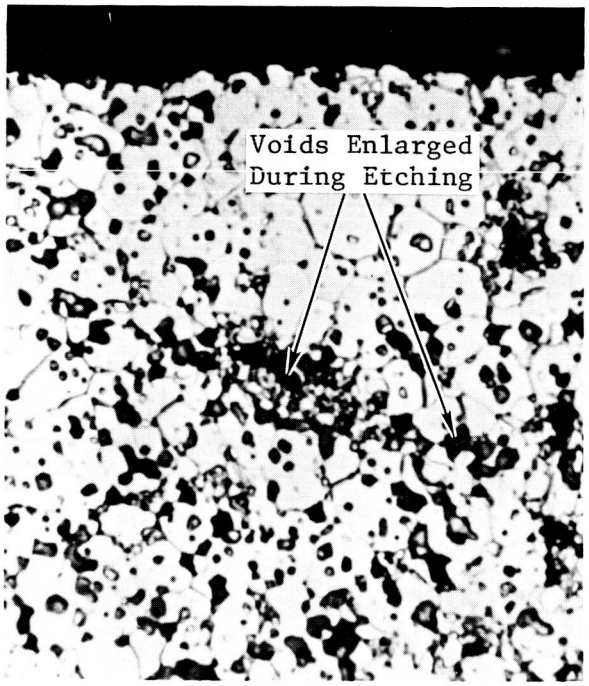

Pre-Test (A051513)

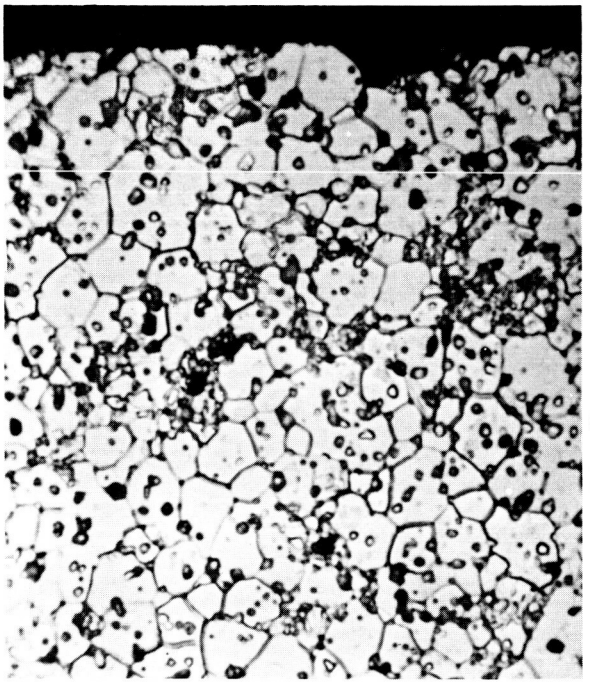

800°F-Liquid Zone
Post Test (A880912)

B1072-15

Figure 15. Microstructure of Transverse Sections of TiC+5%W Before and After Exposure to Potassium for 1000 Hours at 800°, 1200°, and 1600°F.

Etchant: $80HNO_3$+20HF

Magnification: 2000X
N.A.: 1.30

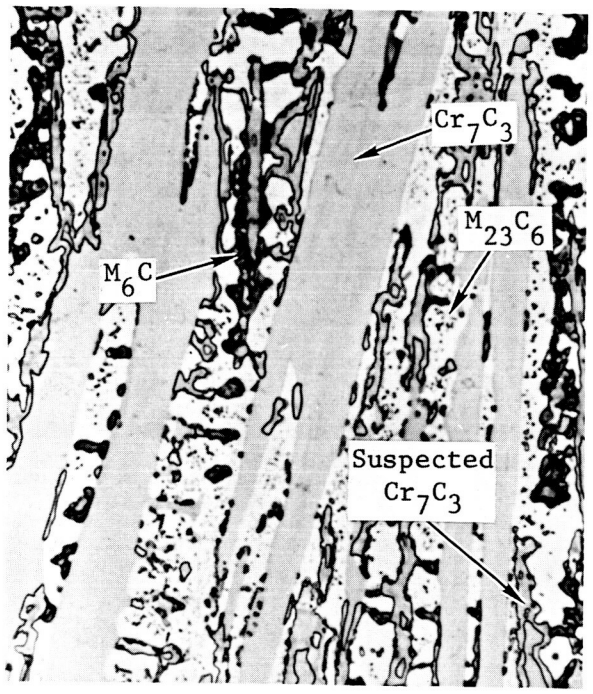

1600°F-Vapor Zone
Post Test (A050622)

1200°F-Vapor Zone
Post Test (A331222)

0 0.001
Inch

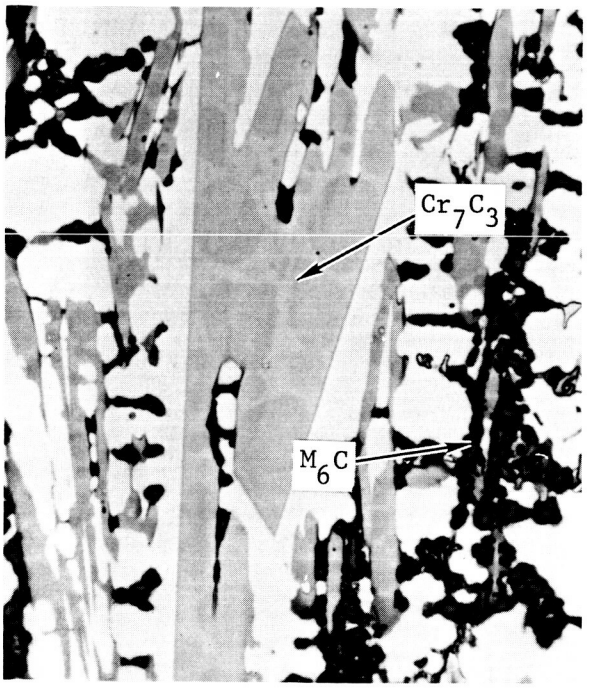

Pre-Test (A050611)

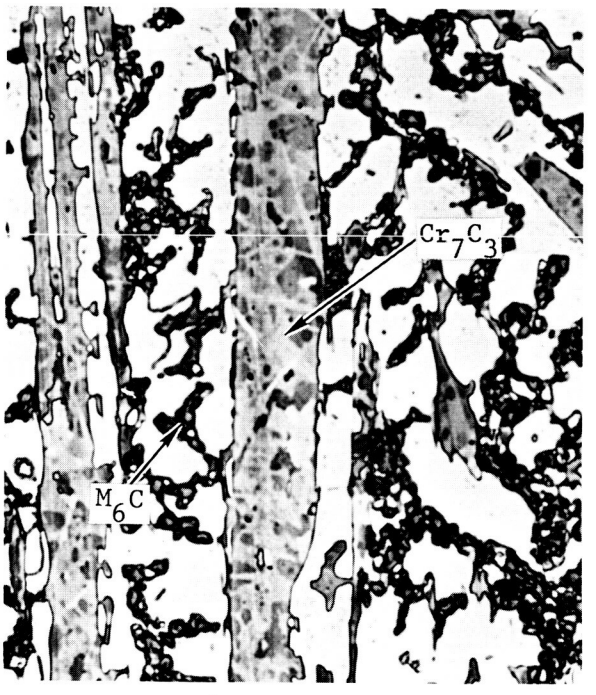

800°F-Vapor Zone
Post Test (A881222)

B1072-16

Figure 16. Microstructure of Transverse Sections of Star J Before and After Exposure to Potassium for 1000 Hours at 800°, 1200°, and 1600°F.

Etchant: 2% Chromic Acid, Electrolytic + Grosbeck's Reagent

Magnification: 1000X
N.A.: 0.85

TABLE IV. SURFACE PHASE CHANGES OF CANDIDATE BEARING MATERIALS AFTER EXPOSURE TO POTASSIUM LIQUID AND VAPOR FOR 1000 HOURS AT 1600°F

Material	Phases Present[a]					
	Pre-Test		Post Test			
			Specimen In Liquid		Specimen In Vapor	
	Major	Minor	Major	Minor	Major	Minor
Carboloy 999	WC	--	W	WC, Co_2W_4C, $(Co,W)_xC$	WC	--
Carboloy 907	WC	TaC	W	TaC, Co_2W_4C, $(Co,W)_xC$	WC	TaC, Co_2W_4C, $(Co,W)_xC$
K601	WC, $(W,Ta)_2C$	--	W	WC, $(W,Ta)_2C$	WC, $(W,Ta)_2C$	W
TiC	TiC	--	TiC	--	TiC	--
TiC+5%W	(Ti,W)C	--	(Ti,W)C	--	(Ti,W)C	--
TiC+10%Mo	(Ti,Mo)C	--	(Ti,Mo)C	--	(Ti,Mo)C	--
TiC+10%Cb	(Ti,Cb)C	--	(Ti,Cb)C	--	(Ti,Cb)C	--
Grade 7178	WC	$(Mo,Cb)_2C$	W	$(Mo,Cb)_2C$, WC	WC	$(Mo,Cb)_2C$
Lucalox	α-Al_2O_3	--	α-Al_2O_3	--	α-Al_2O_3	--
Zircoa 1027	ZrO_2 (cubic)	ZrO_2 (monoclinic)	ZrO_2 (cubic) ZrO_2 (monoclinic)	--	ZrO_2 (monoclinic)	ZrO_2 (cubic)
TiB_2	TiB_2	--	TiB_2	--	TiB_2	--

(a) Identified by x-ray diffraction (CuKα)

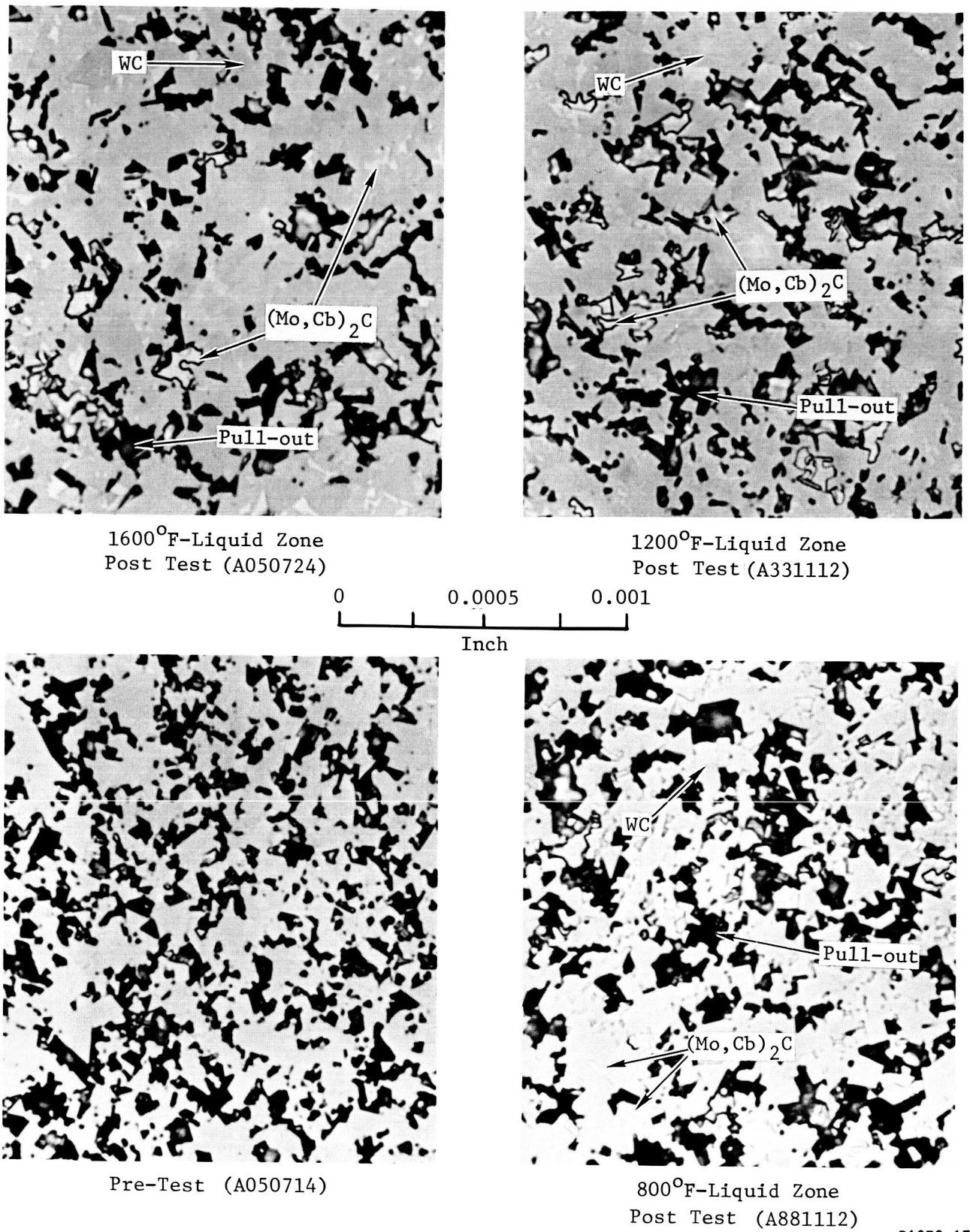

Figure 17. Microstructure of Transverse Sections of Grade 7178 Before and After Exposure to Potassium for 1000 Hours at 800°, 1200°, and 1600°F.

Etchant: 10%NaOH, Electrolytic

Magnification: 2000X
N.A.: 1.30

The greater stability of carbon in the Carboloy 907, K601, and Grade 7178 materials over the Carboloy 999 material, as indicated by the amount of carbon transfer to the Cb-1Zr alloy capsules might be explained by the presence of the more stable carbides TaC, $(W,Ta)_2C$, and $(Mo,Cb)_2C$, respectively, in these materials.

The Zircoa 1027 specimens exhibited an inversion of the cubic ZrO_2 to monoclinic ZrO_2 during testing at 1600°F in both potassium liquid and vapor. These results are in agreement with the large dimensional changes observed in these specimens.[8] From the dimensional stability tests on Zircoa 1027 in vacuum,[8] which revealed dimensional changes considerably smaller than those observed in the corrosion testing in potassium at 1600°F, and the metallographic and visual examinations of the Zircoa 1027 corrosion specimens tested at 1600°F, it appears that the potassium is reacting with the stabilizers in the Zircoa 1027 resulting in the conversion of the cubic ZrO_2 to the more stable monoclinic ZrO_2 at lower temperatures.

Candidate Bearing Material Combinations

The nine Cb-1Zr alloy capsules containing the candidate bearing materials combinations and which were exposed to potassium for 1000 hours at 800°, 1200°, and 1600°F have been opened under argon, the potassium was drained, and the specimens were cleaned by vacuum distillation in the manner described in Quarterly Progress Report No. 7.[8] Three capsules containing specimens of the following material combination both in the liquid and vapor regions were tested at each of the three test temperatures:

Mo-TZM	vs	Carboloy 907
Mo-TZM	vs	TiC+10%Cb
Mo-TZM	vs	Grade 7178

The weight and dimensional measurements of the specimen paris tested at 800°, 1200°, and 1600°F were obtained and the data are reported in Tables V, VI, and VII respectively, along with the pre-test data and observed changes. A summary of the data is given in Table VIII. The data were evaluated in the same manner as that described in Quarterly Progress Report No. 7.[8]

The weight losses observed in the Carboloy 907 specimens (MCN 1036-A13 and MCN 1036-A14) tested at 1600°F in combination with Mo-TZM alloy are believed to be the result of carbon transfer to the Cb-1Zr alloy containment capsule and possibly to the Mo-TZM alloy specimens. The Gibbs free energy change for the later reaction is:

$$0.449\ WC_{(s)} + Mo_{(s)} = \alpha - MoC_{0.449(s)} + 0.449W_{(s)}$$

and at 1143°K:

$$\Delta G_{1143^\circ K} = 2430 \text{ cal (9)}$$

TABLE V. DIMENSIONAL AND WEIGHT CHANGES OF CANDIDATE BEARING MATERIAL COMBINATIONS EXPOSED IN POTASSIUM FOR 1000 HOURS AT 800°F

Material	MCN No.	Specimen Location	Specimen Length, Inches Before Test	Specimen Length, Inches After Test	Dimensional Change Inches x 10^{-3}	Dimensional Change Percent	Specimen Width$_1$, Inches Before Test	Specimen Width$_1$, Inches After Test	Dimensional Change Inches x 10^{-3}	Dimensional Change Percent	Specimen Width$_2$, Inches Before Test	Specimen Width$_2$, Inches After Test	Dimensional Change Inches x 10^{-3}	Dimensional Change Percent	Specimen Weight in Grams Before Test	Specimen Weight in Grams After Test	Weight Change Milligrams	Weight Change Mg Cm^{-2}
Capsule No. BIC-56																		
Carboloy 907	1036-A9	Liquid	2.00264	2.00326	+0.62	+0.031	0.25099	0.25167	+0.68	+0.272	0.25194	0.25219	+0.25	+0.100	30.4390	30.4423	+3.3	+0.240
Mo-TZM(1)	1037-A21	Liquid	1.99909	1.99911	+0.02	+0.001	0.25190	0.25232	+0.42	+0.167	0.25225	0.25280	+0.55	+0.218	21.1107	21.1125	+1.8	+0.131
Carboloy 907	1036-A10	Vapor	2.00275	2.00293	+0.18	+0.009	0.25158	0.25178	+0.20	+0.079	0.25151	0.25161	+0.10	+0.040	30.5477	30.5489	+1.2	+0.087
Mo-TZM(1)	1037-A22	Vapor	1.99924	1.99918	-0.06	-0.003	0.25185	0.25187	+0.02	+0.008	0.25233	0.25231	-0.02	-0.008	21.1088	21.1095	+0.7	+0.051
Capsule No. BIC-59																		
TiC-10%Cb	1045-A7	Liquid	1.97591	1.97619	+0.28	+0.014	0.25260	0.25291	+0.31	+0.123	0.25242	0.25242	0.00	0.000	10.8126	10.8283	+15.7	+1.145
Mo-TZM(1)	1037-A13	Liquid	1.99967	1.99975	+0.08	+0.004	0.24930	0.24948	+0.18	+0.072	0.24797	0.24826	+0.29	+0.117	20.5351	20.5364	+1.3	+0.094
TiC+10%Cb	1045-A8	Vapor	2.00097	2.00112	+0.15	+0.008	0.25239	0.25239	0.00	0.000	0.25261	0.25260	-0.01	-0.004	10.9361	10.9463	+10.2	+0.744
Mo-TZM(1)	1037-A14	Vapor	2.00038	2.00047	+0.09	+0.004	0.24730	0.24730	0.00	0.000	0.24758	0.24755	-0.03	-0.012	20.3552	20.3556	+0.4	+0.029
Capsule No. BIC-55																		
Grade 7178	1046-A11	Liquid	2.00274	2.00270	-0.04	-0.002	0.25151	0.25162	+0.11	+0.044	0.25117	0.25123	+0.06	+0.024	29.6641	29.6640	-0.1	-0.007
Mo-TZM(1)	1037-A11	Liquid	2.00035	2.00040	+0.05	+0.002	0.24906	0.24939	+0.33	+0.132	0.24745	0.24832	+0.87	+0.352	20.4814	20.4857	+4.3	+0.313
Grade 7178	1046-A12	Vapor	2.00289	2.00284	-0.05	-0.002	0.25132	0.25151	+0.19	+0.076	0.25128	0.25157	+0.29	+0.116	29.7338	29.7325	-1.3	-0.094
Mo-TZM(1)	1037-A12	Vapor	2.00081	2.00040	-0.41	-0.021	0.24815	0.24847	+0.32	+0.129	0.24938	0.24992	+0.54	+0.217	20.5855	20.5911	+5.6	+0.408

(1) Stress Relieved 1/2 Hour at 2250°F

TABLE VI. DIMENSIONAL AND WEIGHT CHANGES OF CANDIDATE BEARING MATERIAL COMBINATIONS EXPOSED IN POTASSIUM FOR 1000 HOURS AT 1200°F

Material	MCN No.	Specimen Location	Specimen Length, Inches Before Test	Specimen Length, Inches After Test	Dimensional Change Inches x 10^{-3}	Dimensional Change Percent	Specimen $Width_1$, Inches Before Test	Specimen $Width_1$, Inches After Test	Dimensional Change Inches x 10^{-3}	Dimensional Change Percent	Specimen $Width_2$, Inches Before Test	Specimen $Width_2$, Inches After Test	Dimensional Change Inches x 10^{-3}	Dimensional Change Percent	Specimen Weight in Grams Before Test	Specimen Weight in Grams After Test	Weight Change Milligrams	Weight Change Mg/Cm^2
Capsule No. BIC-57																		
Carboloy 907	1036-A11	Liquid	2.00265	2.00337	+0.72	+0.036	0.25181	0.25190	+0.09	+0.036	0.25215	0.25225	+0.10	+0.039	30.5680	30.5668	-1.2	-0.087
Mo-TZM(1)	1037-A23	Liquid	1.99920	1.99931	+0.11	+0.006	0.25219	0.25246	+0.27	+0.107	0.25200	0.25245	+0.45	+0.179	21.1091	21.1140	+4.9	+0.357
Carboloy 907	1036-A12	Vapor	2.00265	2.00327	+0.62	+0.031	0.25080	0.25091	+0.11	+0.044	0.25087	0.25108	+0.21	+0.084	30.3309	30.3318	+0.9	+0.065
Mo-TZM(1)	1037-A24	Vapor	1.99895	1.99941	+0.46	+0.023	0.25221	0.25230	+0.09	+0.036	0.25187	0.25192	+0.05	+0.020	21.1068	21.1083	+1.5	+0.109
Capsule No. BIC-60																		
TiC+10%Cb	1045-A9	Liquid	1.97576	1.97593	+0.17	+0.009	0.25269	0.25274	+0.05	+0.020	0.25231	0.25260	+0.29	+0.115	10.8179	10.8336	+15.7	+1.145
Mo-TZM(1)	1037-A17	Liquid	1.99913	1.99989	+0.76	+0.038	0.25267	0.25265	-0.02	-0.008	0.25193	0.25222	+0.29	+0.115	21.1186	21.1204	+1.8	+0.131
TiC+10%Cb	1045-A10	Vapor	1.97599	1.97615	+0.16	+0.008	0.25235	0.25237	+0.02	+0.008	0.25256	0.25263	+0.07	+0.028	10.8507	10.8613	+10.6	+0.773
Mo-TZM(1)	1037-A18	Vapor	1.99893	1.99944	+0.51	+0.026	0.25190	0.25202	+0.12	+0.048	0.25226	0.25242	+0.16	+0.064	21.1058	21.1071	+1.3	+0.095
Capsule No. BIC-54																		
Grade 7178	1046-A9	Liquid	2.00300	2.00298	-0.02	-0.001	0.25131	0.25128	-0.03	-0.012	0.25154	0.25153	-0.01	-0.004	29.6927	29.6930	+0.3	+0.021
Mo-TZM(1)	1037-A9	Liquid	2.00088	2.00084	-0.04	-0.002	0.24832	0.24817	-0.03	-0.012	0.24940	0.24939	-0.01	-0.004	20.5763	20.5771	+0.8	+0.058
Grade 7178	1046-A10	Vapor	2.00213	2.00219	+0.06	+0.003	0.25151	0.25150	-0.01	-0.004	0.25128	0.25126	-0.02	-0.008	29.6311	29.6317	+0.6	+0.043
Mo-TZM(1)	1037-A10	Vapor	2.00069	2.00052	-0.17	-0.008	0.24747	0.24745	-0.02	-0.008	0.24832	0.24829	-0.03	-0.012	20.4377	20.4381	+0.4	+0.029

(1) Stress Relieved 1/2 Hour at 2250°F.

TABLE VII. DIMENSIONAL AND WEIGHT CHANGES OF CANDIDATE BEARING MATERIAL COMBINATIONS EXPOSED IN POTASSIUM FOR 1000 HOURS AT 1600°F

Material	MCN No.	Specimen Location	Specimen Length, Inches Before Test	Specimen Length, Inches After Test	Dimensional Change Inches x 10^{-3}	Dimensional Change Percent	Specimen $Width_1$, Inches Before Test	Specimen $Width_1$, Inches After Test	Dimensional Change Inches x 10^{-3}	Dimensional Change Percent	Specimen $Width_2$, Inches Before Test	Specimen $Width_2$, Inches After Test	Dimensional Change Inches x 10^{-3}	Dimensional Change Percent	Specimen Weight in Grams Before Test	Specimen Weight in Grams After Test	Weight Change Milligrams	Weight Change Mg/Cm^2
Capsule No. BIC-58																		
Carboloy 907	1036-A13	Liquid	2.00280	2.00278	-0.02	-0.001	0.25090	0.25101	+0.11	+0.044	0.25161	0.25178	+0.17	+0.068	30.3926	30.3823	-10.3	-0.751
Mo-TZM (1)	1037-A25	Liquid	1.99909	1.99867	-0.42	-0.021	0.25230	0.25246	+0.16	+0.064	0.25201	0.25228	+0.27	+0.107	21.1127	21.1160	+ 3.3	+0.240
Carboloy 907	1036-A14	Vapor	2.00274	2.00276	+0.02	+0.001	0.25172	0.25176	+0.04	+0.016	0.25181	0.25183	+0.02	+0.008	30.5359	30.5339	- 2.0	-0.145
Mo-TZM (1)	1037-A26	Vapor	1.99966	1.99902	-0.64	-0.032	0.25194	0.25197	+0.03	+0.012	0.25220	0.25224	+0.04	+0.016	21.1167	21.1174	+ 0.7	+0.051
Capsule No. BIC-61																		
TiC+10%Cb	1045-A11	Liquid	1.97595	1.97595	0.00	0.000	0.25265	0.25265	0.00	0.000	0.25233	0.25231	-0.02	-0.008	10.8513	10.8597	+ 8.4	+0.612
Mo-TZM (1)	1037-A19	Liquid	1.99870	1.99852	-0.18	-0.009	0.25223	0.25239	+0.16	+0.064	0.25197	0.25221	+0.24	+0.096	21.1047	21.1058	+ 1.1	+0.080
TiC+10%Cb	1045-A12	Vapor	1.97598	1.97597	-0.01	-0.001	0.25233	0.25232	-0.01	-0.004	0.25265	0.25264	-0.01	-0.004	10.8496	10.8572	+ 7.6	+0.554
Mo-TZM (1)	1037-A20	Vapor	1.99873	1.99862	-0.11	-0.006	0.25228	0.25234	+0.06	+0.024	0.25200	0.25203	+0.03	+0.012	21.1233	21.1239	+ 0.6	+0.043
Capsule No. BIC-53																		
Grade 7178	1046-A7	Liquid	2.00298	2.00314	+0.16	+0.008	0.25150	0.25170	+0.20	+0.079	0.24993	0.25008	+0.15	+0.060	29.5962	29.5946	- 1.6	-0.116
Mo-TZM (1)	1037-A7	Liquid	2.00114	2.00098	-0.16	-0.008	0.24813	0.24845	+0.32	+0.129	0.24941	0.24968	+0.27	+0.107	20.5815	20.5850	+ 3.5	+0.255
Grade 7178	1046-A8	Vapor	2.00271	2.00262	-0.09	-0.004	0.25155	0.25147	-0.08	-0.032	0.25127	0.25120	-0.07	-0.028	29.6450	29.6448	- 0.2	-0.014
Mo-TZM (1)	1037-A8	Vapor	2.00018	2.00012	-0.06	-0.003	0.24820	0.24815	-0.05	-0.020	0.24926	0.24926	0.00	0.000	20.5550	20.5555	+ 0.5	+0.036

(1) Stress Relieved 1/2 Hour at 2250°F.

TABLE VIII. SUMMARY OF DIMENSIONAL AND WEIGHT CHANGES OF CANDIDATE BEARING MATERIAL COMBINATIONS EXPOSED IN POTASSIUM FOR 1000 HOURS

Pair No.	Material	Specimen Location	Dimensional Changes[1], Inches x 10^3									Weight Change[2], mg/cm^2		
			Specimens Exposed at 1600°F[3]			Specimens Exposed at 1200°F[4]			Specimens Exposed at 800°F[5]			Specimens Exposed at 1600°F[3]	Specimens Exposed at 1200°F[4]	Specimens Exposed at 800°F[5]
			Length	$Width_1$	$Width_2$	Length	$Width_1$	$Width_2$	Length	$Width_1$	$Width_2$			
4	Carboloy 907	Liquid	-0.02	+0.11	+0.17	+0.72	+0.09	+0.10	+0.62	+0.68	+0.25	-0.751	-0.087	+0.240
	Mo-TZM[6]	Liquid	-0.42	+0.16	+0.27	+0.11	+0.27	+0.45	+0.02	+0.42	+0.55	+0.210	+0.357	+0.131
	Carboloy 907	Vapor	+0.02	+0.04	+0.02	+0.62	+0.11	+0.21	+0.18	+0.20	+0.10	-0.145	+0.065	+0.087
	Mo-TZM[6]	Vapor	-0.64	+0.03	+0.04	+0.46	+0.09	+0.05	-0.06	+0.02	-0.02	+0.051	+0.109	+0.051
6	TiC-10%Cb	Liquid	0.00	0.00	-0.02	+0.17	+0.05	+0.29	+0.28	+0.31	0.00	+0.612	+1.145	+1.145
	Mo-TZM[6]	Liquid	-0.18	+0.16	+0.24	+0.76	-0.02	+0.29	+0.08	+0.18	+0.29	+0.080	+0.131	+0.094
	TiC-10%Cb	Vapor	-0.01	-0.01	-0.01	+0.16	+0.02	+0.07	+0.15	0.00	-0.01	+0.554	+0.773	+0.744
	Mo-TZM[6]	Vapor	-0.11	+0.06	+0.03	+0.51	+0.12	+0.16	+0.09	0.00	-0.03	+0.043	+0.095	+0.029
1	Grade 7178	Liquid	+0.16	+0.20	+0.15	-0.02	-0.03	-0.01	-0.04	+0.11	+0.06	-0.116	+0.021	-0.007
	Mo-TZM[6]	Liquid	-0.16	+0.32	+0.27	-0.04	-0.03	-0.01	+0.05	+0.33	+0.87	+0.255	+0.058	+0.313
	Grade 7178	Vapor	-0.09	-0.08	-0.07	+0.06	-0.01	-0.02	-0.05	+0.19	+0.29	-0.014	+0.043	-0.094
	Mo-TZM[6]	Vapor	-0.06	-0.05	0.00	-0.17	-0.02	-0.03	-0.41	+0.32	+0.54	+0.036	+0.029	+0.408

(1) Specimen dimensions: 2.00 inches x 0.25 inch x 0.25 inch.

(2) Calculated by dividing actual weight loss by specimen surface area (13.738 cm^2).

(3) Complete data found on page 37 of this report.

(4) Complete data found on page 38 of this report.

(5) Complete data found on page 39 of this report.

(6) Stress-relieved 1/2 hour at 2250°F.

Therefore, the decomposition of WC in Carboloy 907 to form $MoC_{0.449}$ at the Mo-TZM alloy surface would not be unexpected. A significant weight gain observed for the Mo-TZM specimen (MCN 1037-A25) tested along with the Carboloy 907 specimen in the liquid zone would appear to substantiate the possibility of carbon transfer from the Carboloy 907 to Mo-TZM alloy, The significance of the observed decrease in length of the two Mo-TZM alloy specimens (MCN 1037-A25 and MCN 1037-A26) tested at 1600°F in combination with Carboloy 907 is not evident at this time and little importance is attached to the changes.

The weight loss observed in the Carboloy 907 specimen (MCN 1036-A11) tested at 1200°F in combination with Mo-TZM alloy in liquid potassium is considerably less than that observed in the 1600°F test; no weight loss was observed in the Carboloy 907 specimen (MCN 1036-A12) tested at 1200°F in combination with Mo-TZM alloy in potassium vapor. Both Mo-TZM alloy specimens (MCN 1037-A23 and MCN 1037-A24) which were tested at 1200°F in combination with Carboloy 907 exhibited weight gains similar to the Mo-TZM alloy specimens tested at 1600°F in combination with Carboloy 907 with the weight increase of the specimen in the liquid zone being greater. Although these increases may be the result of carbon transfer, the increase in weight in the Mo-TZM alloy cannot be completely accounted for from the weight changes observed in the Carboloy 907 specimens. Significant dimensional increases were observed in the $width_2$ (surfaces perpendicular to surface facing Carboloy 907 specimen) of the Mo-TZM alloy specimen (MCN 1036-A23) from the liquid zone, the length of the Mo-TZM alloy specimen (MCN 1037-A24) in the vapor zone, and the lengths of both Carboloy 907 specimens.

The Carboloy 907 specimens (MCN 1036-A9 and MCN 1036-A10) tested at 800°F in combination with Mo-TZM alloy show weight gains in contrast to weight losses observed in the 1600° and 1200°F tests. The Carboloy 907 specimen (MCN 1036-A9) tested in liquid potassium showed a significant increase in length and $width_1$ (surfaces facing Mo-TZM alloy specimen). The Mo-TZM alloy specimen (MCN 1037-A21) tested at 800°F in combination with Carboloy 907 in liquid potassium exhibited a slight increase in weight and in width.

Weight gains were observed in all of the TiC+10%Cb specimens tested at 800°, 1200°, and 1600°F in combination with Mo-TZM alloy with the largest weight gains occurring in the 800° and 1200°F tests. The TiC+10%Cb specimens (MCN 1045-A9 and MCN 1045-A7) tested in the liquid zone exhibited weight changes of identical magnitude in both the 800° and 1200°F tests. Although of smaller magnitude than observed for the specimens tested in potassium liquid, the weight gain of the TiC+10%Cb specimens tested in potassium vapor at 800° and 1200°F also were essentially the same. Slight weight gains also were observed in all of the Mo-TZM alloy specimens (MCN 1037-A13, MCN 1037-A17, and MCN 1037-A19) tested in liquid potassium with TiC+10%Cb specimens at 800°, 1200°, and 1600°F. An explanation for the weight changes observed in the TiC+10%Cb/Mo-TZM alloy tests is lacking and it is hoped that further evaluation will clarify these changes. Significant positive dimensional changes in random directions were observed only in the TiC+10%Cb and Mo-TZM alloy specimens tested at 800° and 1200°F.

The slight weight loss observed in the Grade 7178 specimen (MCN 1046-A7) tested at 1600°F in combination with Mo-TZM alloy in liquid potassium is attributed to carbon transfer and/or edge chipping. The weight gain observed in the Mo-TZM alloy specimen (MCN 1037-A7) adjacent to the Grade 7178 specimen (MCN 1046-A7) can be attributed only partially to carbon transfer since the magnitude of the change is too large in comparison to the loss observed in the Grade 7178 specimen. The significant dimensional increase observed in the Mo-TZM alloy specimen (MCN 1037-A7) in the direction perpendicular to the adjacent faces of the specimens during testing indicates a possible layer formation as the result of the suspected carbon transfer.

No significant weight or dimensional changes were observed in any of the Grade 7178 or Mo-TZM alloy specimens tested at 1200°F. The slight weight loss observed in the Grade 7178 specimen (MCN 1046-A11) tested at 800°F in potassium vapor probably is the result of edge chipping. A significant increase in $width_2$ (surface perpendicular to surface facing Mo-TZM alloy specimen) was observed in the Grade 7178 specimen (MCN 1046-A12) tested at 800°F in potassium vapor. Significant weight gains and dimensional changes were observed in both the Mo-TZM alloy specimens (MCN 1037-A11 and MCN 1037-A12) tested in combination with Grade 7178 at 800°F.

Generally, significantly larger or erratic changes in weight and dimensions were observed for Mo-TZM alloy specimens in combination with other candiate materials and for Carboloy 907 and TiC+10%Cb in combination with Mo-TZM alloy than were observed for similar specimens exposed individually to potassium. Metallographic and x-ray diffraction studies in progress may provide an explanation for these anomalies.

A visual examination of the test specimen combinations exposed to potassium liquid and vapor for 1000 hours at 800°, 1200°, and 1600°F was made and the results are summarized in Tables IX, X, and XI, respectively. Subsequently, bearing material test specimens were sectioned for metallographic examination and chemical analyses or x-ray diffraction analyses in the same manner described in Quarterly Report No. 8.[7] The metallographic preparation of these specimens, and chemical analyses or x-ray diffraction analyses have been completed and their evaluation is in progress.

The Cb-1Zr alloy containment capsules used for the 1600°F, 1000-hour isothermal corrosion tests of the candidate bearing material combinations have been sectioned and samples obtained from the inner 0.020-inch thick layer in the liquid zone for chemical analyses of oxygen, hydrogen, nitrogen and carbon in the same manner reported in Quarterly Progress Report No. 8.[7] The data are presented in Table XII. A significant increase in carbon content was observed only in the capsule containing the Carboloy 907 versus Mo-TZM alloy specimens. Carbon transfer also was observed in earlier tests of individual candidate materials and was discussed in Quarterly Progress Report No. 8[7] and on page 23 of this report.

Results of metallographic examination of samples obtained from the liquid zone of the Cb-1Zr alloy capsules is in agreement with the chamical analyses. A layer of CbC was identified by stain etching techniques on the ID of the capsule con-

TABLE IX. VISUAL EXAMINATION OF CORROSION TEST SPECIMENS OF CANDIDATE BEARING MATERIAL COMBINATIONS AFTER A 1000-HOUR EXPOSURE TO POTASSIUM AT 800°F

Capsule No.	Material	MCN No.	Specimen Location	Description
BIC-55	Mo-TZM	1037-A11	Liquid	The specimen was a dark charcoal color with crystalline patterns on the surface. Discolorations were observed where the Cb-1Zr alloy cage made contact with the specimen.
		1037-A12	Vapor	The appearance of the specimen was a dark charcoal color with crystalline patterns on the surface. Discolorations were evident where the wires of the Cb-1Zr alloy cage were in contact with the specimen.
	Grade 7178	1046-A11	Liquid	The specimen was light grey in appearance with light discolorations where the Cb-1Zr alloy cage touched the specimen.
		1046-A12	Vapor	The specimen was light grey in color with light discolorations where the Cb-1Zr alloy cage was in contact with the specimen.
BIC-56	Mo-TZM	1037-A21	Liquid	The appearance of the specimen was medium grey with dark spots in some areas. Discolorations were observed where the wires of the Cb-1Zr alloy cage touched the specimen.
		1037-A22	Vapor	The appearance of the specimen was light grey with a darker crystalline pattern on the surface. Discolorations were observed where the wires of the Cb-1Zr alloy cage touched the specimen.
	Carboloy 907	1036-A9	Liquid	The appearance of the specimen was light grey with brown stain areas on the surface. Discolorations were observed where the wires of the Cb-1Zr alloy cage touched the specimen.
		1036-A10	Vapor	The appearance of the specimen was light grey with brown stain areas on the surface. No apparent reaction was observed between the Cb-1Zr alloy cage and the specimen.

TABLE IX (Cont'd)

Capsule No.	Material	MCN No.	Specimen Location	Description
BIC-59	Mo-TZM	1037-A13	Liquid	The specimen has a shiny appearance with discolorations where the wires from the Cb-1Zr alloy cage touched the specimen.
		1037-A14	Vapor	The specimen has a shiny surface appearance with discolorations where the wires from the Cb-1Zr alloy cage touched the specimen.
	TiC+10%Cb	1045-A7	Liquid	The specimen was light grey in color with no apparent marks from the Cb-1Zr alloy cage.
		1045-A8	Vapor	The specimen has a light grey appearance with no discolorations from the Cb-1Zr alloy cage.

TABLE X. VISUAL EXAMINATION OF CORROSION TEST SPECIMENS OF CANDIDATE BEARING MATERIAL COMBINATIONS AFTER A 1000-HOUR EXPOSURE TO POTASSIUM AT 1200°F

Capsule No.	Material	MCN No.	Specimen Location	Description
BIC-54	Mo-TZM	1037-A9	Liquid	The specimen was light grey in appearance with some stains on the surface. No evidence or eaction between the specimen and Cb-1Zr alloy cage is visible.
		1037-A10	Vapor	The appearance of the specimen is light grey in color with rust colored stains on the surface. No discolorations from the Cb-1Zr alloy cage touching the specimen.
	Grade 7178	1046-A9	Liquid	The specimen was light grey in color with discolorations where the wires from the Cb-1Zr alloy cage touched the specimen.
		1046-A10	Vapor	The specimen appearance was light grey with discolorations where the wires of the Cb-1Zr alloy cage touched the specimen.
BIC-57	Mo-TZM	1037-A23	Liquid	The specimen was dark grey in color with a crystalline pattern on the surface. Discolorations are evident where the wires of the Cb-1Zr alloy cage touched the specimen.
		1037-A24	Vapor	The appearance of the specimen is blue grey in color with a scattered crystalline pattern. Discolorations were observed where the wires of the Cb-1Zr alloy cage were in contact with the specimen.
	Carboloy 907	1036-A11	Liquid	The specimen was rust colored in appearance with no visible discolorations where the Cb-1Zr alloy cage touched the specimen.
		1036-A12	Vapor	The appearance of the specimen was rust colored with dark brown spots on the surface. Very light discolorations were observed where the Cb-1Zr alloy cage touched the specimen.

TABLE X (Cont'd)

Capsule No.	Material	MCN No.	Specimen Location	Description
BIC-60	Mo-TZM	1037-A17	Liquid	The specimen was dark grey in color with a scattered crystalline pattern and discolorations where the Cb-1Zr alloy cage was in contact with the specimen.
		1037-A18	Vapor	The appearance of the specimen was light grey with discolorations observed where the wires of the Cb-1Zr alloy cage were in contact with the specimen.
	TiC+10%Cb	1045-A9	Liquid	The specimen was light grey in appearance with discolorations observed where the wires of the Cb-1Zr alloy cage were in contact with the specimen.
		1045-A10	Vapor	The appearance of the specimen was medium grey with discolorations where the Cb-1Zr alloy cage touched the specimen.

TABLE XI. VISUAL EXAMINATION OF CORROSION TEST SPECIMENS OF CANDIDATE BEARING MATERIAL COMBINATIONS AFTER A 1000-HOUR EXPOSURE TO POTASSIUM AT 1600°F

Capsule No.	Material	MCN No.	Specimen Location	Description
BIC-53	Mo-TZM	1037-A7	Liquid	The appearance of the specimen is light grey with bright spots. Discoloration was observed where the wires from the Cb-1Zr alloy cage touched the specimen. A few pit marks were observed at either ends of the specimen.
		1037-A8	Vapor	The appearance of the specimen is light grey with discolorations where the wires from the Cb-1Zr alloy cage touched the specimen.
	Grade 7178	1046-A7	Liquid	The appearance of the specimen is light grey in color with discolorations where the wires from the Cb-1Zr alloy cage touched the specimen.
		1046-A8	Vapor	The appearance of the specimen is light grey with discolorations where the wires from the Cb-1Zr alloy cage was in contact with the specimen. The surface of the specimen gives the appearance of having a longitudinal structure.
BIC-58	Mo-TZM	1037-A25	Liquid	The specimen has a blue color overall with scattered crystalline patterns and rust colored areas. No marks were observed from the Cb-1Zr alloy cage touching the specimen.
		1037-A26	Vapor	The specimen has a shiny appearance with a blue streak running down the center. Light discolorations were observed where the Cb-1Zr alloy cage had touched the specimen
	Grade 907	1036-A13	Liquid	The appearance of the specimen was shiny with some black smears in a few scattered areas. Light discolorations were observed where the wires of the Cb-1Zr alloy cage touched the specimen.
		1036-A14	Vapor	The surface of the specimen has a dull metallic luster with shiney marks where the Cb-1Zr alloy cage touched the specimen.

TABLE XI. (Cont'd)

Capsule No.	Material	MCN No.	Specimen Location	Description
BIC-61	Mo-TZM	1037-A19	Liquid	The surface of the specimen has a variety of colors including blue, red, green and brown. A crystalline pattern resembling a palm leaf covers the surface.
		1037-20	Vapor	The specimen has a dull metallic appearance with the marks, left by the Cb-1Zr alloy cage, having the brightest appearance. The crystalline pattern that has been evident on all previous specimens is dark instead of light grey color as observed previously.
	TiC+10%Cb	1045-A11	Liquid	The specimen has a light grey surface color with no evidence of marks from the Cb-1Zr alloy cage.
		1045-A12	Vapor	The specimen is blue-grey in color with no observed marks from the Cb-1Zr alloy cage.

TABLE XII. CHEMICAL ANALYSES OF Cb-1Zr ALLOY CAPSULES CONTAINING CANDIDATE BEARING MATERIAL COMBINATION TEST SPECIMENS AND EXPOSED TO POTASSIUM FOR 1000 HOURS AT 1600°F

Capsule No.	Material Combinations	Chemical Analyses[1], ppm			
		C	O	N	H
BIC-58	Carboloy 907 vs Mo-TZM	260/260	309/361	100/106	2/6
BIC-61	TiC+10%Cb vs Mo-TZM	80/70	218/221	96/96	<1/1
BIC-53	Grade 7178 vs Mo-TZM	60/60	276/287	104/110	<1/4
Control (1005-7)	----	50/30	275/300	77/77	1/<1
Control (1005-4)	----	50/70	370/394	90/89	6/1
As-Received (Bulk[2])	----	40	184	95	1

[1]Analyses of Inner 0.020-Inch Thick Layer of Cb-1Zr Alloy Capsule in the Liquid Zone. Gas Analyses by Vacuum Fusion Techniques; Carbon Analyses by Combustion Conductometric.

[2]0.080-Inch Thick Wall.

taining the Carboloy 907 versus Mo-TZM alloy specimens, Figure 18. No other significant changes were observed in any of the containment capsules.

B. Potassium Wetting

A sample of potassium was transferred from the titanium-lined, zirconium-gettered hot trap into an 18-inch length of 0.5-inch OD x 0.020-inch thick wall stainless steel tubing for use in the wetting measurements. Purification of the potassium was described in Quarterly Progress Report No. 7.[8] Half of the 18-inch long sample was utilized for chemical analyses for oxygen by the amalgamation technique (helium cover gas) and for metallic impurities by emission spectrographic methods. Duplicate oxygen analyses showed oxygen content to be 6.1 and 7.3 ppm. Metallic impurities were generally below the detection limits as shown in the following tabulation:

METALLIC IMPURITIES (PPM) IN POTASSIUM USED FOR WETTING MEASUREMENTS

Lab No.	Ag	Al	Ca	Cb	Co	Cr	Cu	Fe	Mg	Mn	Mo	Na	Ni	Pb	Si	Sn	Ti	Zr
201	<1	<1	1	<1	<1	<1	<1	1	<1	<1	<1	1	<1	<1	1	<5	<1	<5

A 4-inch section of the remaining stainless steel sample tube, containing approximately 10 grams of potassium, was inserted into the potassium reservoir of the wetting apparatus under high purity argon. The transfer was made in a glove box that had been evacuated to a pressure of 10^{-6} torr prior to backfilling with high purity argon. The potassium reservoir was sealed under the argon cover by means of an ultra-high vacuum valve and subsequently was removed from the glove box and attached to the wetting apparatus and the system evacuated and baked out. During bakeout, the lower portion of the reservoir containing the potassium was cooled externally with tap water; after bakeout, with the system at room temperature, the pressure was 5×10^{-9} torr as indicated by the discharge gauge.

Formation of Potassium Drop

The potassium flow rate from the reservoir to the condenser as a function of temperature was calculated in order to estimate the time and temperature required to distill sufficient potassium to the condenser to form a drop. Factors involved in this calculation are the conductances of the various components in the flow path, i.e., the reservoir itself, the ultra-high vacuum valve and the potassium inlet tube. A description of these various parts of the system has been given in previous Quarterly Report No. 8.[7] Also required for the calculation is the equilibrium potassium vapor pressure as a function of temperature.[10] Calculations for both molecular flow and transition region flow were made utilizing methods described by Dushman.[11] The results of these calculations are shown in Figure 19 along with the equilibrium potassium vapor pressure. It is estimated that about 0.1 gram of potassium on the condenser will be required to form the drop and from the data of Figure 19, a distilling time of about one hour at 220°C is necessary to give the desired quantity of potassium.

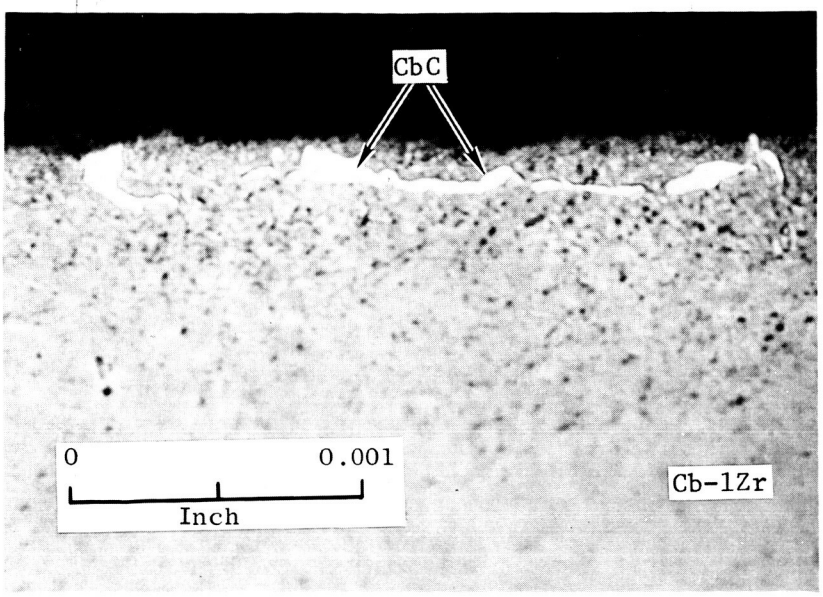

(A770111)

B1072-18

Figure 18. Transverse Section of Cb-1Zr Containment Capsule BIC-53 in Liquid Zone Showing CbC on the ID Surface After Exposure to Potassium for 1000 Hours at 1600°F. The Capsule Contained Specimens of Carboloy 907 and Mo-TZM Alloy in the Liquid and Vapor Zones.

Etchant: Stain Etched (Ref. 6) Magnification: 1500X
N.A.: 0.95

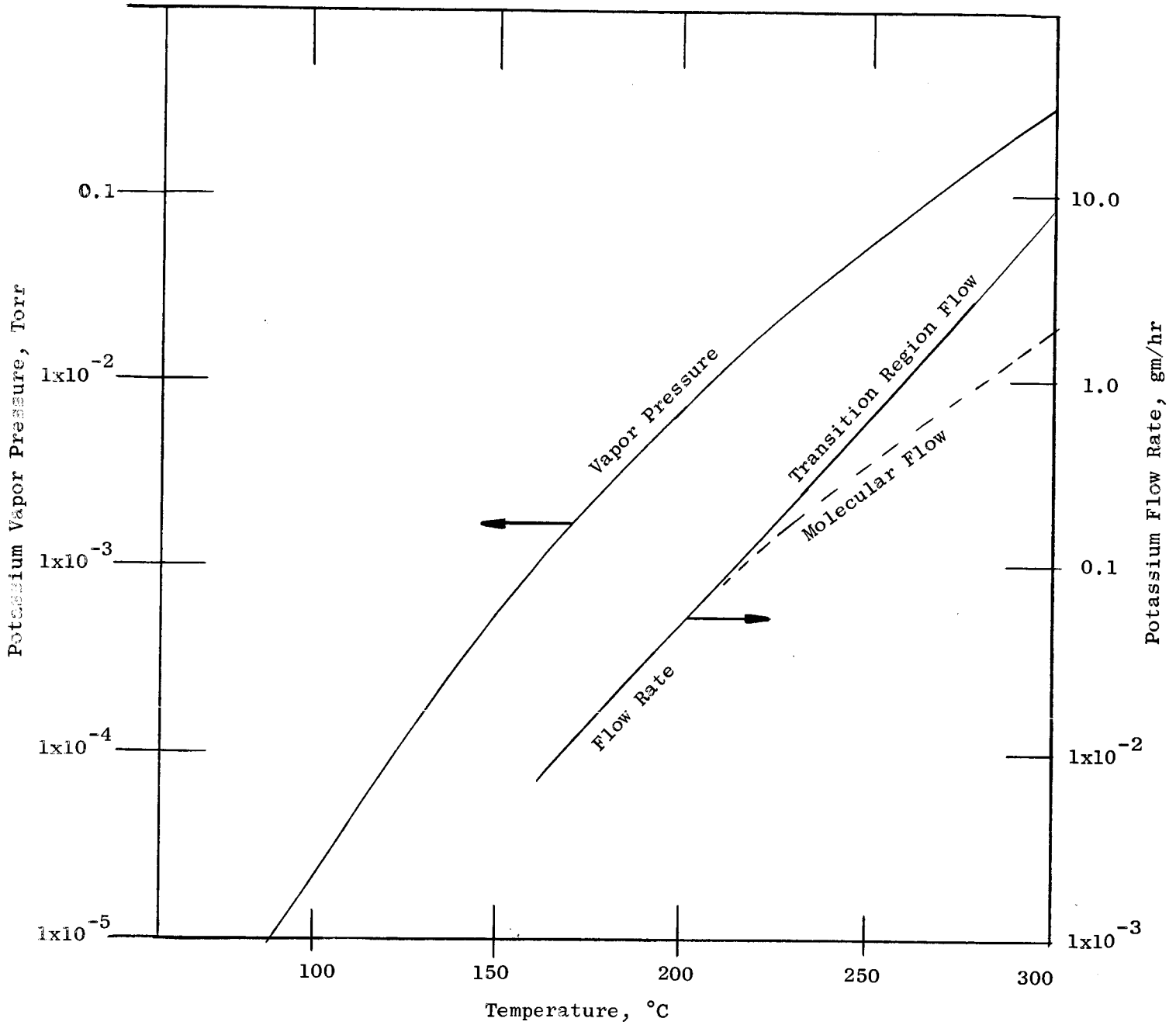

Figure 19. Vapor Pressure of Potassium (Ref. 9) and Calculated Rate of Potassium Transfer from the Reservoir to the Condenser of the Wetting Apparatus.

B1072-19

Before attempting to form the drop, the potassium in the reservoir was outgassed. This was accomplished by heating the reservoir, the valve, and the potassium inlet tube while cooling the condenser with water. The remainder of the system was at room temperature and the valve between the test chamber and the getter-ion pump was open. Little gas was evolved from the potassium except at the melting point at which time some pressure surges were noted. In attempting to heat the potassium to a higher temperature to distill potassium to the condenser, it soon became obvious that the potassium was not completely condensing on the condenser and a visible film of potassium was forming on the interior surfaces of the test chamber, including the specimen and windows. During this attempt, the potassium was heated to about 180°C.

In subsequent trials, a drop was formed successfully by the following procedure. The valve to the pumping system was closed, the upper portion of the system was enclosed by the oven and the condenser was water cooled. The oven was heated at the same time that heat was applied to the reservoir, maintaining the vapor flow path at a higher temperature than the potassium. Distillation was carried out for 1-1/4 hours with the potassium in the reservoir at temperatures between 210° and 220°C; then the entire system was allowed to cool to room temperature. Subsequently, the condenser was heated by a flow of hot air through the condenser tube. As the potassium on the condenser melted, it readily formed a drop and fell to the surface of the specimen. A photograph of the solid drop so formed is shown in Figure 20a; the magnification is about 1.5, the true drop volume is about 0.12 cc and the mass of the drop is about 0.10 gram.

The photographs shown in Figure 20 were made utilizing a Gaertner Model M101AT telemicroscope, a Reichert photomicrographic unit for a monocular microscope, and a 35 mm camera back with Kodak Plus-X film. In these initial photographs, the picture quality is rather poor due to incorrect focus.

Wetting of Mo-TZM Alloy by Potassium

The first wetting measurements were made on a Mo-TZM alloy surface utilizing the drop shown in Figure 20a. The temperature of the system was increased slowly by increasing the oven temperature. During the early portion of this run, the condenser was maintained at a temperature lower than that of the Mo-TZM alloy specimen by a flow of air through the condenser tube. A rather rough measurement of the condenser temperature was obtained from a thermocouple placed on the condenser exit tubulation.

At temperatures between the melting point of potassium and approximately 160°C, the contact angle was constant at 135 degrees. The contact angle was measured directly by utilizing the protractor eyepiece on the telemicroscope. The contact angle is defined as the angle between the liquid and solid surfaces as measured through the liquid at the liquid-solid interface. A photograph of the liquid drop at 98°C is shown in Figure 20b. At a temperature of about 160°C, evaporation of the drop became appreciable resulting in a decrease in the contact angle. It was noted that no spreading occurred and that the decrease in contact angle merely resulted from the decrease in drop volume with the interface remaining stationary. A photo-

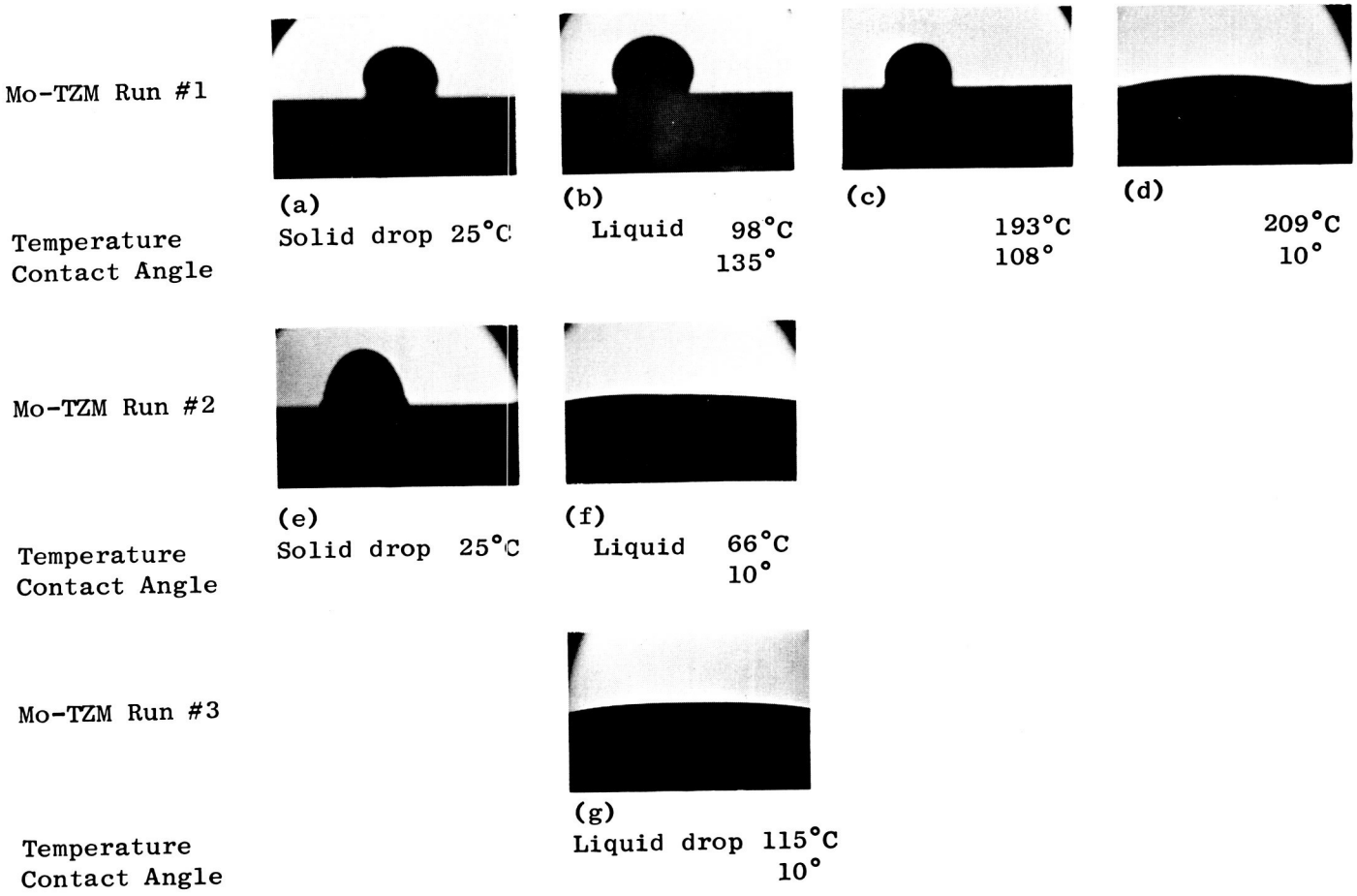

Figure 20. Wetting Characteristics of Potassium on Mo-TZM Alloy Surface.
Magnification Approximately 1.5X

graph of the drop at 193°C is shown in Figure 20c where the decrease in drop volume is quite apparent.

When drop evaporation reached an appreciably rate, the cooling air flow to the condenser was decreased in order to allow the condenser to warm up and prevent further evaporation of the drop. However, as the temperature of the condenser increased and eventually exceeded that of the specimen, residual potassium on the condenser evaporated and condensed on the specimen. At this point, the drop collapsed suddenly and spread out to reach a contact angle of about 10 degrees. A photograph of the drop at 209°C is shown in Figure 20d. In Figure 21, both the specimen temperature and the contact angle are plotted against time for this first run on the TZM alloy surface.

After the completion of Mo-TZM alloy Run #1, the potassium was distilled back to the potassium reservoir and redistilled onto the condenser in an attempt to form a second drop. The potassium wet the condenser much better than on the first run and considerably more potassium was required to form the drop. A photograph of the second drop (solidified at 25°C) is shown in Figure 20e. As may be seen by comparison with Figure 20a, a considerably larger volume of potassium was obtained in the second drop. The oven temperature was increased as in Run #1, except that the condenser was not cooled. In the Mo-TZM alloy Run #2, the potassium immediately spread to the edge of the surface as soon as it melted and again reached a contact angle of about 10 degrees. A photograph of the liquid drop at 66°C is shown in Figure 20f. However, it was noted that a film of potassium had formed on the Mo-TZM alloy surface before melting had occurred. Apparently, either during the drop formation or heating of the oven to melt the drop, sufficient potassium to form a visible film passed from the condenser to the specimen.

The potassium was distilled back to the reservoir a second time and redistilled to the condenser in order to place a drop on a dry surface. This was accomplished by heating the test chamber and cooling the condenser by air flow until the specimen reached a temperature considerably above the melting point. At this time, the condenser was permitted to be heated causing the drop to form and fall to the surface of the specimen. Wetting occurred immediately, the drop spreading to the edge of the specimen as shown in Figure 20g. The specimen temperature was 115°C at the time the drop was formed and the contact angle was about 10 degrees.

These three separate wetting tests on the Mo-TZM alloy specimen demonstrate the general type of behavior to be expected for potassium in contact with the various candidate bearing materials. The contact angle depends on the previous history of the solid surface, and in particular, on whether the surface has been preciously wet by potassium. Although details of the reactions involved are not readily apparent, it seems clear that some modification of the solid surface occurs upon the initial contact of the surface with liquid potassium. Similar behavior has been reported for sodium wetting iron, cobalt and nickel.[12] It was concluded in that study, that changes in contact angle reflect the reduction, by sodium, of the invisible oxide film present on the metal surfaces after abrasion in air. Such reaction might well explain the observations made in the present study.

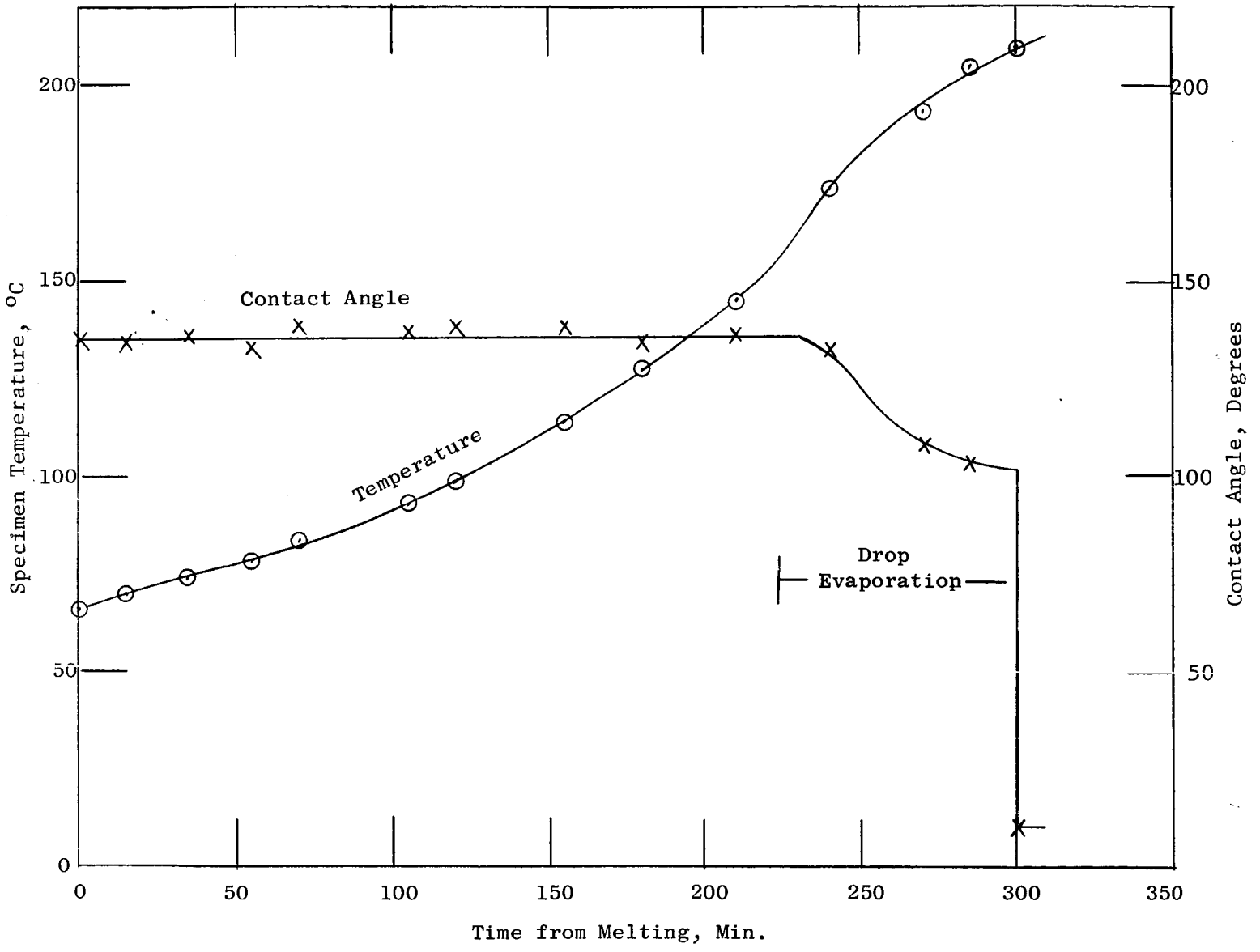

Figure 21. Mo-TZM Alloy Specimen Temperature and Contact Angle as a Function of Time after Melting of Potassium Drop - Wetting Run #1.

B1072-21

It thus appears that wetting of a surface by potassium does not involve a unique contact angle and instead three separate conditions which may yield quite different contact angles may be considered. These are: 1) advancing interface over a freshly prepared surface, 2) advancing interface on a previously wet surface, and 3) receding interface. It is frequently observed that advancing and receding contact angles differ and the effect can be quite large.[13] This phenomenon is generally known as hysteresis of contact angles. Although receding contact angles were not measured directly, it is fairly obvious that the receding angle would be less than the minimum advancing angle, that is, less than 10 degrees for Mo-TZM alloy throughout the temperature range investigated in this study. There is reason to believe that wetting would improve at higher temperatures.

The experience gained thus far shows several operational difficulties with the apparatus. The contact angle can be decreased either by evaporation of the drop to the condenser or by condensation of potassium from the condenser on the specimen. Since the system is heated by the natural convection oven, there is a temperature gradient within the oven with the upper portion of the test chamber appreciably hotter than the lower portion. Also, since the condenser is attached to the upper flange and the specimen is supported by the lower flange, the potassium on the condenser is at a considerably higher temperature than the potassium on the specimen. Therefore, the condenser must be cooled by air flow through the condenser in order to keep the condenser at the same temperature as the specimen to prevent transfer of potassium between the condenser and the specimen. The ideal situation would be to have all the potassium which communicates with the test chamber, i.e., the specimen, the condenser, and the reservoir (if the valve is open), at exactly the same temperature and, in addition, have all other surfaces communicating with the test chamber at a higher temperature.

The first step to obtain better control of the potassium will be to place a thermocouple within the condenser tube extending to a point near the condenser. This thermocouple will indicate more accurately the true condenser temperature and should permit closer determination of the temperature difference between the condenser and the specimen. With better control of the potassium transfer, it should be possible to determine receding contact angles in addition to the advancing angle over a freshly prepared surface and the advancing angle over a previously wet surface. The measurements on the Mo-TZM alloy will be repeated after some improvements have been made in the system and utilizing a freshly prepared surface.

C. Friction and Wear in High Vacuum

Upon reassembly of the modified loading arms in the high vacuum friction and wear tester, test specimens were installed and three tests of Assembly VII were completed. Prior to installation in the tester, the specimens were prepared in a manner described in Quarterly Progress Report No. 9.[5] The 2-lb. capacity load cell was used and was located 0.75 in. from the gimbal in order to magnify the force signal when the force pickup is located in the plane of the dead weights. At this location, any error in the fabrication of the threads or the removal of slack from the force pickup connector cable allows the loading arm to vibrate more during testing than would occur when the force pickup connector is in the plane of the dead weights.

The tests were conducted at room temperature, at speeds of 500 and 800 SFM and at initial pressures in the 10^{-10} to 10^{-9} torr range. The pressure in the chamber remained at less than 1×10^{-8} torr during the tests with the exception of test No. 300705B (Grade 7178 versus Grade 7178). In this test, the high load (6.11 lbs.) resulted in a relatively high wear rate (27.2 $in^3/10^{10}$ ft. for the rider; 347.0 $in^3/10^{10}$ ft for the disc) and a temperature rise in the test specimens (520°F on the rider away from the interface) which caused the pressure to rise to 5×10^{-8} torr. The average coefficient of friction was calculated to be 0.54.

The results of these tests are summarized in Table XIII along with the results of the previous 11 tests. Short testing times of < 60 minutes are the result of high friction between the specimens which leads to slippage in the magnetic drive. The static breakaway torque of the tester is regularly measured at about 50 lb.-in. The Sandborn traces showing the changes in friction coefficient with time, photographs of the test specimens illustrating wear patterns, weight change data, and surface finish measurements are presented in Appendix C. No attempt will be made to present an analysis and interpretation of the test data until a greater number of tests have been employed.

TABLE XIII. SUMMARY OF FRICTION AND WEAR TESTS CONDUCTED IN HIGH VACUUM

Assembly No.	Arm No.	Test No.	Test Material		Test Temp °F	Increase in Rider Specimen Temp, °F(1)	Speed SFM	Compressive Load				Test Duration Minutes	Chamber Pressure, Torr		Average Coefficient Friction	Wear Rate, $in^3/10^{10}$ ft.		Remarks
			Rider	Disc				lbs.	Hertzian Stress Psi	(%)0.2%CYS or UCS Rider	Disc		Start	Maximum		Rider	Disc	
I	1	500905A	Carboloy 907	Carboloy 907	RT	925	500	11.86	581,330	82	82	9.41	4.0×10^{-9}	1.7×10^{-8}(2)	0.77	-2.130	+59.4	Test terminated due to excessive wear of rider.
I	4	500K05A	Carboloy 907	Carboloy 907	RT	5	500	0.141	132,640	19	19	60.00	5.5×10^{-9}	9.4×10^{-9}(2)	0.65	+0.138	- 0.689	--
II	1	400905A	Mo-TZM	Carboloy 907	RT	35	500	0.083	94,810	87	13	60.00	7.0×10^{-9}	1.7×10^{-8}(2)	--(3)	-0.344	+ 1.56	--
II	3	500705A	Carboloy 907	Carboloy 907	RT	190	500	6.90	485,400	69	69	1.92	6.5×10^{-9}	1.2×10^{-8}(2)	0.63	-76.5	+119.0	Test terminated due to slippage in magnetic drive
II	4	404905A	Mo-TZM	Carboloy 907	675	3	500	0.081	91,020	86	13	60.00	3.3×10^{-9}	1.0×10^{-8}(2)	--(3)	+0.955	- 2.37	--
IV	1	504K05A	Carboloy 907	Carboloy 907	720	25	500	0.081	99,980	16	16	60.00	7.2×10^{-9}	9.8×10^{-9}(4)	--(3)	-0.716	- 2.03	--
IV	2	500705B	Carboloy 907	Carboloy 907	RT	835	500	6.90	485,390	69	69	60.00	3.2×10^{-10}	8.5×10^{-9}(4)	0.35	-257.0	+14.2	--
V	1	512705A	Carboloy 907	Carboloy 907	1580	85	500	2.58	106,530	40	40	15.04	5.9×10^{-9}	8.8×10^{-9}(4)	0.78	-1.09	- 0.545	Test terminated due to slippage in magnetic drive.
V	3	512K05A	Carboloy 907	Carboloy 907	1580	5	500	0.117	38,050	14	14	60.00	7.0×10^{-9}	7.6×10^{-9}(4)	0.97	+0.350	-16.0	--
VI	1	300705A	7178	7178	RT	45	500	6.12	484,800	69	69	0.87	1.0×10^{-9}	1.0×10^{-9}(4)	0.56	-26.1	--	Disc fractured on application of load.
VI	2	200K05A	7178	Mo-TZM	RT	13	500	0.080	94,890	13	87	60.00	8.0×10^{-10}	9.0×10^{-10}(4)	--(3)	- 6.37	-170.0	--
VII(5)	1	300705B	7178	7178	RT	520	500	6.11	484,730	69	69	16.00	1.2×10^{-9}	5.0×10^{-8}(4)	0.54	-27.2	-347.0	Test terminated due to slippage in magnetic drive.
VII	2	100K08A	Mo-TZM	7178	RT	52	800	0.080	94,750	87	13	60.00	6.2×10^{-10}	9.0×10^{-10}(4)	1.00	-0.537	- 0.989	--
VII	4	200K05B	7178	Mo-TZM	RT	30	500	0.082	95,500	14	87	60.00	7.0×10^{-10}	1.0×10^{-9}(4)	0.95	-1.35	-74.2	--

(1) Measured with Sheathed Chromel-Alumel Thermocouples Located in Thermowell in Contact with Side of Rider Specimen 1/4 inch Away from Interface.

(2) Main Shaft Angular Contact Bearings (MRC-7207) Lubricated with MoS_2.

(3) Coefficient of Friction Values are not Considered Valid Because of Inaccuracies in Torque Measurement.

(4) Main Shaft Angular Contact Bearings (MRC-7207) Ultrasonically Cleaned and Unlubricated.

(5) Modified Loading Arms Incorporated in Assembly No. VII (See page 7 of this Report).

V. FUTURE PLANS

The summary which follows enumerates the steps to be pursued during the succeeding quarter to implement this study.

A. Complete evaluation of candidate bearing material combinations which were exposed to potassium for 1000 hours at 800^{o}, 1200^{o}, and 1600^{o}F.

B. Complete high speed flow tests and finalize design of high speed pump for potassium friction and wear test rig.

C. Conduct potassium wetting tests on Carboloy 907, TiC+10%Cb, and Grade 7178.

D. Conduct friction and wear tests in high vacuum (10^{-9} torr) for the following material combinations: Grade 7178 vs 7178; Grade 7178 vs Mo-TZM alloy; Mo-TZM alloy vs TiC+10%Cb.

E. Conduct elevated temperature compression tests with the following materials: tungsten, Star J, Carboloy 907, Carboloy 999, and Grade 7178.

REFERENCES

[1]"Materials for Potassium Lubricated Journal Bearings," Quarterly Progress Report 1, Contract NAS 3-2534, For Period Ending July 22, 1963, NASA-CR-54073.

[2]Coffin, L. F., Jr., "Theory and Application of Sliding Contact of Metals in Sodium." Report KAPL-828, Knolls Atomic Power Laboratory, General Electric Company, October 1955.

[3]Zeman, K. P., Young, W. R., and Coffin, L. F., Jr., "Friction and Wear of Refractory Compounds," Report 59GC-23, General Electric Company, May 1959.

[4]AiResearch Manufacturing Company of Arizona, Quarterly Technical Progress Report for Period Ending September 30, 1965, SNAP 50/SPUR Contract AF33(615)-2289 BPSN: 5(6399-675A) 63409124, ADS-5152-R4, p. 7.

[5]"Materials for Potassium Lubricated Journal Bearings," Quarterly Progress Report 9, Contract NAS 3-2534, For Period Ending July 22, 1965, NASA-CR-54892.

[6]Crouse, R. S., "Identification of Carbides, Nitrides, and Oxides of Niobium Alloys by Anodic Staining," ORNL-3821, July, 1965.

[7]"Materials for Potassium Lubricated Journal Bearings," Quarterly Progress Report 8, Contract NAS 3-2534, For Period Ending April 22, 1965, NASA-CR-54646.

[8]"Materials for Potassium Lubricated Journal Bearings," Quarterly Progress Report 7, Contract NAS 3-2534, For Period Ending January 22, 1965, NASA-CR-54345.

[9]Chang, Y. A., "Ternary Phase Equilibria in Transition Metal-Boron-Carbon-Silicon Systems" Part IV Thermochemical Calculations, Vol. I. Thermodynamic Properties of Group IV, V, and VI Binary Transition Metal Carbides, AFML-TR-65-2, June, 1965.

[10]Honig, R. E., "Vapor Pressure Data for the Elements," RCA Review, December, 1962.

[11]Dusham, S., "Scientific Foundations of Vacuum Technique," John Wiley and Sons, Inc., (1955).

[12]Addison, E. C., Iberson, E., and Manning, J. A., Journal Chemical Society, p. 2699, (1962).

[13]Adamson, A. W., "Physical Chemistry of Surfaces," Interscience Publishers, Inc., New York, (1960).

PUBLISHED REPORTS

Quarterly Progress Reports	For Quarter Ending
Report No. 1 (NASA-CR-54006)	July 22, 1963
Report No. 2 (NASA-CR-54007)	October 22, 1963
Report No. 3 (NASA-CR-54073)	January 22, 1964
Report No. 4 (NASA-CR-54113)	April 22, 1964
Report No. 5 (NASA-CR-54169)	July 22, 1964
Report No. 6 (NASA-CR-54264)	October 22, 1964
Report No. 7 (NASA-CR-54345)	January 22, 1965
Report No. 8 (NASA-CR-54646)	April 22, 1965
Report No. 9 (NASA-CR-54892)	July 22, 1965

APPENDICES

APPENDIX A

REDESIGN OF LOADING ARM FOR FRICTION AND WEAR TESTERS

Appendix A

Redesign of Loading Arm for Friction and Wear Testers

Methods of accurately estimating spring rate and other critical design parameters have been employed in order to correct the original approximations. The applicable formulas are (1):

$$K_{\phi} = \frac{M}{\bar{\phi}} = \frac{K_{32} E h^3 R}{2\ell} \qquad \text{(Eq. 1)}$$

$$K_y = \frac{\Delta F_y}{\Delta Y} = \frac{6 K_{32} E h^3 R}{\ell^3} \qquad \text{(Eq. 2)}$$

$$K_{32} = f\left(\frac{b}{a}\right) \qquad \text{(Eq. 3)}$$

$$\ell = NR \qquad \text{(Eq.4)}$$

where:

a = bellows major inside diameter, in.

b = bellows minor inside diameter, in.

E = modulus of elasticity, lb./in^2.

h = bellows wall thickness, in.

K_ϕ = moment constant.

K_y = deflection constant.

K_{32} = coefficient, function of diameter ratio.

ℓ = bellows active length, in.

M = moment, in.-lb.

N = no. of convolutions.

R = length per convolution, in.

ΔF_y = change in force, lb.

ΔY = change in dimension perpendicular to bellows centerline, in.

ϕ = angle of bend of bellows centerline, rad.

The two modes of bending are simple bending of the centerline of the bellows (Eq. 1) and parallel translation of the ends of the bellows (Eq. 2). They may be combined into one statement:

$$M_e = M + X_1 (\Delta F_y)$$

$$M_e = \phi K_\phi + \bar{X}_1 \bar{K}_y \Delta\bar{Y}$$

$$M_e = \frac{\phi K_{32} E h^3 R}{2NR} + \frac{X_1 \Delta Y \, 6 \, K_{32} E h^3 R}{N^3 R^3}$$

$$M_e = K_{32} E h^3 \left(\frac{\phi}{2N} + \frac{6 X_1 \Delta Y}{N^3 R^2} \right) \quad \text{in-lb.} \qquad \text{(Eq. 5)}$$

where: X_1 = distance from gimbal to near end of bellows along bellows centerline, in.

For a bellows of nominal properties and dimensions,

$a = 0.750$ in.

$b = 1.125$ in.

$E = 28 \times 10^6$ lb/in.^{2}

$h = 0.008$ in.

$K_{32} = f\left(\frac{0.750}{1.125}\right) = f\,(0.667) = 46$ from graph.

$R = 0.112$ in./conv.

Eq. 5 becomes:

$$M_e = (46)\,(28 \times 10^6)\,(0.008^3)\left(\frac{\phi}{2N} + \frac{6\,X_1\,\Delta Y}{N^3\,(0.112)^2}\right)$$

$$M_e = 659.46\left(\frac{\phi}{2N} + \frac{478.32\,X_1\,\Delta Y}{N^3}\right) \text{ in.-lb.} \qquad \text{(Eq. 6)}$$

The error force at the specimen, located X_2 in. from the gimbal, is then:

$$F_e = \frac{M_e}{X_2} = \frac{659.46}{X_2}\left(\frac{\phi}{2N} + \frac{478.32\,X_1\Delta Y}{N^3}\right) \text{ lb.} \qquad \text{(Eq. 7)}$$

The existing arm design is shown in Figure A1. Substitution into Eq. 7 gives:

$$F_{eo} = \frac{659.46}{4.880}\left(\frac{0.20491\,w}{2(9)} \quad \frac{478.32\,(1)\,(0.20491\,w)}{9^3}\right)$$

$$F_{eo} = 135.14\ (0.01138\,w + 0.13444\,w)$$

$$F_{eo} = 19.705\,w \text{ lb. where } w = \text{specimen wear, in.}$$

The redesign of the loading arm is shown in Figure A2. It is planned that the X_1 dimension be zero, producing $\Delta Y = 0$; however, let $X_1 = 0.050$

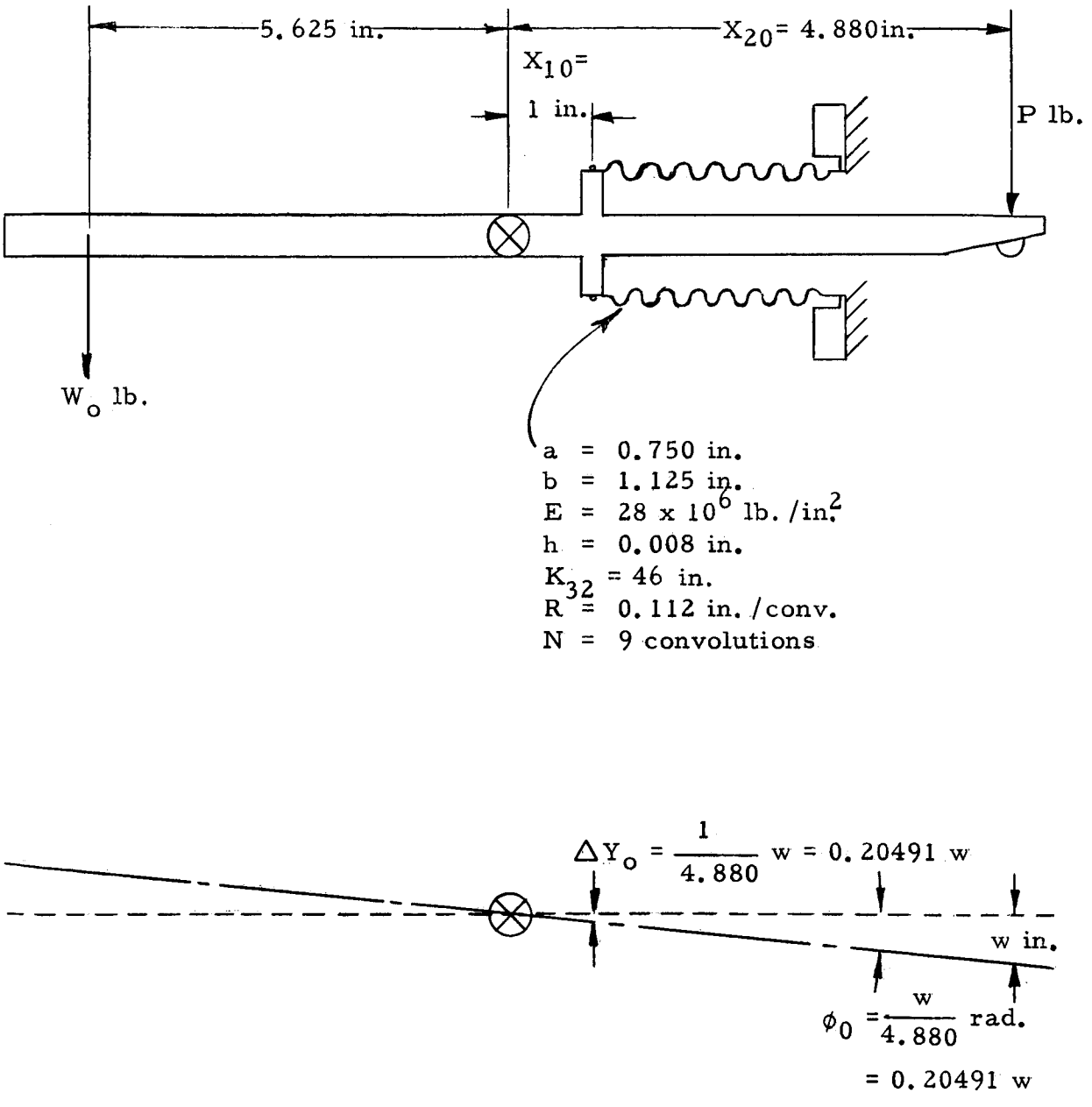

Figure A1. Length and Deflection Characteristics of the Existing Loading Arm Design.

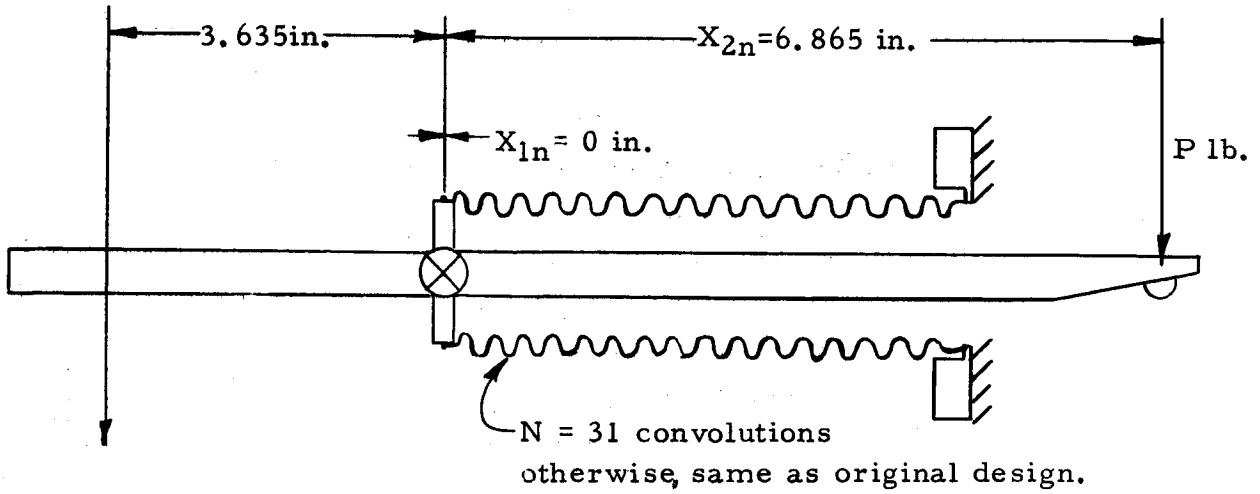

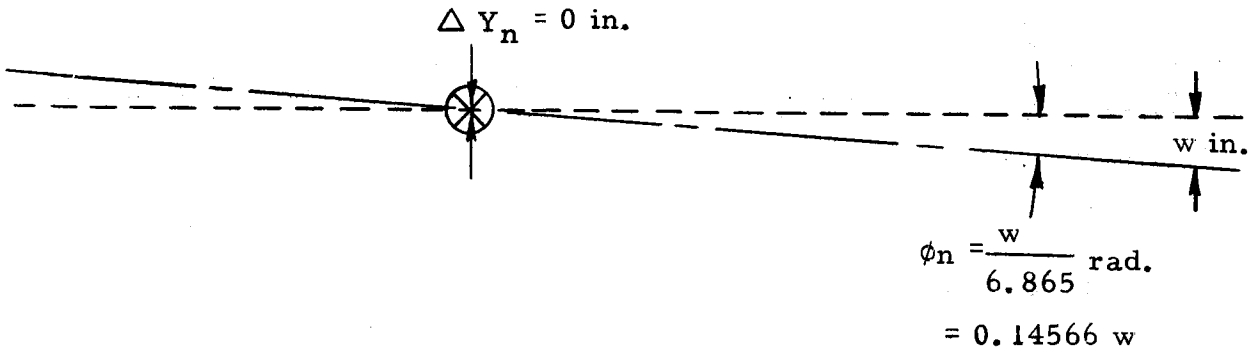

Figure A2. Length and Deflection Characteristics of New Loading Arm Design.

inch as a possible misaglignment error between the gimbal centerline and the line of action of the bellows force. Then the comparative bellows and deflections are as shown by Figure A3 and substitution into Eq. 7 gives:

$$F_{en} = \frac{659.46}{6.865}\left(\frac{0.14566w}{2\ (31)} + \frac{478.32\ (0.050)\ (0.050)\ (0.14566w)}{(31)^3}\right)$$

$$F_{en} = 96.061\ (0.00235w + 0.00001w)$$

$$F_{en} = 0.22670\ w.$$

The force errors, which decrease the load between specimens as wear occurs, are of the order of 0.020 pound per 0.001 inch of specimen wear for the original arm design and 0.0002 pound per 0.001 inch of specimen wear for the new design. Although the absolute magnitude is not large, the 0.020 pound represents an error of about 25% per 0.001 inch wear for the lightest loads to be used.

The preceding proposed change was incorporated into drawing 263E797, shown in Figure A4, and its component drawings. An assembly fixture, drawing SK56131-468, was designed to obtain proper dimensional control of the arms during the welding operation.

The change incorporated a force pickup mounting position of only 0.75 inch from the gimbal centerline, thus giving a magnification factor of $\frac{3.635}{0.750} = 4.847$ over the friction loads which would be produced with the force pickup located in the plan of the tray load.

Specimen Redesign - As an alternate to a loading arm design, it is possible to accept the existing unloading error, and raise the specimen compression forces to a level where the unloading error would be an acceptably small percentage of the smallest compression force P.

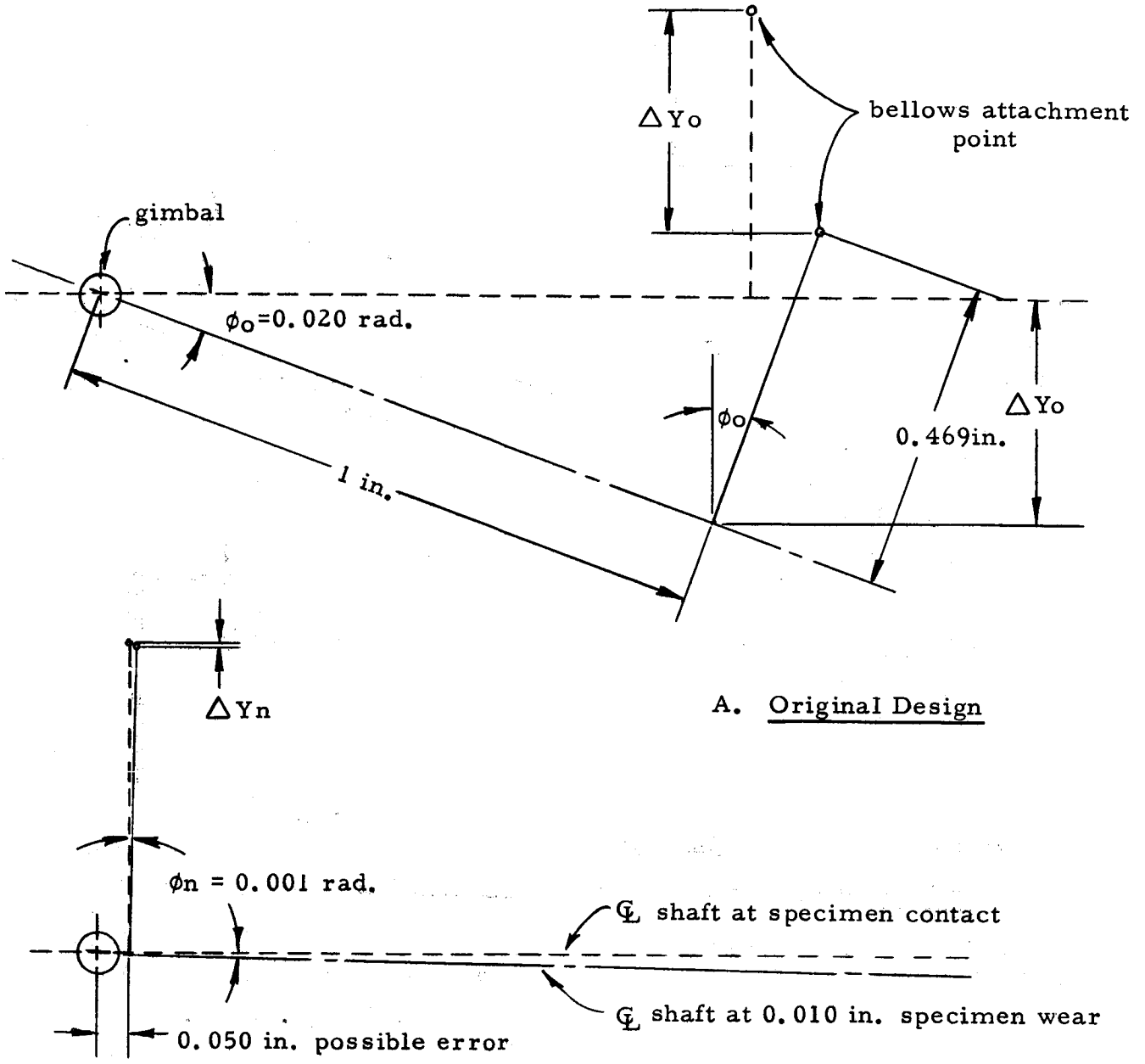

Figure A3. Comparison of Bellows Deflections - Original vs. New Design.

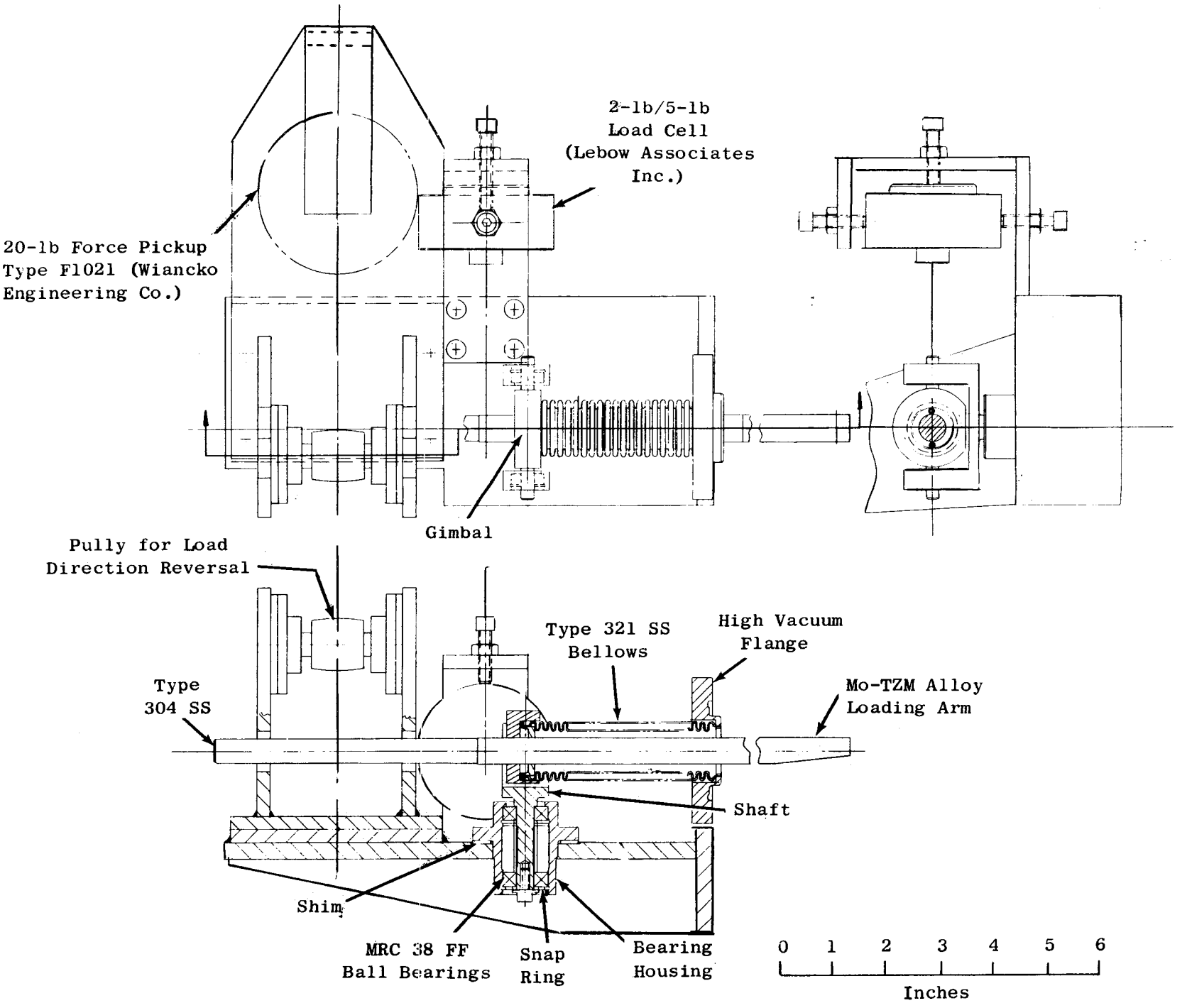

Figure A4. Loading Arm Redesign and Location of Force Cell Assemblies.

If it is considered acceptable to have a 1% error per 0.001 inch of specimen wear:

$$F_{eq} = 19.705\ (0.001)\ \text{lb.} = (0.01)\ (P\ \text{lb.})$$

$$P = 1.97\ \text{lb.}$$

For a sphere loaded against a flat plate (2):

$$\text{Max } Sc = 0.917 \sqrt[3]{\frac{P}{D^2\left[\frac{1-\nu_1^2}{E_1} + \frac{1-\nu_2^2}{E_2}\right]^2}} \qquad \text{(Eq. 8)}$$

Where: ν = Poisson's ratio.

D = sphere diameter, in.

E = modulus of elasticity, lb/in^2.

P = total load, lb.

S_c = unit compressive stress, $lb./in^2$.

Subscripts 1 and 2 refer to bodies 1 and 2.

With no change in material properties, the ratio of sphere diameter to load is:

$$\frac{D_a^2}{P_a} = \frac{D_b^2}{P_b} = \left(\frac{0.917}{\text{max } Sc}\right)^3 \left[\frac{1}{\frac{1-\nu_1^2}{E_1} + \frac{1-\nu_2^2}{E_2}}\right]^2 = \text{constant}$$

For a present light - load condition, $D_a = 0.2495$ in. and $P_a = 0.0701$ lb. When $P_b = 1.97$ lb.:

$$D_b^2 = \frac{D_a^2 P_b}{P_a} = \frac{(0.2495)^2\ (1.97)}{0.0701} = 1.749$$

$$D_b = 1.322 \text{ in.}$$

Although the above diameter could be achieved by the removal of a few thousandths of stock from the existing hemispherical riders, this plan was rejected in favor of correcting the bellows spring rate error.

APPENDIX B

ANALYSIS OF LOADING SYSTEM ERRORS DUE TO DIMENSIONAL INACCURACIES

Appendix B

Analysis of Loading System Errors Due to Dimensional Inaccuracies

Inspection reports of parts fabricated for the high vacuum friction tester were analyzed to determine the deviations from the nominal blueprint dimensions measured at various levels of allowable tolerances. The results are shown in Table I. Primarily, it shows that the part dimensions will be within the allowable tolerance band with 96.4% confidence (1.85 standard deviations). This information will be used to assign probable dimensional errors where no inspection dimensions are available and reported to be within tolerance or where any one of several parts could be fitted into the assembly.

TABLE I. STATISTICAL SAMPLE OF FABRICATION ACCURACY FOR HIGH VACUUM FRICTION TESTER

Act.-Nom. Inch	Allowable Tolerance, Inch						
	0.001	0.002	0.003	0.004	0.009 0.005	0.010	0.016
> +0.016							3
+0.016							1
+0.015							2
+0.014	Number of						1
+0.013	Samples						0
+0.012						1	5
+0.011			Allowable Limits				1
+0.010						2	4
+0.009					0	0	1
+0.008					0	0	1
+0.007					0	0	2
+0.006				1	1	1	3
+0.005					6	0	1
+0.004				0	13	1	3
+0.003			5	0	11	0	5
+0.002	1	0	10	1	9	2	13
+0.001	20	3	9	1	9	3	15
0	68	13	12	3	49	4	29
-0.001	12	6	5	0	11	2	10
-0.002	1	10	6	3	19	0	11
-0.003			10	0	9	0	11
-0.004				0	14	1	5
-0.005					3	0	1
-0.006			1		0	1	2
-0.007					0	1	1
-0.008					0	0	0
-0.009					0	0	1
-0.010						1	1
-0.011							0
-0.012							6
< -0.012							4
Size of Sample	102	32	58	9	154	20	143
Std. Dev. σ, In. x 10^{-3}	0.714	1.046	1.862	2.427	2.555	4.370	10.788
Deviation at 1.85σ, In.	0.001	0.002	0.003	0.004	0.005	0.008	0.020

Coordinate System - The baseline for measurements of dimensional inaccuracies will be the line joining the actual centerline of the arm in the planes of the gimbal and the specimen when the disc and rider specimens have come in contact and when no side forces are applied. The positive directions are as shown in Figure B1.

1.0 Mislocation of Disc Specimen - The disc specimen can be mislocated from its nominal dimension because of the following reasons:

1.1 Tolerance stackup from the surface of the disc which contacts the rider through all dimensions leading to the gimbal centerline (calculated and measured deviations):

$$Y_{1.1} = \pm 0.026 \text{ in.}$$

1.2 Movement allowable in angular contact bearings on the shaft - assume that magnetic attraction holds this to:

$$Y_{1.2} = \pm 0.005 \text{ in.}$$

1.3 Differential thermal expansion - using measured temperatures at the end of the shaft and estimating temperature deterioration:

at R.T.,	$RT^{Y}1.3 = 0$ in.
at 400°F,	$400^{Y}1.3 = + 0.022$ in.
at 800°F,	$800^{Y}1.3 = + 0.044$ in.
at 1200°F,	$1200^{Y}1.3 = + 0.066$ in.
at 1600°F,	$1600^{Y}1.3 = + 0.088$ in.

1.4 No deviations in the X or Z directions have significance except in the location of the wear track on the disc.

1.5 The significance of the total deviation from nominal is that the Y - axis (perpendicular to the arm centerline) is shifted from coincidence with the line of action of gravitational acceleration and the outside tray loads will not be coincident with compressive force P between specimens:

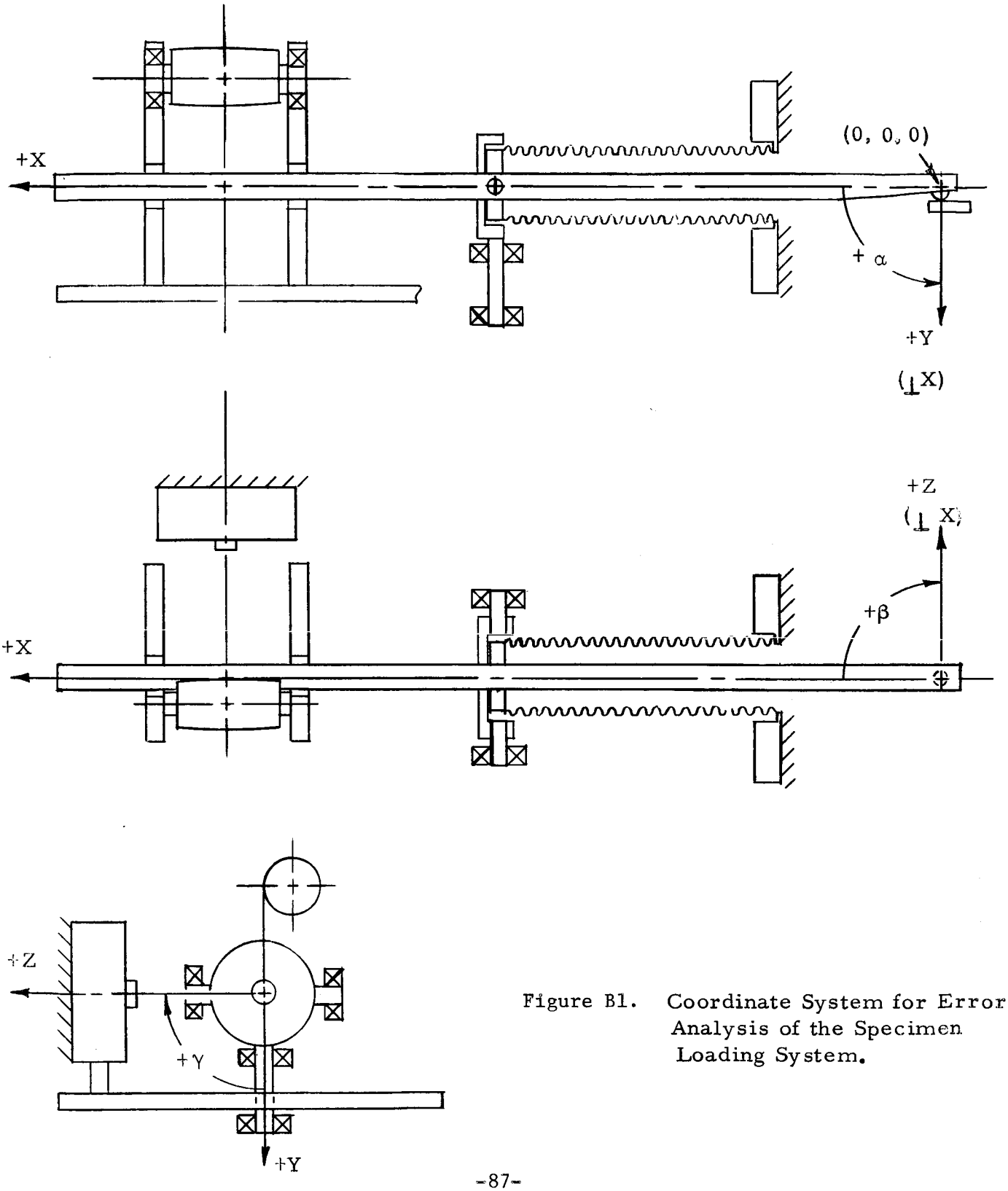

Figure B1. Coordinate System for Error Analysis of the Specimen Loading System.

$$\alpha_{1.5} = \arctan \frac{Y_{1.1} + Y_{1.2} + Y_{1.3}}{X_2}$$

Where X_2 = 6.865 in. (distance between gimbal and specimens), the loading error which results will be:

$$e_{1.5} = 100 \tan \alpha_{1.5} = 100 \tan (0.0451 + 0.000801T) \quad \% \text{ error}$$

The above figures give:

T °F	$e_{1.5}$ %
RT	±0.4
400	+0.7 -0.1
800	+1.1 +0.2
1200	+1.4 +0.5
1600	+1.7 +0.9

The calibration procedure will be ammended to provide for the measurement and correction of the thermal growth to give less than 1% error.

1.6 Out-of-plane rotation (η direction) of ± 0.001 in. can cause sinusoidal loading and unloading of the compression load P between specimens.

Let displacement $Y = Y_{1.6} \omega t$ in.,

velocity $Y' = Y_{1.6} \omega \sin (\omega t + \frac{\pi}{2})$ in./sec,

acceleration $Y'' = Y_{1.6} \omega^2 \sin (\omega t + \pi)$ in./sec^2

where: t = time, sec.

ω = angular velocity, rad./sec.

$$= \left(\frac{N \text{ rev}}{\text{min}}\right) \left(\frac{2 \text{ rad}}{\text{rev.}}\right) \left(\frac{\text{min}}{60 \text{ sec.}}\right) = 0.10471N \quad \frac{\text{rad}}{\text{sec}}$$

Acceleration peaks will occur at $\omega t = 0.5\pi$ and 1.5π.

$$Y'' \text{ max} = Y_{1.6}\, \omega^2\, (\pm 1)$$

$$= Y_{1.6}\, (0.10471\ N)^2$$

$$= \pm\ 0.01096\ Y_{1.6}\ N^2$$

The effective mass m_a of the arm which is accelerated is approximately:

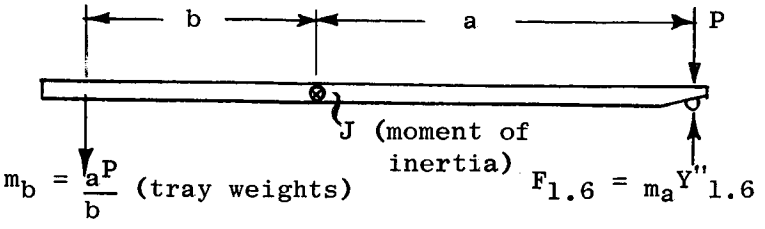

$$m_a = \frac{J + m_b b^2}{a^2} = \frac{J + ab\ P}{a^2}$$

$$m_a = \left[0.24383 + 1.3717\ P\right] \times 10^{-3} \quad \frac{\text{lb sec}^2}{\text{in.}}$$

From $F = ma \doteq ma\ Y''$ lb.,
the error will be:

$$e_{1.6} = \left[\frac{F_{1.6}}{P}\right] 100 \quad \% \text{ error}$$

$$= 100 \left[\frac{(0.24383 + 1.2717P)}{1000P} \left(\pm\ 0.01096\ Y_{1.6} N^2\right)\right]$$

$$= \pm \left[\frac{0.26734 + 1.5040}{1000P}\right] Y_{1.6} N^2$$

which amounts to $_{50}e_{1.6} = \pm \left(\frac{6.1043}{P} + 34.341\right)$ %
at 4778 RPM for ± 0.001 in. runout.

This error can be discovered by rotating the main drive shaft by hand when the specimens are loaded slightly in excess of the tare weight. Runout will be indicated by a dial indicator touching the loading arm.

1.7 Gross deivations from flatness of the disc specimens will effectively cause loading errors by changing the compressive stresses between the specimens. The spherical diameter of the deviated surface will be:

$$D_1 = \frac{4b^2 + c^2}{4b}$$

and the stress between the specimens will be (1):

$$\max s_c = 0.918 \sqrt[3]{P \frac{\left(\frac{D_1 \pm D_2}{D_1 D_2}\right)^2}{\left[\frac{1 - \nu_1^2}{E_1} + \frac{1 - \nu_2^2}{E_2}\right]^2}}$$

where the ± sign is + for a sphere on a sphere and
- for a sphere in a spherical socket

b = chordal rise, in.

c = chord length, 0.500 in. (width of disc)

D_1 = diameter of the deviated disc surface, in.

D_2 = rider specimen diameter, 0.250 in.

E = modulus of elasticity, psi.

P = compressive load between specimens, lb.

s_c = unit compressive stress, psi.

ν = Poisson's ratio.

For a sphere on a flat plate

$$\max s_c = 0.918 \sqrt[3]{\frac{P}{D_2^2 \left[\frac{1 - \nu_1}{E_1} + \frac{1 - \nu_2}{E_2}\right]^2}}$$

The load required to produce stress s_c between the imperfect surfaces is:

$$P_d = \left(\frac{D_1 D_2}{D_1 \pm D_2}\right)^2 \left(\frac{\max s_c}{0.918}\right)^3 \left[\frac{1 - \nu_1^2}{E_1} + \frac{1 - \nu_2^2}{E_2}\right]^2$$

The normal load is:

$$P = D_2^2 \left(\frac{\max s_c}{0.918}\right)^3 \left[\frac{1-\nu_1^2}{E_1} + \frac{1-\nu_2^2}{E_2}\right]^2$$

The loading error is:

$$e_{1.7} = \left[\frac{P - P_d}{P}\right] 100 = \left[1 - \frac{P_d}{P}\right] 100 \quad \% \text{ error}$$

$$= \left[1 - \left(\frac{D_1 D_2}{D_1 \pm D_2}\right)^2 \left(\frac{1}{D_2}\right)^2\right] 100$$

$$= \left[1 - \left(\frac{\frac{4b^2 + 0.500^2}{4b}}{\frac{4b^2 + 0.500^2}{4b} \pm 0.250}\right)^2\right] 100$$

$$= \left[1 - \left(\frac{4b^2 + 0.250}{4b^2 + 0.250 \pm b}\right)^2\right] 100$$

$$\approx \left[1 - \left(\frac{0.250}{0.250 \pm b}\right)^2\right] 100$$

$$\approx 100 - \left(\frac{2.50}{0.250 \pm b}\right)^2 \quad \text{(neglecting the } b^2 \text{ terms)}$$

This error is approximately 0.8% for b=0.001 in. Therefore, the load should be adjusted before testing or the results should be reported on the basis of true stresses imposed. The latter method will be used.

1.8 Mislocation of the disc specimen in the α direction changes the point of contact between the specimens in the X direction, leading to a small speed error.

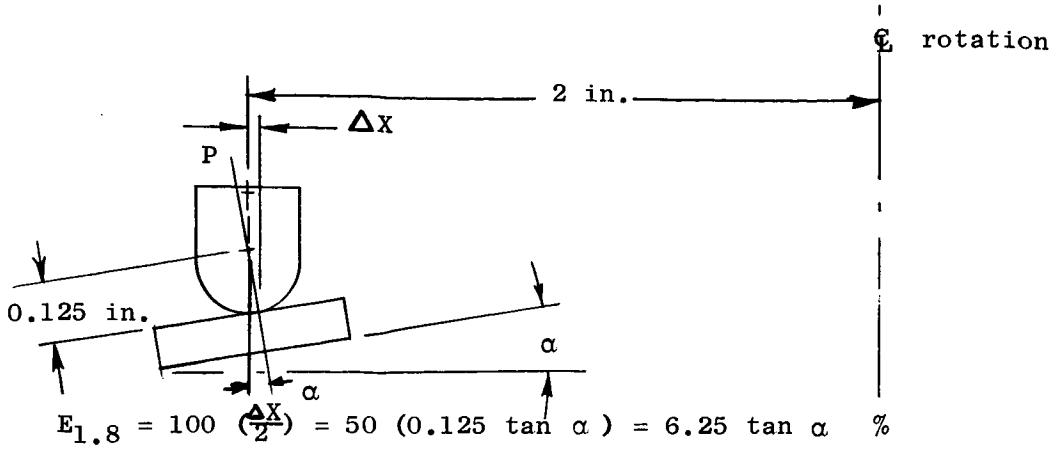

$E_{1.8} = 100 \left(\frac{\Delta X}{2}\right) = 50\ (0.125 \tan \alpha) = 6.25 \tan \alpha$ %

The loading error associated with the above is:

$$e_{1.8} = 100 \tan \alpha .$$

Therefore, the blueprint flatness requirements of 0.001 inch TIR and assembly requirement of 0.003 in. max. gap under specimens would make the probable errors completely negligible:

$$\tan \alpha = \frac{0.001 + 0.003}{4} = 0.001$$

$$E_{1.8} = 0.006\%$$

$$e_{1.8} = 0.1\%$$

1.9 Mislocation of the disc specimen in the β direction is meaningless because this is the direction of rotation.

1.10 Mislocations of the disc specimen in the γ direction has been discussed under 1.6 above; however, an additional loading error can occur. Putting this on the same basis of ± 0.001 runout gives:

$$e_{1.10} = 100 \tan \gamma \quad \% \text{ error}$$

$$= 100 \left(\frac{Y_{1.6}}{2}\right)$$

$$= 50\ Y_{1.6}$$

$$= 0.05\%/\pm\ 0.001 \text{ in. runout}$$

Therefore, it is considered negligible.

2.0 Mislocation of Rider Specimen -

2.1 No errors of consequence can occur in this location because the specimen is press-fitted into the arm. The actual distance between the centerline of the specimen hole and the gimbal pivot pins is carefully measured and used in calculating tray weights needed to produce the desired compressive force between specimens. The protrusion of the rider from the arm is absorbed in the definition of the centerline of the arm in the plan of the rider as being 0.250 in. from the specimen interface.

2.2 Deviations in the diameter of the riders will cause effective loading errors by changing the compressive stresses between the specimens. From 1.7 above, the load P_d required to produce stress s_c between the imperfect specimens would be:

$$\max s_c = 0.918 \sqrt[3]{\frac{P_d}{D_{2d}^2 \left[\frac{1-\nu_1^2}{E_1} + \frac{1-\nu_2^2}{E_2}\right]^2}}$$

and between the perfect specimens would be:

$$\text{mas } s_c = 0.918 \sqrt[3]{\frac{P}{D_2^2 \left[\frac{1-\nu_1^2}{E_1} + \frac{1-\nu_2^2}{E_2}\right]^2}}$$

The loading error would be:

$$e_{2.2} = \left[\frac{P - P_d}{P}\right] 100 = \left[1 - \frac{P_d}{P}\right] 100 \quad \text{\% error}$$

$$= \left[1 - \frac{D_{2d}^2}{D_2^2}\right] 100$$

Let $D_{2d} = D_2 + \Delta d$

$$e_{2.2} = \left[1 - \frac{D_2^2 \pm 2 D_2 \Delta d + \Delta d^2}{D_2^2}\right] 100$$

$$= \left[1 - \left(1 \pm \frac{2\Delta d}{D_2} + \left(\frac{\Delta d}{D_2}\right)^2\right)\right] 100$$

$$e_{2.2} = \frac{\pm 200\Delta d}{0.2495} - 100 \left(\frac{\Delta d}{0.2495}\right)^2$$

$$= \pm 801.60\ \Delta d - 1606.4\ \Delta d^2$$

Since this error reaches 1% when $\Delta d = 0.00125$ in., it should be accounted for by recalculating required loads prior to testing or the results reported on the basis of true stress imposed. The latter method will be used.

2.3 Mislocation of the rider in the α direction has a speed effect of:

$$E_{2.3} = 100 \frac{(0.125 \tan\alpha)}{2} = 6.25 \tan\alpha \ \%$$

Inspection shows $\tan\alpha$ to be of the order of 0.005; therefore the error is about 0.03% and negligible.

The loading error is:

$$e_{2.3} = 100 \left(\frac{0.125 \tan\alpha}{6.865}\right) = 1.8209 \tan\alpha \ \%$$

This error is of the order of 0.01% when $\tan\alpha = 0.005$, and also is negligible.

2.4 Mislocation of the rider in the β or γ directions has no effect on loading.

3.0 Mislocation of the Vacuum Flange -

The vacuum flange mislocation from its blueprint nominal position with respect to the gimbal may occur in the X, Y, Z, α, β, and γ directions or in rotation about its centerline. The effect of the mislocations is to impose axial loads on the arm which are absorbed by the gimbal bearings; and moments which are fully accounted for by the tare weight and force pickup calibrations immediately prior to each test. The spring rate of the bellows is verified as acceptable by the tare weight test.

4.0 Mislocation of Gimbal Components -

4.1 No mislocation of the gimbal centerline with respect to the rider specimen can occur, however, errors with respect to the centerline of rotation will cause speed errors. The stackup of measured and probable dimensions gives:

$$E_{4.1} = \left(\frac{0.026}{2}\right) 100 = 1.3\% \text{ error}$$

4.2 No mislocation of the gimbal centerline in the Y and Z directions is possible, by definition. Mislocation in the α and β directions causes no error because of the freedom to rotate about the bearings. Although bearing friction can produce errors in vertical loading, force pickup calibration, and force signal readout, these errors appear to be eliminated by externally induced vibration of the gimbal support during calibration to break static friction and by the presence of sufficient natural vibrations during testing.

4.3 Tilting of the gimbal in the γ direction (see Figure 1) will not cause proportional loading errors directly because the rider specimen has a hemispherical contour. Its effect will be upon the geometry of the dead weight loading system and the force pickup, to be discussed later.

5.0 Thermocouples -

The presence of the arm thermocouples causes an error in spring rate of the system, changing the load between the specimens as wear occurs. This error is minimized by the attachment of the rigid thermocouple sheath as close as possible to the gimbal centerline. From this point, wires are run to an attachment point several feet away. It is accounted for as part of the bellows spring rate discovered by the tare weight test.

6.0 Mislocation of the Dead Weight Loading Point -

6.1 Essentially, there is no error in the X direction (see Figure 1) because this dimension is measured and entered into calculations

which define the dead weight required to produce the desired compressive P between specimens. However, the actual application of the load is through screw threads which have some clearance and runout in the β direction.

The loading error associated with this dimension will be:

$$e_{6.1} = 100 \left(\frac{X_{6.1}}{X_1} \right) \qquad \% \text{ error}$$

Where X_1 = 3.635 in. (distance from gimbal to loading point)

$X_{6.1}$ = 0.005 in. (probable thread clearance)

$e_{6.1}$ = 0.14% and is negligible

Loading through the screw by a free-swinging steel loop assures that the line of action of the load passes through the center of the measured loading point, whether the loading direction is coincident or opposite to the direction of gravity.

6.2 An error in the Y dimension of the dead-weight loading point has no effect upon the load. It is measured when the specimens are in contact as a baseline for aligning the force pickup and force pickup calibration bearing.

6.3 An error in the Z dimension has no effect upon the load (or counterweight) which hangs down through the support, it does effect the load in the anti-gravity direction.

By careful loading of the arm with loads both in the direction of gravity and opposite the direction of gravity, it is believed that the dimensional error $Z_{6.3}$ can be held to within 0.010 in. with confidence, giving a force pickup error of:

$$f = \frac{Z_{6.3} W_{ag}}{\sqrt{1.5^2 + Z_{6.3}^2}} = \frac{0.010 \ (1.8886 \ P)}{1.5000}$$

$$= 0.0126 \ P \quad \text{lb.}$$

$$f_{6.3} = 100 \left(\frac{F}{F_{fp}}\right) = 100 \left(\frac{0.0126\ P}{1.8886\ f_{fp}}\right) = \frac{0.667}{f_f} \quad \% \text{ error}$$

F_{fp} = force transmitted to the force pickup, lb.

f_f = coefficient of friction

P = compressive load between specimens, lb.

$W_{ag}\ max = \frac{6.865}{3.635} P = 1.8886\ P$

and a dead weight load error of:

$$e_{6.3} = \left(1 - \frac{W_{6.3}}{W_{ag}}\right) 100$$

$$= 1 - \left(\frac{1.5\ W_{ag}}{W_{ag}\ \sqrt{1.5^2 + 0.010^2}}\right) 100$$

$$= 0.002\% \text{ (considered negligible)}$$

The above loading error exists only when the anti-gravity load W_{ag} is the full tray load W_o necessary to produce the desired compressive force between specimens. The error is less when the W_{ag} load is merely a counterbalance load required to unbalance the arm in order to obtain good tare test points.

6.4 Misalignment of the loading screw in the α direction is meaningless because the loading hooks swing freely in that direction.

6.5 Misalignment of the loading screw in the β direction is eliminated when the lines of action of the loads in the direction of gravity and opposite to it pass through the measured centerline of the loading point. Careful use of the hooks eliminate this source of error (see 6.3) on the load.

β - direction misalignment and fabrication inaccuracies misalign the force pickup and force pickup calibration load attachment points. These points are located at approximately 0.580 inch

from the arm centerline. With a 2.5 inch long flexible connector attached to the force pickup, the force signal error is:

$$f_{6.5} = \left(1 - \frac{F_{6.5}}{F_{fp}}\right) 100$$

$$= \left(1 - \frac{2.5F_{fp}}{F_{fp}\sqrt{2.5^2 + (0.580 \text{ Tan}\beta)^2}}\right) 100$$

$$= 0\%$$

where $F_{6.5}$ = erroneous force signal to the pickup

F_{fp} = true force pickup signal

$\text{Tan}\beta$ = 0.010 by measurement and estimation

Similarly, the calibration force $f'_{6.3}$ is affected because its arc distance is about 1.25 in:

$$f'_{6.5} = \left(1 - \frac{1.25}{\sqrt{1.25^2 + 0.0058^2}}\right) 100 = 0\%$$

6.6 Misalignments in the γ direction have the same effect upon the force pickup as $f_{6.5}$ and $f'_{6.5}$ above. They would, in fact, tend to be slightly less because the vertical error vector of the force would try to align the centers of each end of the flexible connectors.

The vertical loading error is:

$$e_{6.6} = \frac{100\ F_{fp} \sin\beta}{W_o} \quad \% \text{ error}$$

$$= \frac{F_{fp}}{W_o} = f_f \quad \% \text{ (Coefficient of friction)}$$

where W_o = dead weight loads to produce desired compressive stress, lb.

6.7 The errors in the Z and β dimensions of the 0.25 in. hole through the center of the loading arm have an effect upon the force signal because gauges fitting into this hole are utilized to align the force pickup centerline perpendicular to the arm centerline. If the dimension $Z_{6,4}$ = 0.004 in. at 2.885 in. from a base point $\tan\beta_{6.4}$ = 0.0025 by measurement, and the gauges align the force pickup face centerlines within 0.005 in., at distances of 2.430 in. and 4.660 in. from the arm centerline, the associated force error will be:

$$\tan\beta = 0.0025 + \frac{0.004}{2.885} = 0.0039$$

$$0.0039\ (4.660 - 2.430) + 0.005 + 0.005 = 0.019$$

$$f_{6.7} = \left(1 - \frac{2.230\ F_{fp}}{F_{fp}\ \sqrt{2.230^2 + 0.019^2}}\right) 100$$

$$= 0.005\% \text{ (considered negligible)}$$

6.8 An error similar to $f_{6.7}$ can occur because of the use of gauges to align the force pickup calibration forces perpendicular to the arm centerline. With $\tan\beta$ = 0.039 as before and a possible error of 0.010 in. in aligning the force connector at 1.25 in. from the arm centerline, the force pickup calibration signal error is:

$$0.0039\ (1.25) + 0.010 = 0.015 \text{ in.}$$

$$f'_{6.8} = \left(1 - \frac{1.25\ F_{fp}}{F_{fp}\ \sqrt{1.25^2 + 0.015^2}}\right) 100$$

$$= 0.007\% \text{ (considered negligible).}$$

7.0 Inaccuracies in Force Pickup Location -

7.1 Mislocation of the centerline of the force pickup with respect to the arm loading point in the X direction is expected to be about 0.005 in. because of the fact that gauges are used. With a force pickup connector length of 2.5 in., the force signal error is:

$$f_{7.1} = \left(1 - \frac{2.5\ F_{fp}}{F_{fp}\ \sqrt{2.5^2 + 0.005^2}}\right) \qquad 100 = 0\%\ \text{error}$$

7.2 Mislocation of the centerline of the force pickup with respect to the arm loading point in the Y direction is expected to be about 0.005 in., because of the fact that jo-blocks are used. The force signal error $f_{7.2} = 0\%$, as in 7.1.

7.3 Mislocation of the force pickup in the Z direction with respect to the arm loading point is manifested as slack in the force pickup cable. Tension causes no error and only changes the point on the disc specimen were the specimens come in contact. The possible error is minimized by the following method during force pickup calibration:

a) The approximate tare load is applied to the arm in the direction of gravity and opposite the direction of gravity in the absence of any horizontal forces. The arm is locked at the point of specimen contact.

b) The force pickup connector is attached to the arm.

c) An adjusting screw is locked in the position at which slack has been removed from the connector and the tension load barely can be seen at the Sanborn recorder.

d) The X and Y dimensions of the force pickup are set equal to those of the arm loading point, using special gauges and jo-blocks, simultaneously with step (c).

If the calibration were completed with slack in the connector the friction force produced between the specimens immediately would remove it or the true force would be transmitted through the slack connector. The effect of clearances in the threads would be similar to connector slack. Both are accounted for by the pre-test calibration of the force pickup. During loading, the connector will stretch a negligible amount and the flexible end of the force pickup will move about 0.005 in. in the direction of the load (if loaded to full rated capacity).

Since slack of only 0.001 in. causes the connector to deviate 0.035 in. from a straight line (circular arc assumed), it is believed that connector slack can reliably be held to less than 0.001 in. by visual inspection alone.

The effect of thread clearance can probably be completely accounted for by careful analysis of the force pickup calibration trace. The most probable maximum motion of the connector will be about 0.0025 in. because the force pickups will be chosen to have a load range of about twice the expected frictional forces. The connector will stretch no more than 0.0015 in. at the highest expected loads (calibration). The total maximum expected slack to be taken out of the force pickup connector system thus is of the order of 0.005 in., which translates to $0.005 \left(\frac{6.875}{3.635}\right) = 0.009$ in. in the plane of the specimens. The equivalent spring rate of the bellows (see monthly report for August 1965) is of the order of 0.2 lb/in. Therefore the force error is:

$$f_{7.3} = (0.009 \text{ in.})\ (0.2 \text{ lb./in.}) = 0.0018 \text{ lb.}$$

Considering this error with respect to the pickup force F_{fp} to be transmitted:

$$F_{fp} = f_f P \left(\frac{6.865}{3.635}\right)$$

$$= 1.8886\ f_f P \quad \text{lb.}$$

$$f_{7.3} = 100 \left(\frac{0.0018}{1.8886\ f_f P}\right)$$

$$= \frac{0.1}{f_p P} \quad \%$$

7.4 Mislocation of the force pickup in the α direction produces no error because the pickup is insensitive to such a mislocation.

7.5 Mislocation of the force pickup in the β and γ directions cause negligible force errors, their effects being similar to those of 6.5 and 6.6 above.

7.6 The spring rate of the force pickup connector will cause an unloading error of approximately 0.001 lb./0.001 in. wear. This rate will be discovered as a part of the tare test, and may be accounted for after the tests.

8.0 Mislocation of the Force Pickup Calibration Bearing -

8.1 The location of the force pickup calibration bearing with respect to the arm loading point is set with a special gauge. The probable maximum mislocation is about 0.010 in., leading to a calibration force error of:

$$f'_{8.1} = 100 \left(1 - \frac{1.25F'}{F' \sqrt{1.25^2 + 0.010^2}} \right) = 0.004\% \text{ (considered negligible)}$$

where the distance from the center of the calibration bearing to the calibration force cable attachment point is 1.25 in.

8.2 The mislocation of the centerline of the calibration force cable in the Y direction is held with jo-blocks to about 0.010 in., giving an error, as above, of:

$$f'_{8.2} = 0.004\% \text{ (considered negligible).}$$

8.3 Deviations of the position of the calibration bearing in the Z, α, β, or γ directions have no significance. The hysteresis of the system from such sources as the bearing friction and the cable stiffness is thought to be removed by vibrating the arm support during calibration to break static friction.

9.0 Mislocation of the Gravity - Reversal Shaft -

9.1 The gravity-reversal shaft is located above the loading arms primarily for the purpose of allowing the dead weights to pull upward on loading arms numbers 1 and 2, where the riders load downward on the discs. On loading arms numbers 3 and 4, a counterweight is sometimes used in this location for tare weight determination. The shaft may be mislocated in the X dimension by about 0.104 in. maximum. The resulting loading error is:

$$e_{9.1} = \left(1 - \frac{1.5\ W_{ag}}{W_{ag}\sqrt{1.5^2 + 0.104^2}}\right) \quad 100 \text{ \% error}$$

$$= 0.24\% \text{ (considered negligible).}$$

The above error is a loading error only when the anti-gravity load W_{ag} is the full dead weight load. It will be less when the load is counterweight only. Also, the wide belt used over this shaft will allow the load vector to center itself, to a certain degree.

9.2 Mislocation in the Y dimension has no significance.

9.3 Mislocation in the Z dimension can be about 0.050 in. maximum, giving a loading error of:

$$e_{9.2} = \left(1 - \frac{1.5\ W_{ag}}{W_{ag}\sqrt{1.5^2 + 0.050^2}}\right) \quad 100 \text{ \% error}$$

$$= 0.06\% \text{ (considered negligible)}$$

Again, this value will be less if the W_{ag} load is merely a counterweight load. Also, the calibration procedure is expected to hold the actual mislocation to less than 0.010 in.

9.4 Shaft mislocations in the α, β, and γ directions have no significance. The friction in the shaft bearings is another possible source of loading error, but it is believed that externally induced vibration of the support during calibration breaks the static friction and that natural vibrations during testing will accomplish the same result.

9.5 Use of Dial Indicator - A dial indicator located on the outboard end of the loading arm has been found to be indispensable in determining the exact point of specimen contact during tare weight tests and other calibration steps. To prevent its presence from adding a spring rate unloading error, its spring has been disconnected. The weight of its moving parts has been measured so that accurate corrections can be made if the dial indicator is present during tare weight tests and removed during actual testing. In general, the dial indicator is always present. Sticking of the dial indicator shaft is overcome by externally induced vibration of the support during calibration, and by natural vibrations during testing.

Summary of Loading System Errors Due to Dimensional Inaccuracies

A. Summary of Loading Errors:

$$e_{1.5} = 1.00\% \text{ (calibration procedure to be changed)}$$

$$e_{1.6} = \left[\frac{0.26734 + 1.5040}{1000\ P}\right] Y_{1.6} N^2 \quad \%$$

$$e_{1.7} = 100 - \left(\frac{2.50}{0.250 \pm b}\right)^2 \quad \%$$

$$e_{1.8} = 0.1\%$$

$$e_{1.10} = 50\ Y_{1.6} \quad \%$$

$$e_{2.2} = \mp 801.60\Delta d - 16.04\Delta d^2 \quad \%$$

$$e_{2.3} = 0.01\%$$

$$e_{6.1} = 0.14\%$$

$$e_{6.3} = 0.002\%$$

$$e_{6.6} = f_f\%$$

$$e_{9.1} = 0.24\%$$

$$e_{9.2} = 0.06\%$$

$$\sum e = 0.552 + 100 \tan (0.00451 + 0.000801\ T) + \left[\frac{0.26734 + 1.5040}{1000\ P}\right] Y_{1.6} N^2 + \left[100 - \left(\frac{2.50}{0.250 \pm b}\right)^2\right] + 50\ Y_{1.6} \mp 801.60\ \Delta d - 16.04\ \Delta d^2 + f_f \quad \%$$

Where:

- T = test temperature, $^\circ F \times 10^2$
- $Y_{1.6}$ = vertical runout of disc specimen when rotated about main shaft axis, in.
- N = rotating speed, RPM
- b = out-of-plane deviation of disc specimen surface to be tested, in.
- Δd = deviation of rider specimen diameter from 0.2495 in., in.

With a test procedure which holds 100 tan (0.00451 + 0.000801T) to 1% and $Y_{1.6}$ to ± 0.001 in.,

$$\sum e = 101.522 + 0.001 \left(\left[\frac{0.26734 + 1.5040P}{1000\ P} \right] N^2 + 50 \right) - \left(\frac{2.50}{0.250 \pm b} \right)^2 \mp 801.60\ \Delta d - 1606.3\ \Delta d^2 + f_f$$

at 764 RPM,

$$\sum_8 e = 102.45 + \frac{0.15605}{P} - \left(\frac{2.50}{0.250 \pm b} \right)^2 \mp 801.60\ \Delta d - 1606.4\ \Delta d^2 + f_f \quad \%$$

At 4778 RPM,

$$\sum 50e = 135.91 + \frac{6.1032}{P} - \left(\frac{2.50}{0.250 \pm b} \right)^2 \mp 801.60\ \Delta d - 1606.4\ \Delta d^2 + f_f \quad \%$$

With no errors due to the variables in the equations, the constant portions of the errors would be:

$$\sum_8 e_c = 2.45\%$$

$$\sum_{50} e_c = 35.91\%$$

Which emphasizes the strong effect of the ± 0.001 in. runout in the disc specimen at 4778 RPM.

B. Summary of Speed Errors

$E_{1.8} = 0.006\%$

$E_{2.3} = 0.03\%$

$E_{4.1} = 1.3\%$

$\sum E = 1.336\%$ (considered acceptable)

C. Summary of Force Errors:

$$f_{6.3} = \frac{0.667}{f_f} \quad \%$$

$$f_{6.5} = 0\%$$

$$f_{6.6} = 0\%$$

$$f_{6.7} = 0.005\%$$

$$f_{7.1} = 0\%$$

$$f_{7.2} = 0\%$$

$$f_{7.3} = \frac{0.1}{f_f P} \quad \%$$

$$f_{7.5} = 0\%$$

$$\sum f = 0.005 + \frac{0.1}{f_f P} + \frac{0.667}{f_f} = 0.005 + \frac{1}{f_f}\left(\frac{0.1}{p} + 0.667\right) \quad \%$$

This figure will probably be around $0.005 + \frac{1}{1}\left(\frac{0.1}{0.07} + 0.667\right) = 2.10\%$ or less.

D. Summary of Pickup Calibration Force Errors:

$$f'_{6.5} = 0\%$$

$$f'_{6.6} = 0\%$$

$$f'_{6.8} = 0.007\%$$

$$f'_{7.5} = 0\%$$

$$f'_{8.1} = 0.004\%$$

$$f'_{8.2} = 0.004\%$$

$\sum f' = 0.015\%$ (considered acceptable)

The above error summaries refer only to those sources of errors discussed, primarily dimensional discrepancies. They cannot be considered as full system errors until the electronics errors and dynamic inaccuracies due to specimen wear also are considered.

APPENDIX C

FRICTION AND WEAR DATA - HIGH VACUUM FRICTION AND WEAR TEST PROGRAM

FRICTION AND WEAR TEST DATA FOR CARBOLOY 907 VS CARBOLOY 907 IN HIGH VACUUM

Test No. - 500905A

Assembly No. - I

Loading Arm No. - 1

Test Date - 6/11/65

Rider
Material - Carboloy 907
Specimen No. - 1036-E-1

Disc
Material - Carboloy 907
Specimen No. - 1036-F-1A

Test Temperature, ^{o}F - RT

Max. ΔT of Rider, ^{o}F - 925

Speed, SFM - 500

Test Duration, Min. - 9.41

Compressive Load, Lbs - 11.860 (P_9)

Compressive Stress, psi - 581,330

Load/Material UCS or 0.2%CYS -
Rider - 82
Disc - 82

Average Coefficient of Friction - 0.77

Chamber Pressure, Torr. -
Start - 4.0×10^{-4}
Max. - 1.7×10^{-8}

Remarks - Test terminated due to excessive wear of rider.

Change in Coefficient of Friction with Time -

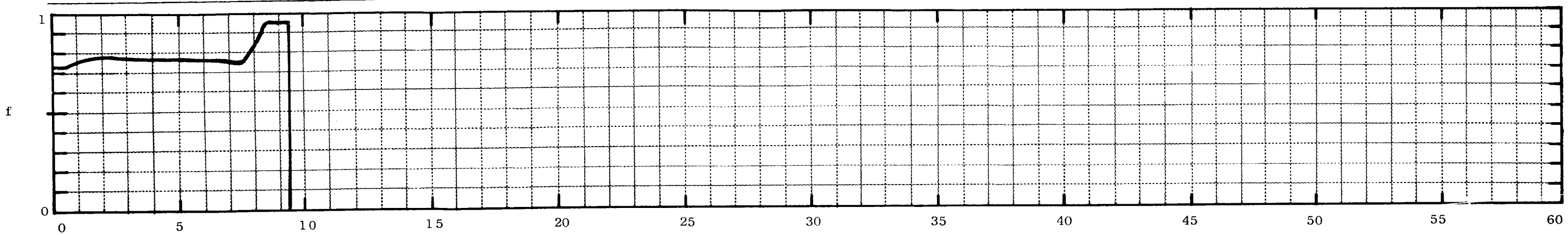

WEAR - RIDER

Initial Surface Finish - Not measured, <6

Wear Scar Dia., In. - 0.214

Weight, Gms -
Start - 3.5222
Finish - 3.2782
Change - -0.2440

Material Density, Gms Cm^3 - 14.684

Volume Change, Mm^3 - -16.62

Wear Rate, $In^3 \cdot 10^{10}$ / - -2130

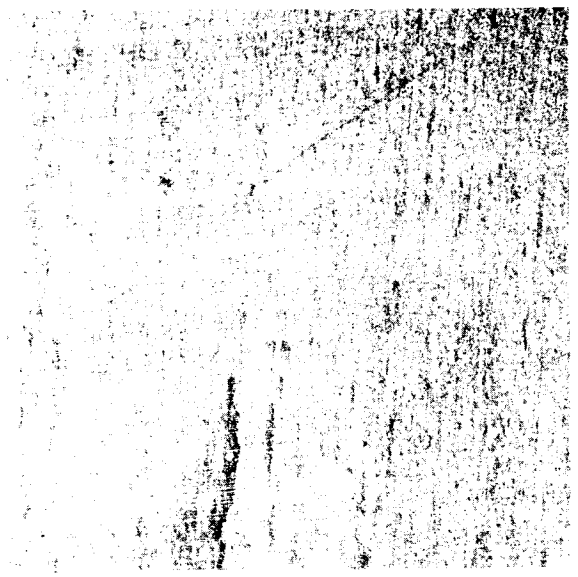

(C66081666) Mag.: 28.5X

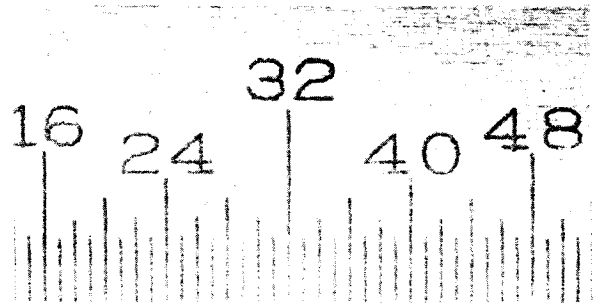

(C65081331) Mag.: 5X

WEAR - DISC

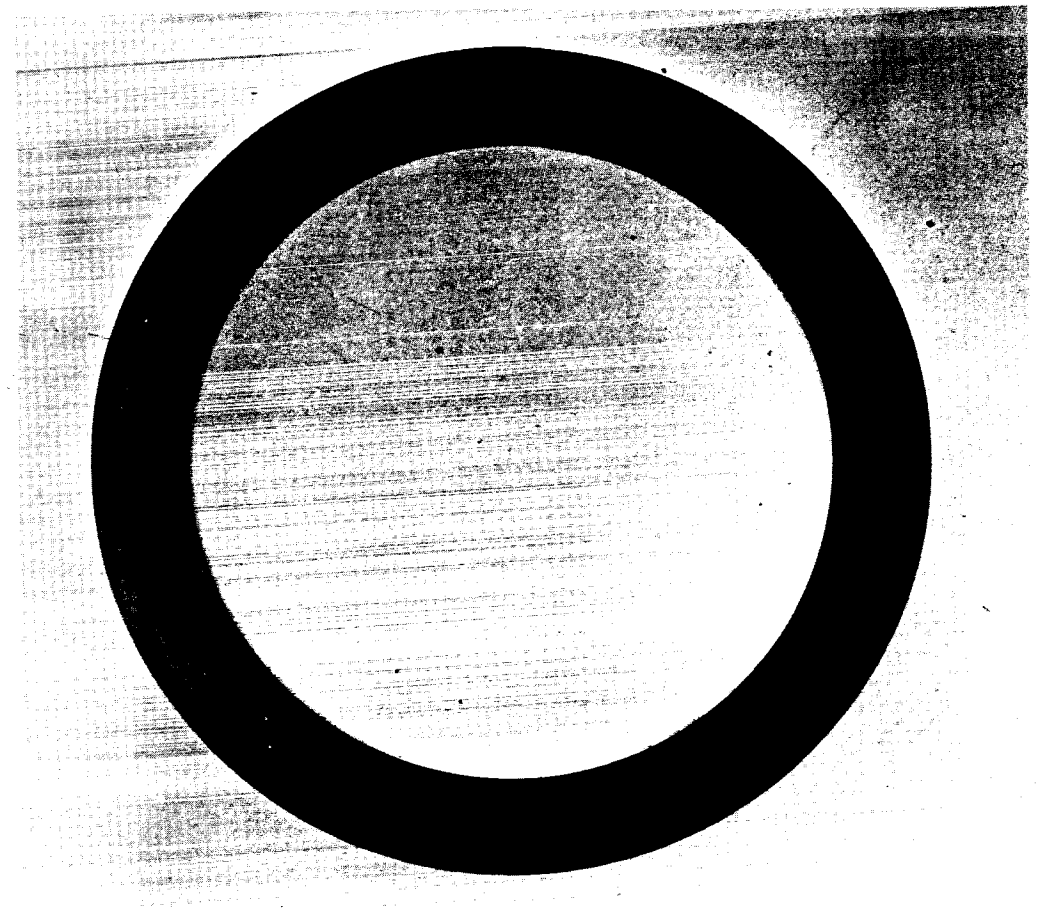

(C65081301) Mag.: 1X

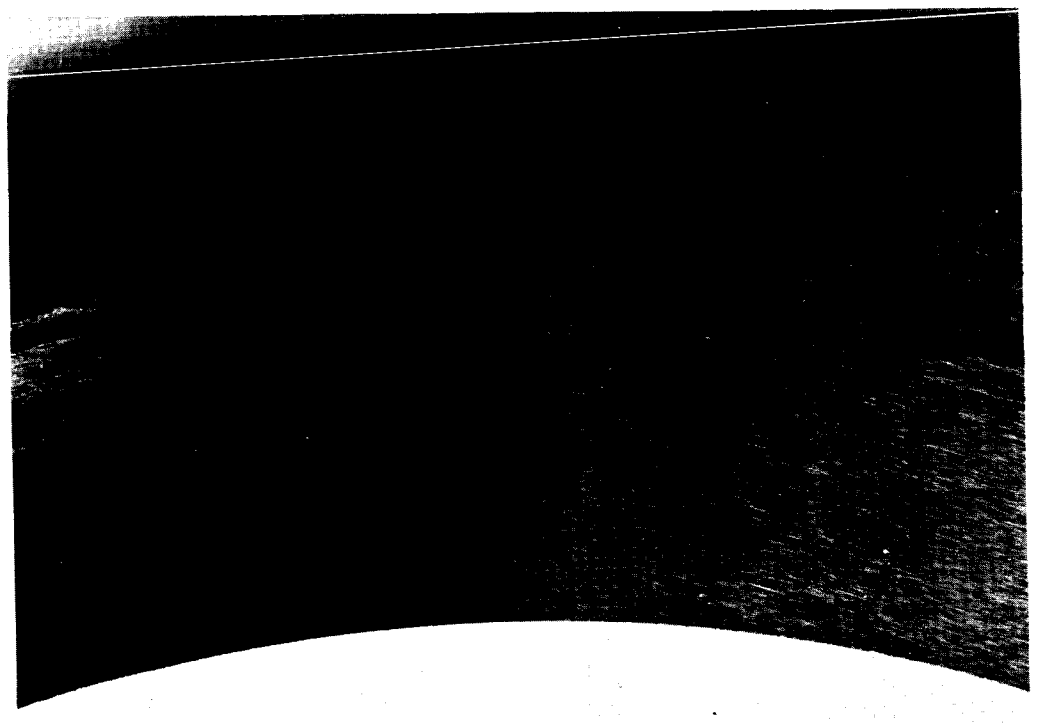

(C65081339) Mag.: 5X

Initial Surface Finish, Avg. RMS - 3-4

Wear Scar Width, In. - 0.172

Weight, Gms /Cm^3 -
Start - 226.8239
Finish - 226.8307
Change - +0.0068

Material Density, Gms /Cm^3 - 14.684

Volume Change, Mm^3 - +0.463

Wear Rate, $In^3/10^{10}ft$ - +59.4

Post-Test Profilometer Trace - Circumferential at 90° CW from S/N

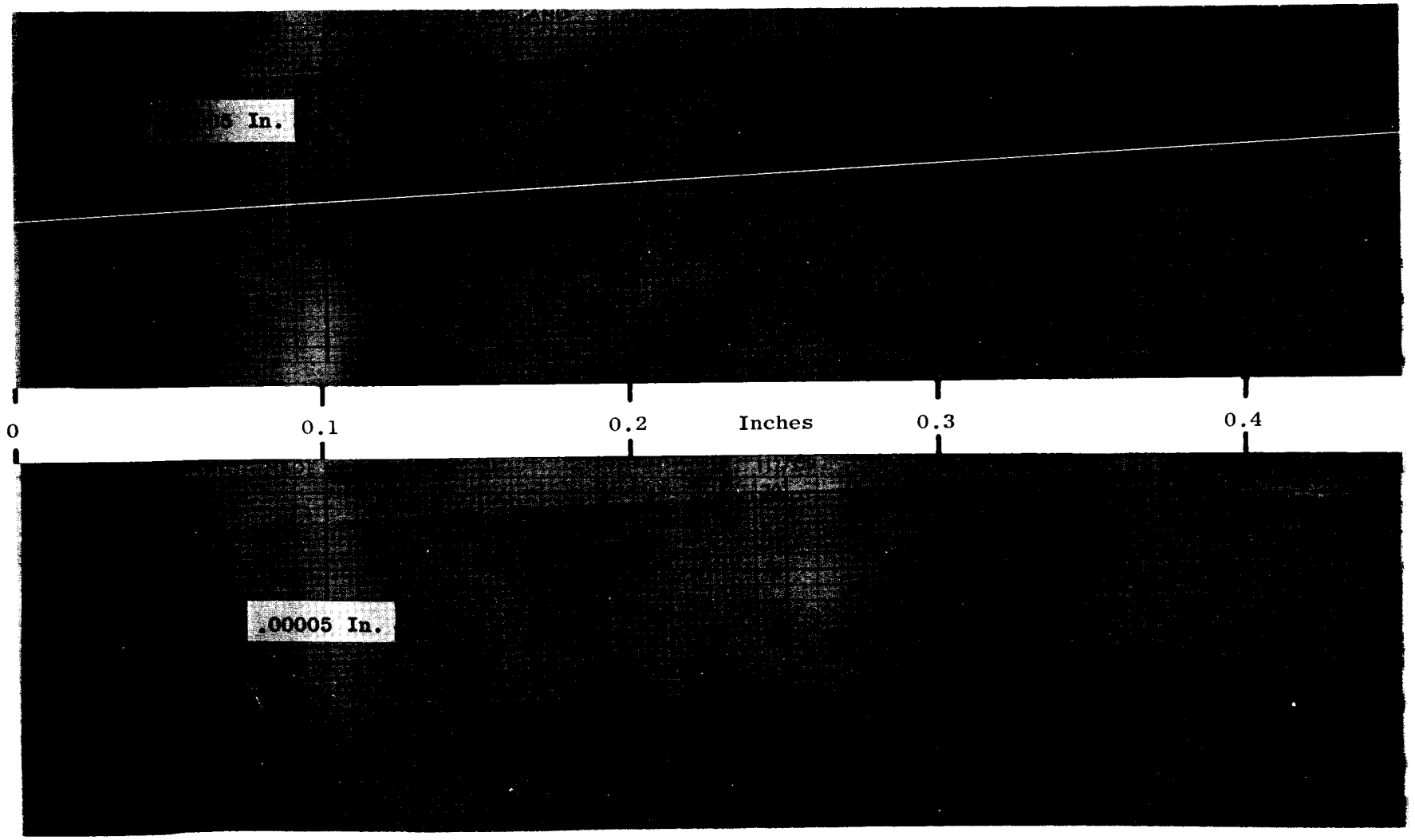

Post-Test Profilometer Trace - Radial at 90° CW from S/N

FRICTION AND WEAR TEST DATA FOR CARBOLOY 907 VS CARBOLOY 907 IN HIGH VACUUM

Test No. - 500K05A

Assembly No. - I

Loading Arm No. - 4

Test Date - 6/11/65

Rider
Material - Carboloy 907
Specimen No. - 1036-E-4

Disc
Material - Carboloy 907
Specimen No. - 1036-F-4B

Test Temperature, °F - RT

Max. ΔT of Rider, °F - 5

Speed, SFM - 500

Test Duration, Min. - 60.00

Compressive Load, Lbs - 0.141(K)

Compressive Stress, psi - 132,640

Load/Material UCS or 0.2%CYS -
Rider - 19
Disc - 19

Average Coefficient of Friction - 0.65

Chamber Pressure, Torr -
Start - 5.5×10^{-9}
Max. - 9.4×10^{-9}

Remarks -

Change in Coefficient of Friction with Time -

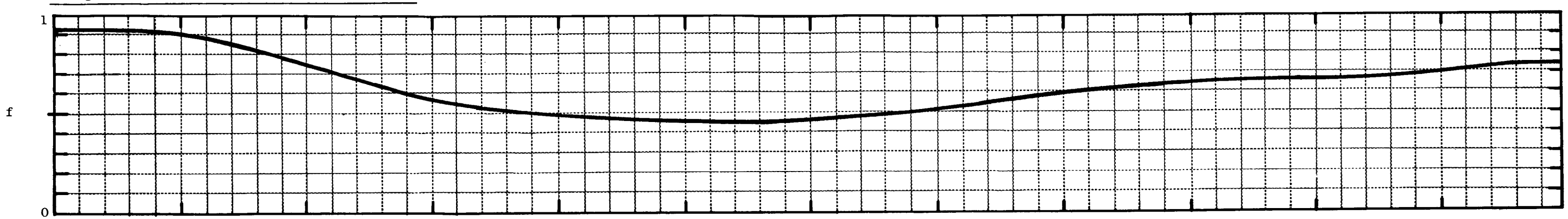

WEAR - RIDER

Initial Surface Finish - Not measured, <6

Wear Scar Dia., In. - 0

Weight, Gms -
Start - 3.5031
Finish - 3.5032
Change - +0.0001

Material Density, Gms/Cm^3 - 14.684

Volume Change, Mm^3 - +0.007

Wear Rate, $In^3/10^{10}ft$ - +0.138

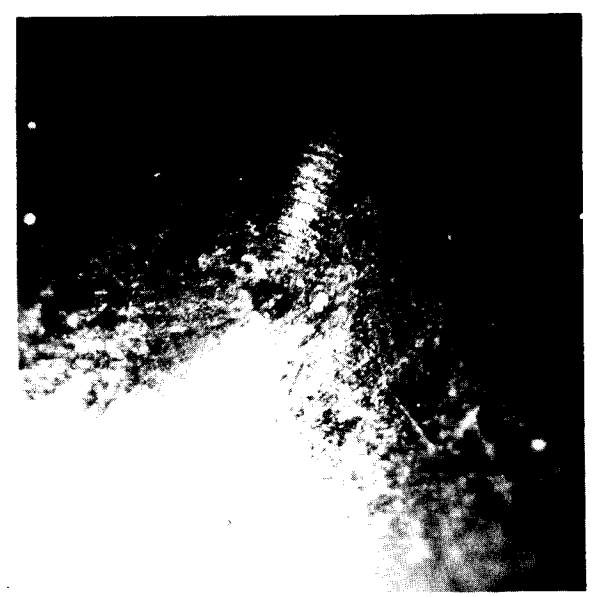

(C66081625) Mag.: 28.5X

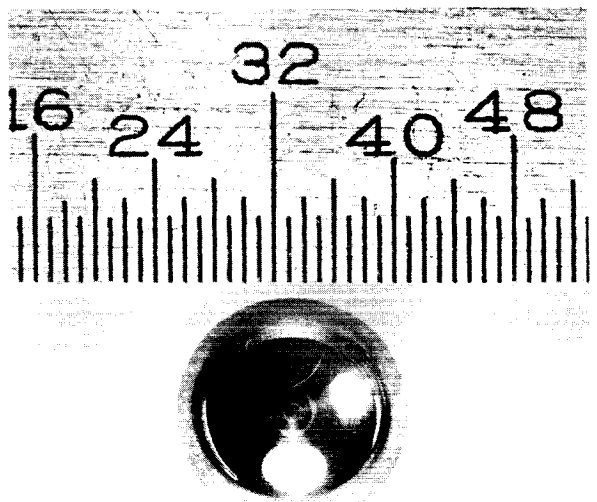

(C65081332) Mag.: 5X

WEAR - DISC

Test No. - 500K05A

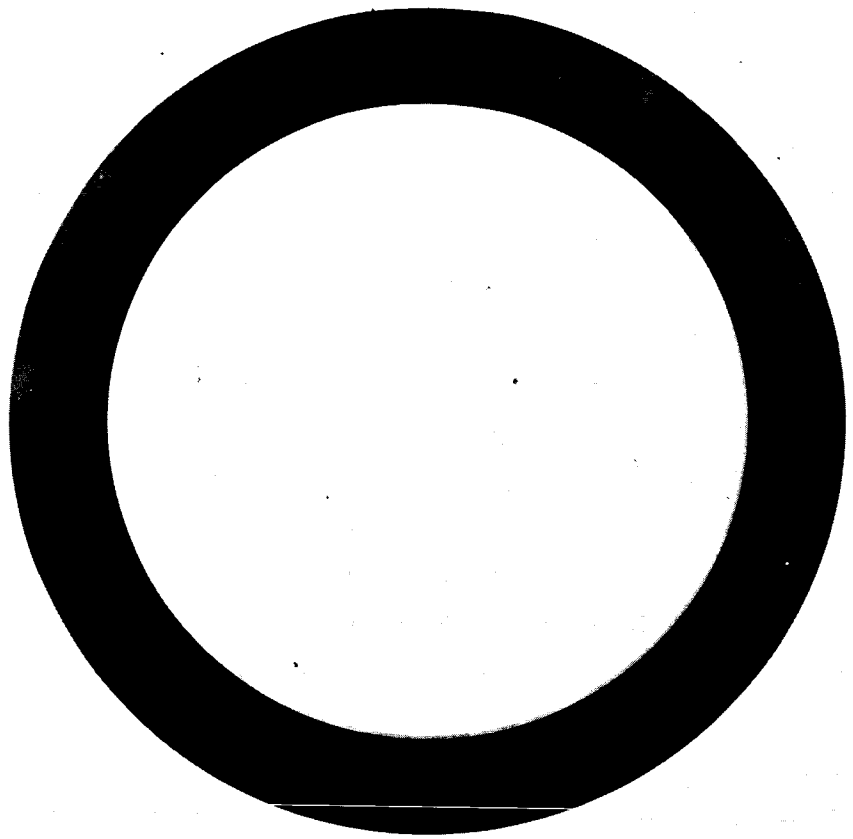

(C65081304) Mag.: 1X

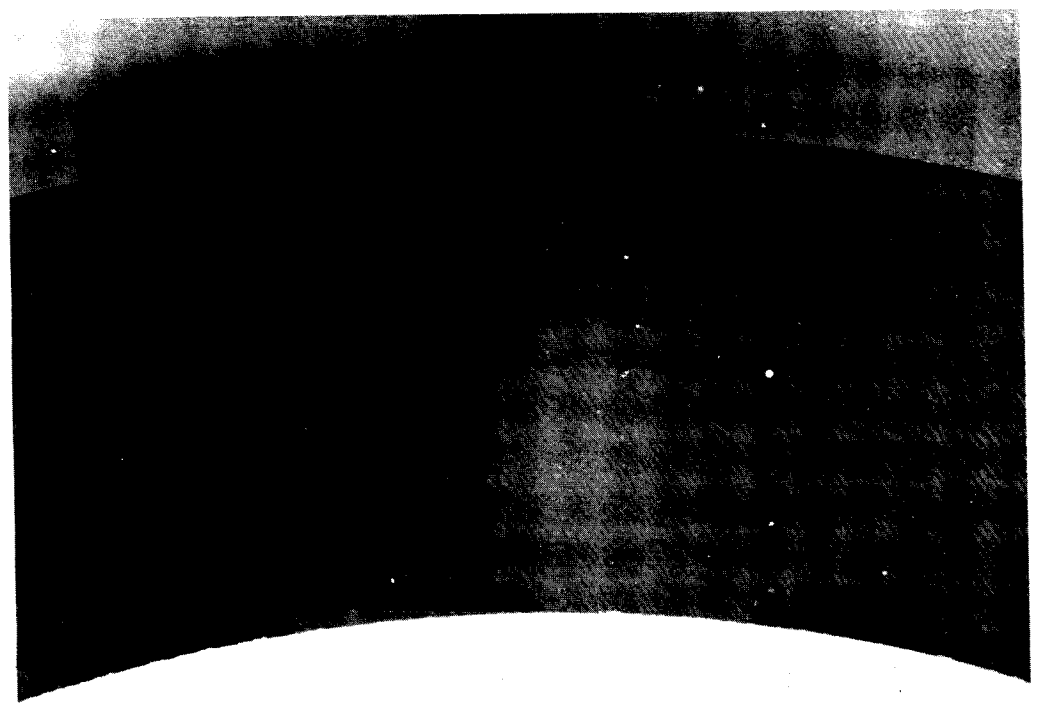

(C65081338) Mag.: 5X

Initial Surface Finish, Avg. RMS - 3-4

Wear Scar Width, In. - 0.010

Weight, Gms /Cm^3 -
Start - 226.0991
Finish - 226.0986
Change - -0.0005

Material Density, Gms /Cm^3 - 14.684

Volume Change, Mm^3 - 0.034

Wear Rate, $In^3/10^{10}ft$ - -0.689

Post-Test Profilometer Trace - Circumferential at 90° CW from S/N

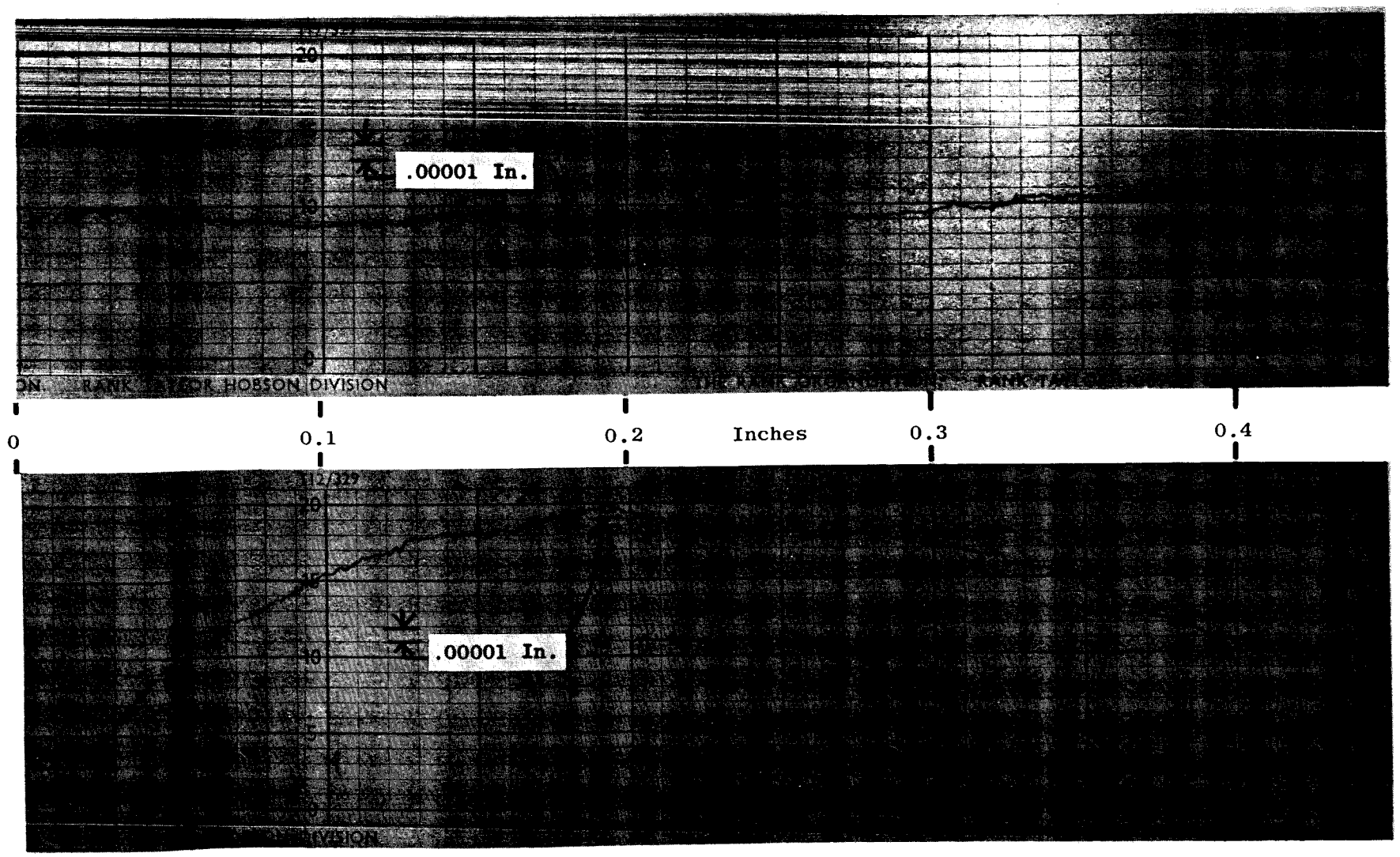

Post-Test Profilometer Trace - Radial at 90° CW from S/N

FRICTION AND WEAR TEST DATA FOR Mo-TZM ALLOY VS CARBOLOY 907 IN HIGH VACUUM

Test No. - 400905A

Assembly No. - II

Loading Arm No. - 1

Test Date - 6/19/65

Rider
Material - Mo-TZM
Specimen No. - 1037-E-5

Disc
Material - Carboloy 907
Specimen No. - 1036-F-5A

Test Temperature, ^{o}F - RT

Max. ΔT of Rider, ^{o}F - 35

Speed, SFM - 500

Test Duration, Min. - 60.00

Compressive Load, Lbs - 0.083(P9)

Compressive Stress, psi - 94,810

Load/Material UCS or 0.2%CYS -
Rider - 87
Disc - 13

Average Coefficient of Friction - -

Chamber Pressure, Torr -
Start - 7.0×10^{-9}
Max. - 1.7×10^{-8}

Remarks - Coefficient of friction value not considered valid because of inaccuracies in torque measurement.

Change in Coefficient of Friction with Time - No Plot

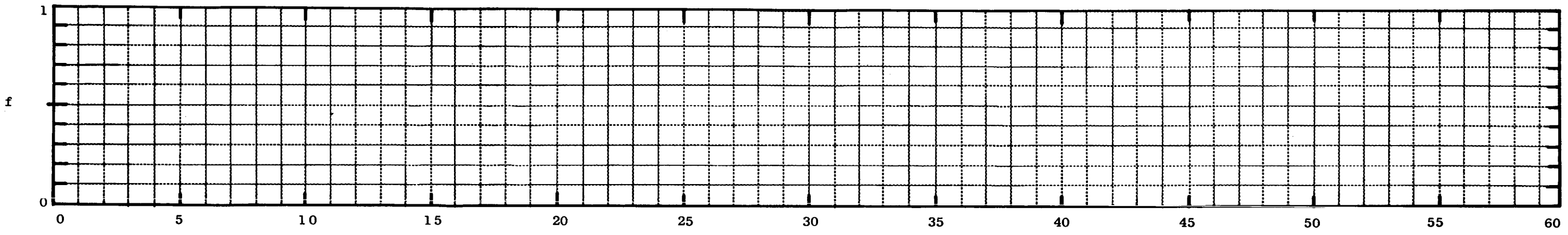

WEAR - RIDER

Initial Surface Finish - Not measured, < 6

Wear Scar Dia., In. - 0.080

Weight, Gms -
Start - 2.3877
Finish - 2.3875
Change - -0.0002

Material Density, Gms/Cm^3 - 10.139

Volume Change, Mm^3 - -0.0197

Wear Rate, $In^3/10^{10}ft$ - -0.344

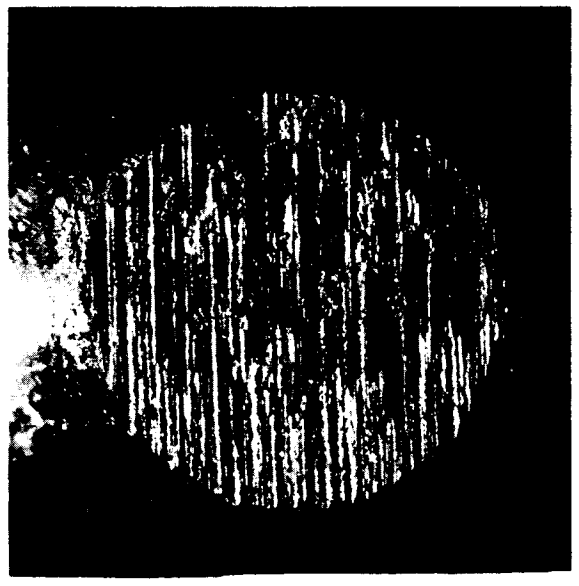

(C66081663) Mag.: 28.5X

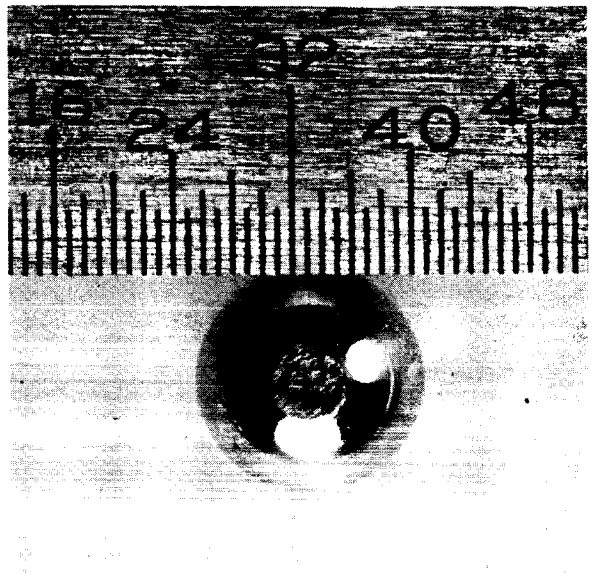

(C65081334) Mag.: 5X

WEAR - DISC

Test No. - 400905A

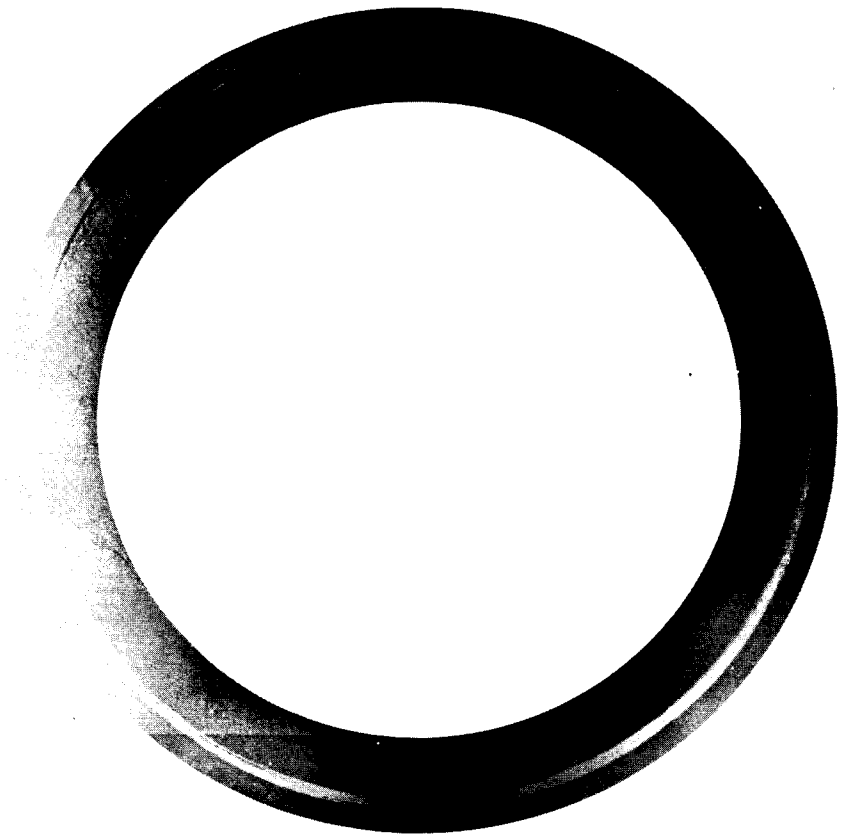

Mag.: 1X

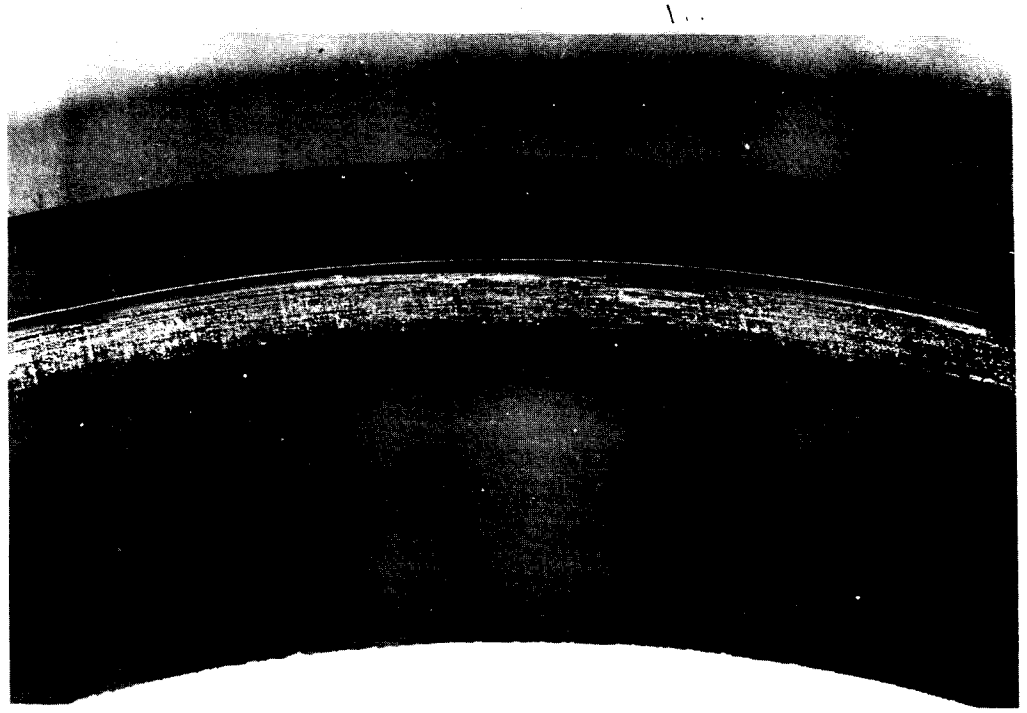

(C65081341) Mag.: 5X

Initial Surface Finish, Avg. RMS - 1.5-3

Wear Scar Width, In. - 0.063

Weight, Gms /Cm^3 -
Start - 225.9902
Finish - 225.9911
Change - +0.0009

Material Density, Gms /Cm^3 - 10.139(1)

Volume Change, Mm^3 - +0.089(1)

Wear Rate, $In^3/10^{10}ft$ - +1.56

Notes -

(1) Based on transfer of Mo-TZM alloy rider material.

Post-Test Profilometer Trace - Circumferential at 90° CW from S/N

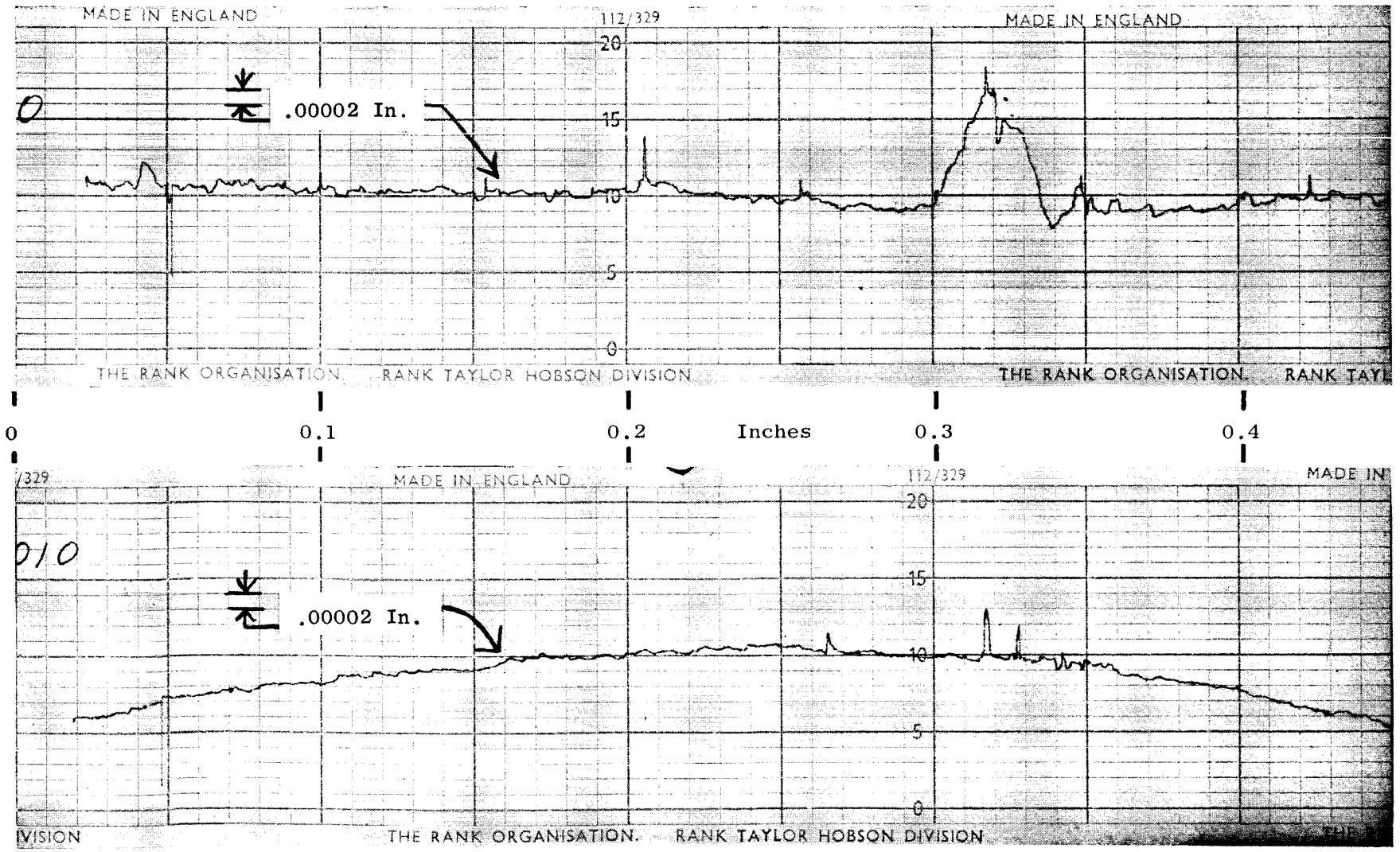

Post-Test Profilometer Trace - Radial at S/N

FRICTION AND WEAR TEST DATA FOR CARBOLOY 907 VS CARBOLOY 907 IN HIGH VACUUM

Test No. - 500705A

Assembly No. - II

Loading Arm No. - 3

Test Date - 6/19/65

Rider
Material - Carboloy 907
Specimen No. - 1036-E-3

Disc
Material - Carboloy 907
Specimen No. - 1036-F-3B

Test Temperature, ^{o}F - RT

Max. ΔT of Rider, ^{o}F - 190

Speed, SFM - 500

Test Duration, Min. - 1.92

Compressive Load, Lbs - 6.90(P_7)

Compressive Stress, psi - 485,400

Load/Material UCS or 0.2%CYS -
Rider - 69
Disc - 69

Average Coefficient of Friction - 0.63

Chamber Pressure, Torr -
Start - 6.5×10^{-9}
Max. - 1.2×10^{-8}

Remarks - Test terminated due to slippage of magnetic drive.

Change in Coefficient of Friction with Time -

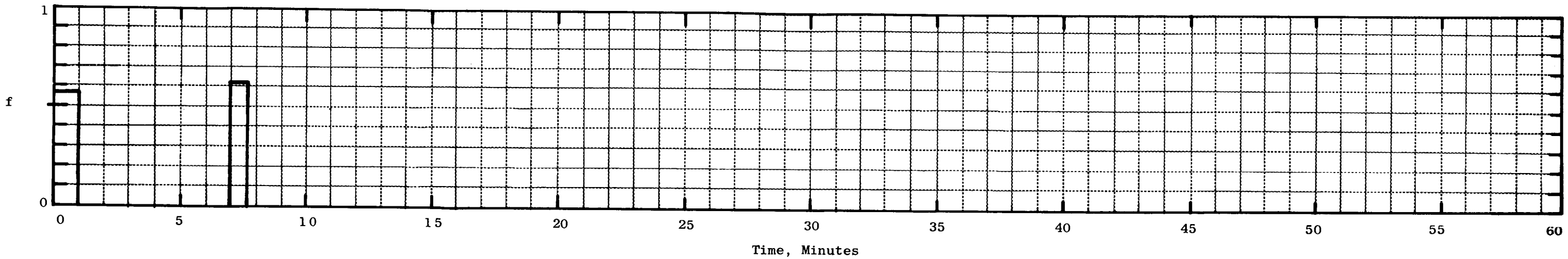

WEAR - RIDER

Initial Surface Finish - Not measured, <6

Wear Scar Dia., In. - 0.109

Weight, Gms -
Start - 3.4934
Finish - 3.4816
Change - -0.0018

Material Density, Gms/Cm^3 - 14.684

Volume Change, Mm^3 - -122.58

Wear Rate, $In^3/10^{10}ft$ - -76.5

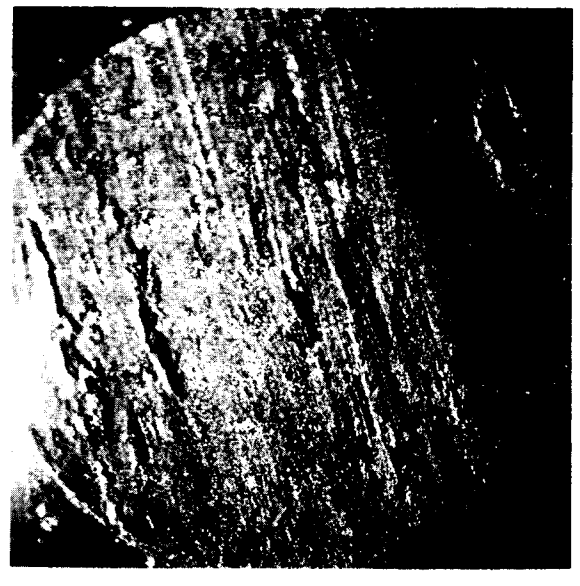

(C66081604) Mag.: 28.5X

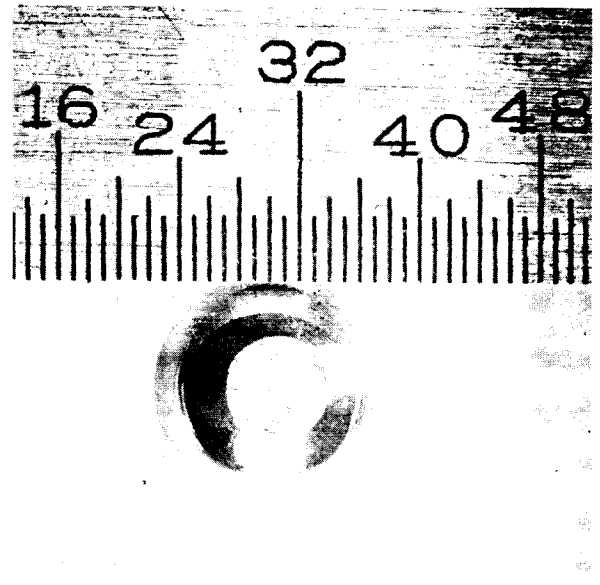

(C65081333) Mag.: 5X

WEAR - DISC

Test No. - 500705A

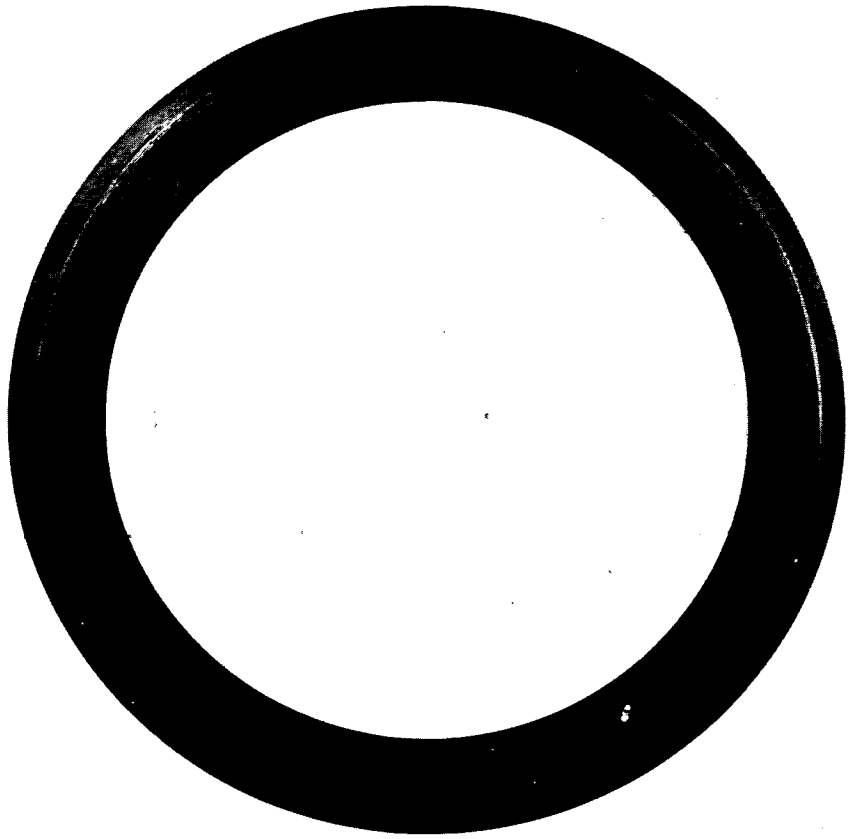

Mag.: 1X

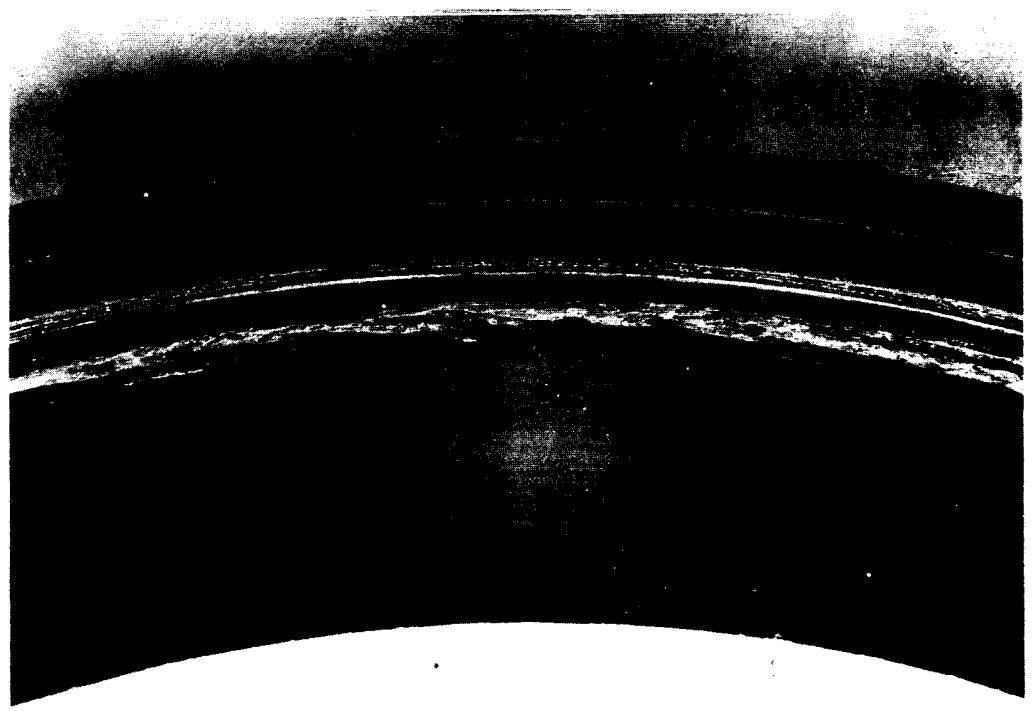

(65081337)

Mag.: 5X

Initial Surface Finish, Avg. RMS - N/A, < 6

Wear Scar Width, In. - 0.078

Weight, Gms /Cm^3 -
Start - 226.5416
Finish - 226.5444
Change - +0.0028

Material Density, Gms /Cm^3 - 14.684

Volume Change, Mm^3 - +0.191

Wear Rate, $In^3/10^{10}ft$ - +119

Post-Test Profilometer Trace - Circumferential at 90° CW from S/N

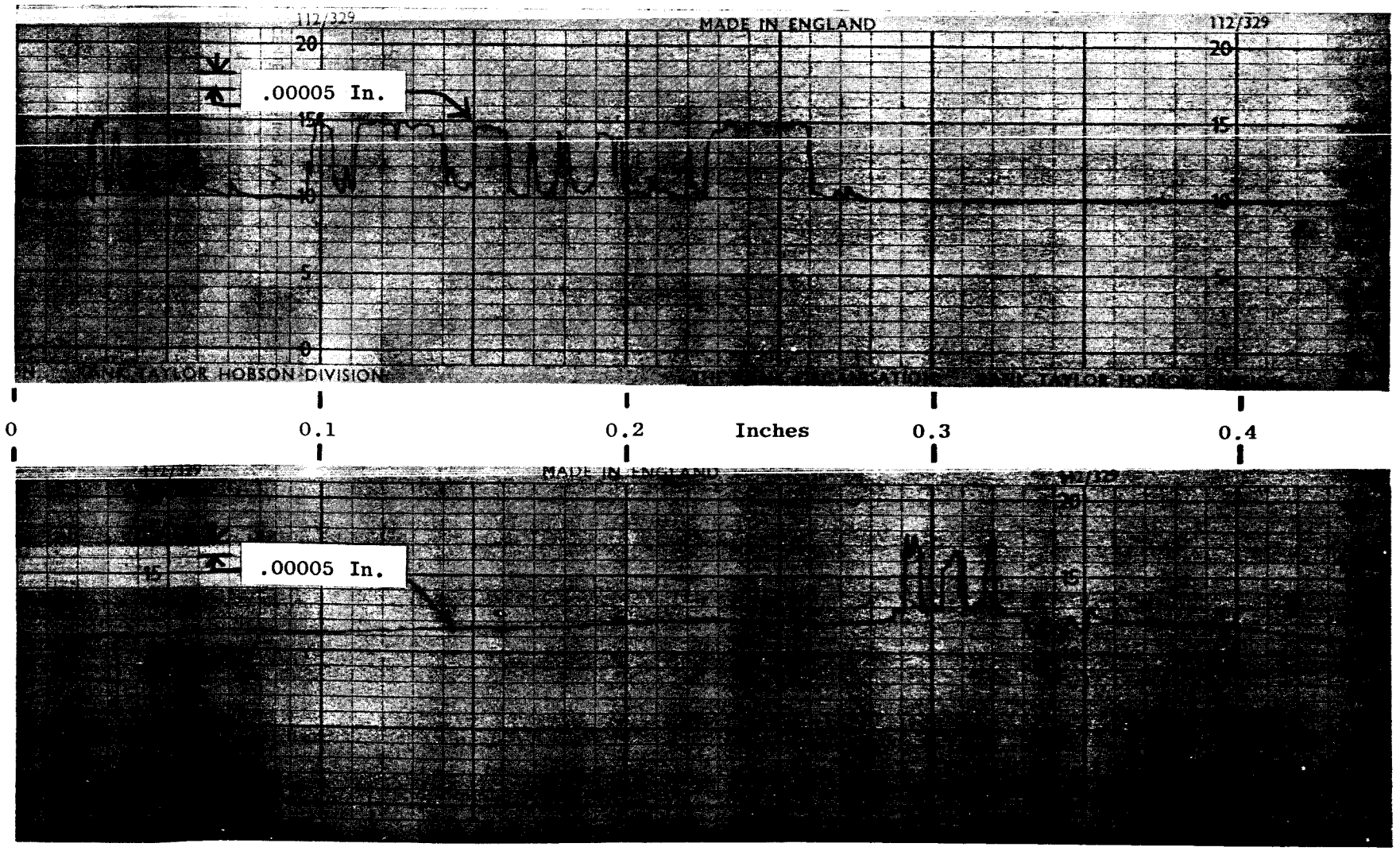

Post-Test Profilometer Trace - Radial at 90° CW from S/N

FRICTION AND WEAR TEST DATA FOR Mo-TZM ALLOY VS CARBOLOY 907 IN HIGH VACUUM

Test No. - 404905A

Assembly No. - II

Loading Arm No. - 4

Test Date - 6/21/65

Rider
Material - Mo-TZM
Specimen No. - 1037-E-6

Disc
Material - Carboloy 907
Specimen No. - 1036-F-6A

Test Temperature, ^{o}F - 675

Max. ΔT of Rider, ^{o}F - 0

Speed, SFM - 500

Test Duration, Min. - 60.00

Compressive Load, Lbs - 0.081(P_9)

Compressive Stress, psi - 91,020

Load/Material UCS or 0.2%CYS -
Rider - 86
Disc - 13

Average Coefficient of Friction - -

Chamber Pressure, Torr -
Start - 3.3×10^{-9}
Max. - 1.0×10^{-8}

Remarks - Coefficient of friction values not considered valid because of inaccuracies in torque measurement.

Change in Coefficient of Friction with Time - No Plot

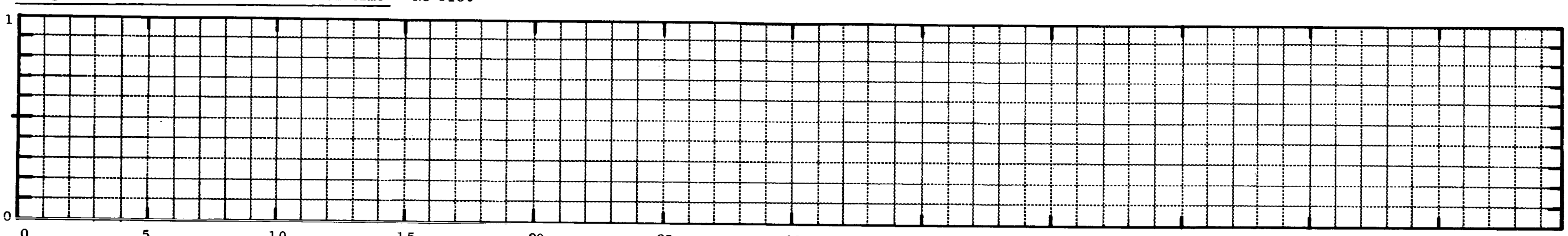

WEAR - RIDER

Initial Surface Finish - Not measured, <6

Wear Scar Dia., In. - 0.040

Weight, Gms -
Start - 2.3909
Finish - 2.3917
Change - +0.0008

Material Density, Gms/Cm^3 - 14.684(1)

Volume Change, Mm^3 - +0.0545(1)

Wear Rate, $In^3/10^{10}ft$ - +0.955

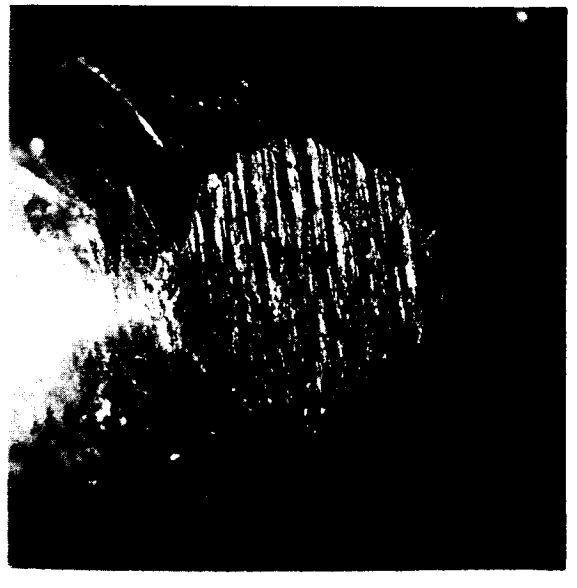

(C66081601) Mag.: 28.5X

(C65081335) Mag.: 5X

WEAR - DISC

Test No. - 404905A

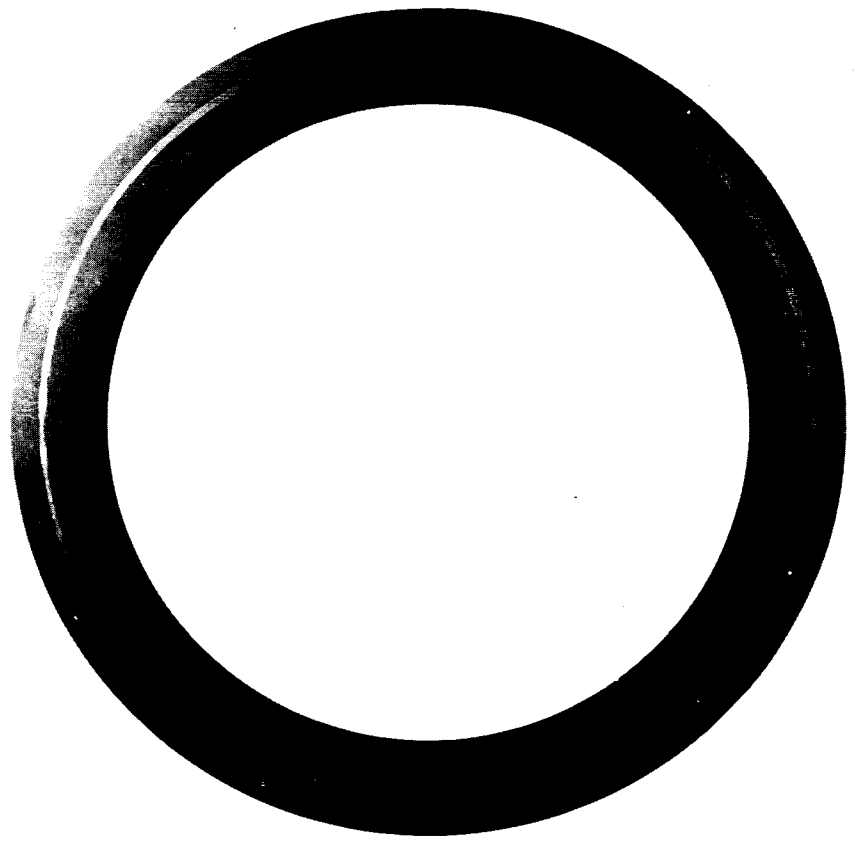

Mag.: 1X

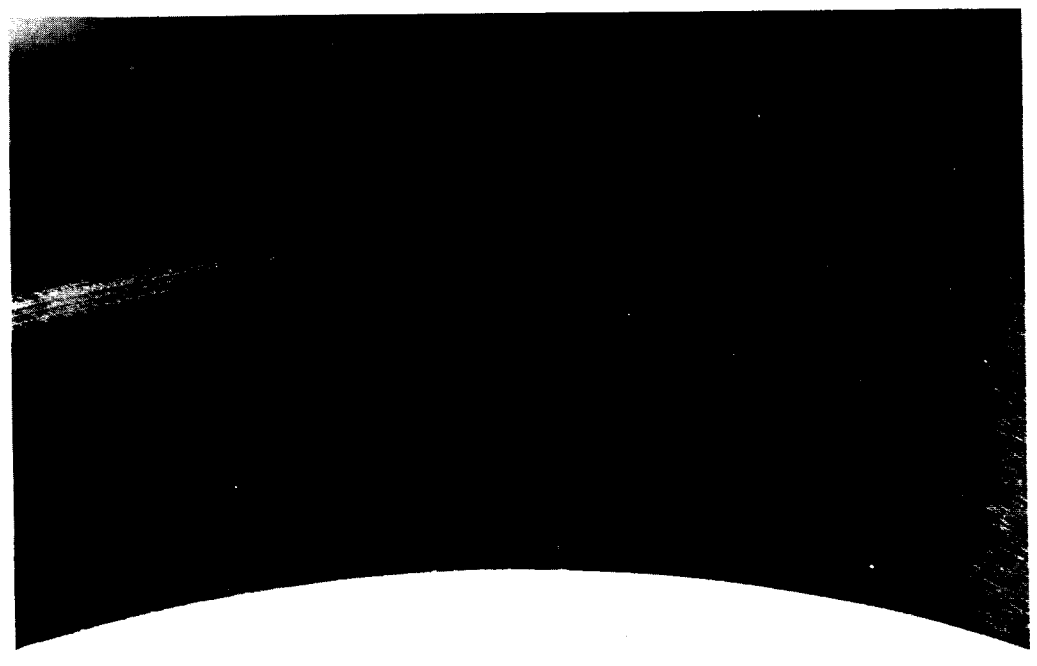

(C65081342)

Mag.: 5X

Initial Surface Finish, Avg. RMS - 2-3

Wear Scar Width, In. - 0.031

Weight, Gms /Cm^3 -
Start - 226.6134
Finish - 226.6114
Change - -0.0020

Material Density, Gms /Cm^3 - 14.684

Volume Change, Mm^3 - -0.136

Wear Rate, $In^3/10^{10}ft$ - -2.37

Notes -
(1) Based on transfer of Carboloy 907 disc material.

Post-Test Profilometer Trace - Circumferential at 90° CW from S/N

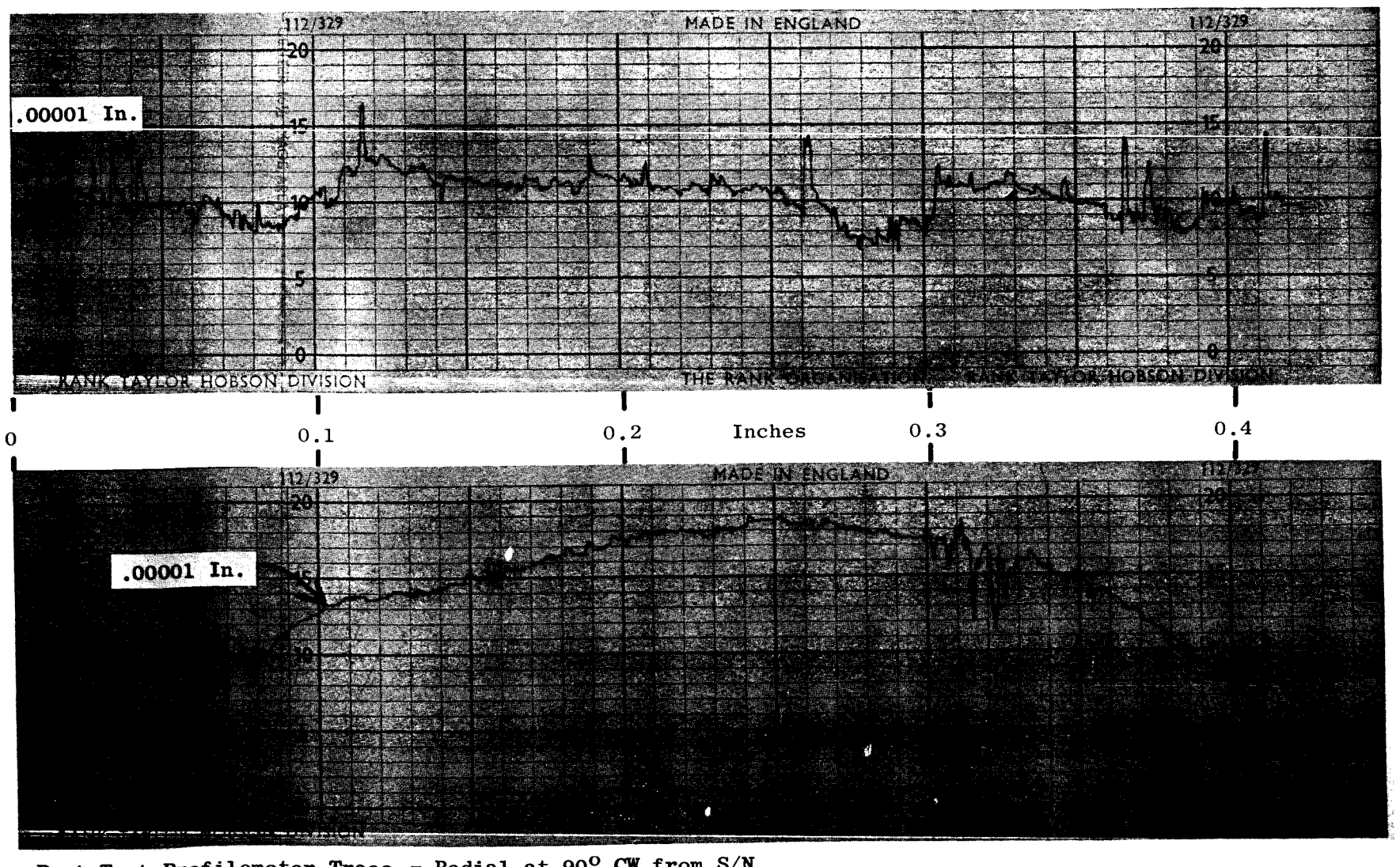

Post-Test Profilometer Trace - Radial at 90° CW from S/N

FRICTION AND WEAR TEST DATA FOR CARBOLOY 907 VS CARBOLOY 907 IN HIGH VACUUM

Test No. - 504K05A

Assembly No. - IV

Loading Arm No. - 1

Test Date - 7/9/65

Rider
Material - Carboloy 907
Specimen No. - 1036-E-5

Disc
Material - Carboloy 907
Specimen No. - 1036-F-7A

Test Temperature, ^{o}F - 720

Max. ΔT of Rider, ^{o}F - 25

Speed, SFM - 500

Test Duration, Min. - 60.00

Compressive Load, Lbs - 0.081(K)

Compressive Stress, psi - 99,980

Load/Material UCS or 0.2%CYS -
Rider - 16
Disc - 16

Average Coefficient of Friction - -

Chamber Pressure, Torr -
Start - 7.2×10^{-9}
Max. - 9.8×10^{-9}

Remarks - Coefficient of friction values not considered valid because of inaccuracies in torque measurement.

Change in Coefficient of Friction with Time - No Plot

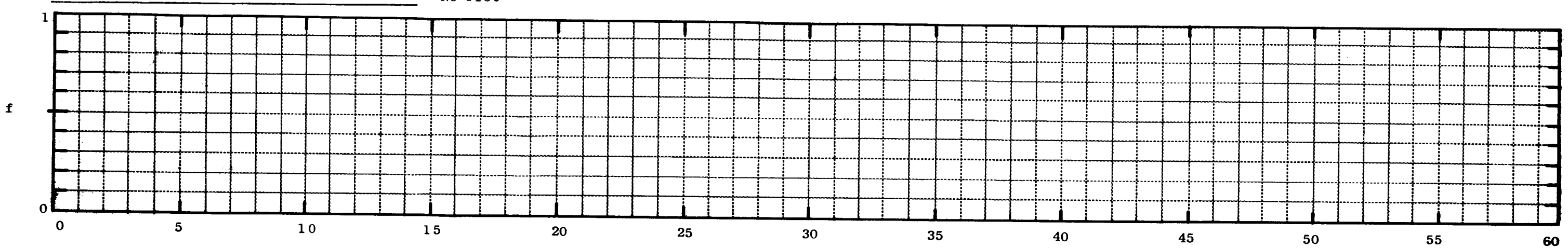

WEAR - RIDER

Initial Surface Finish -

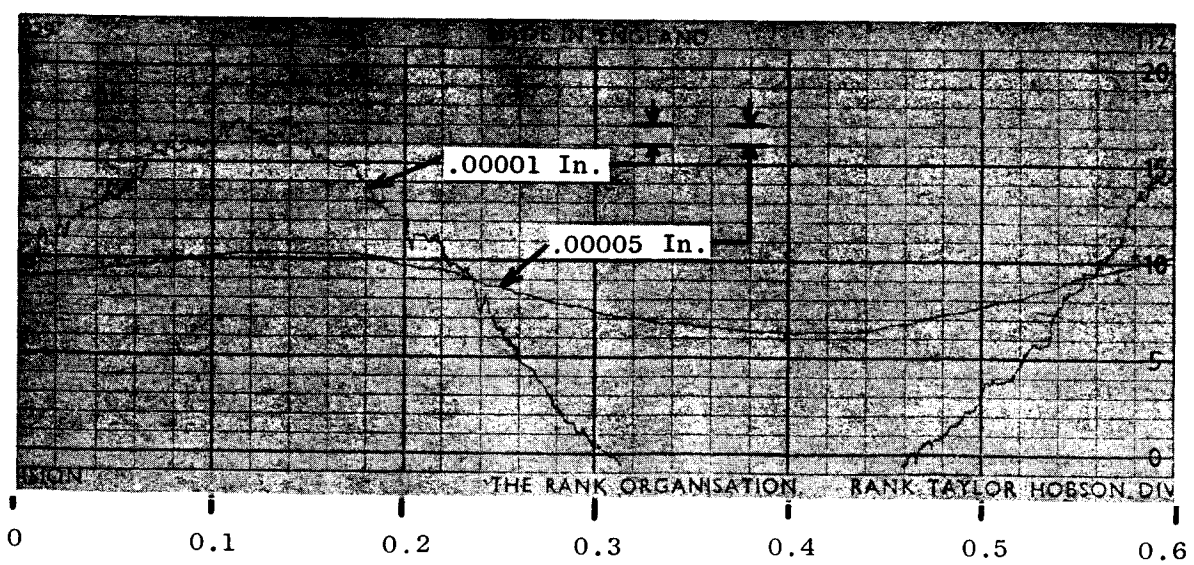

Wear Scar Dia., In. - 0

Weight, Gms -
Start - 3.5028
Finish - 3.5022
Change - -0.0006

Material Density, Gms/Cm^3 - 14.684

Volume Change, Mm^3 - -0.0409

Wear Rate, $In^3/10^{10}ft$ - -0.716

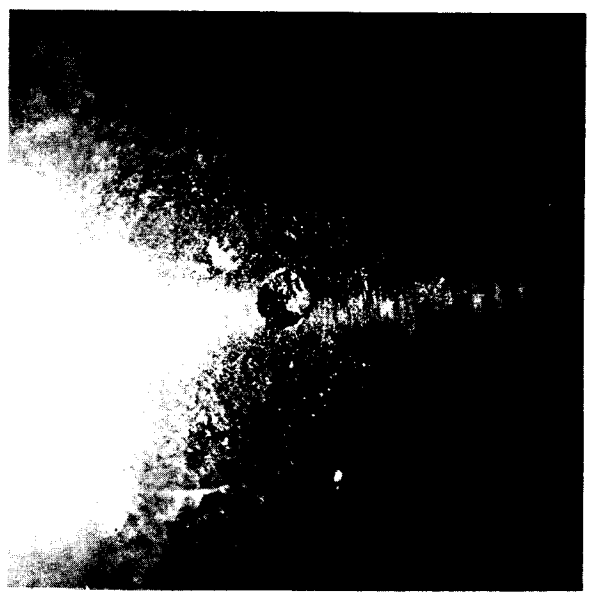

(C66081646) Mag.: 28.5X

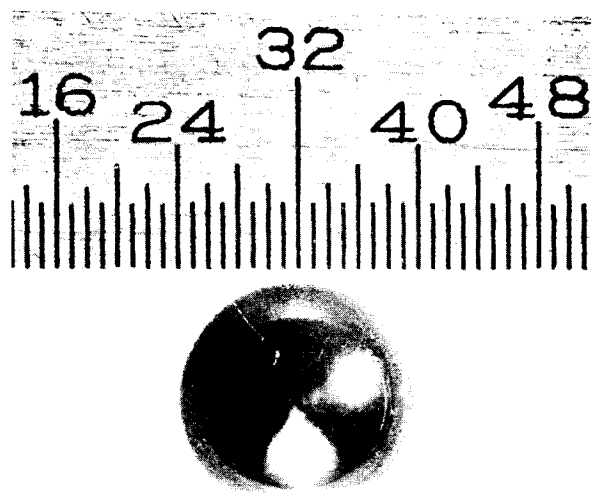

(C65081329) Mag.: 5X

WEAR - DISC

Test No. - 504K05A

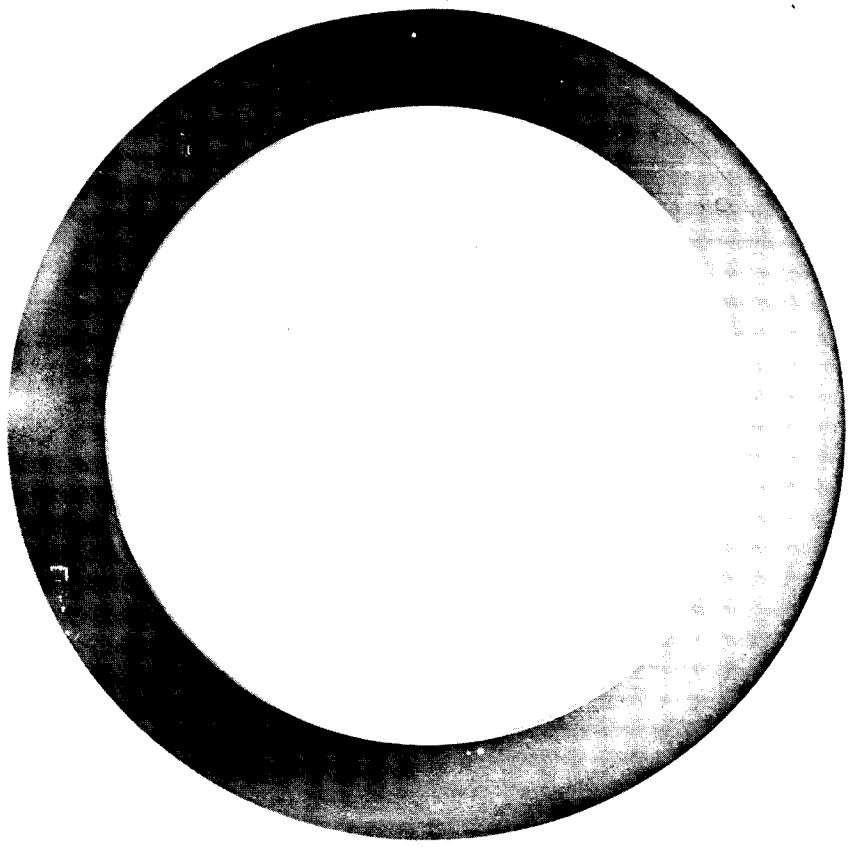

(C65081307) Mag.: 1X

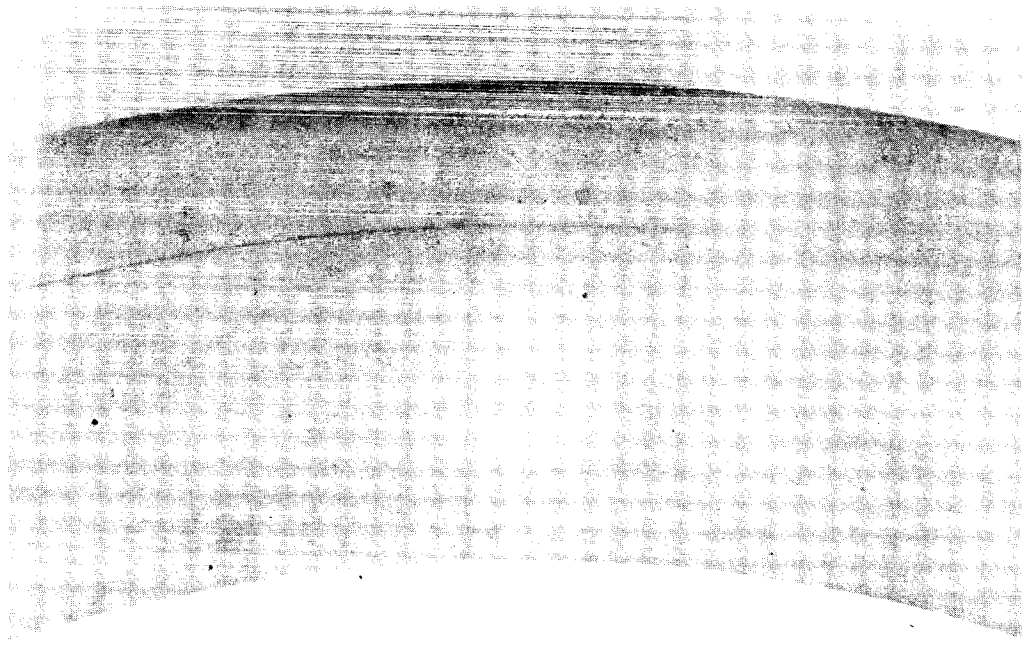

(C65081336) Mag.: 5X

Initial Surface Finish, Avg. RMS - 2.5-3.5

Wear Scar Width, In. - 0.016

Weight, Gms /Cm^3 -
Start - 225.9531
Finish - 225.9514
Change - -0.0017

Material Density, Gms /Cm^3 - 14.684

Volume Change, Mm^3 - -0.116

Wear Rate, $In^3/10^{10}ft$ - -2.03

Post-Test Profilometer Trace - Circumferential at 90° CW from S/N

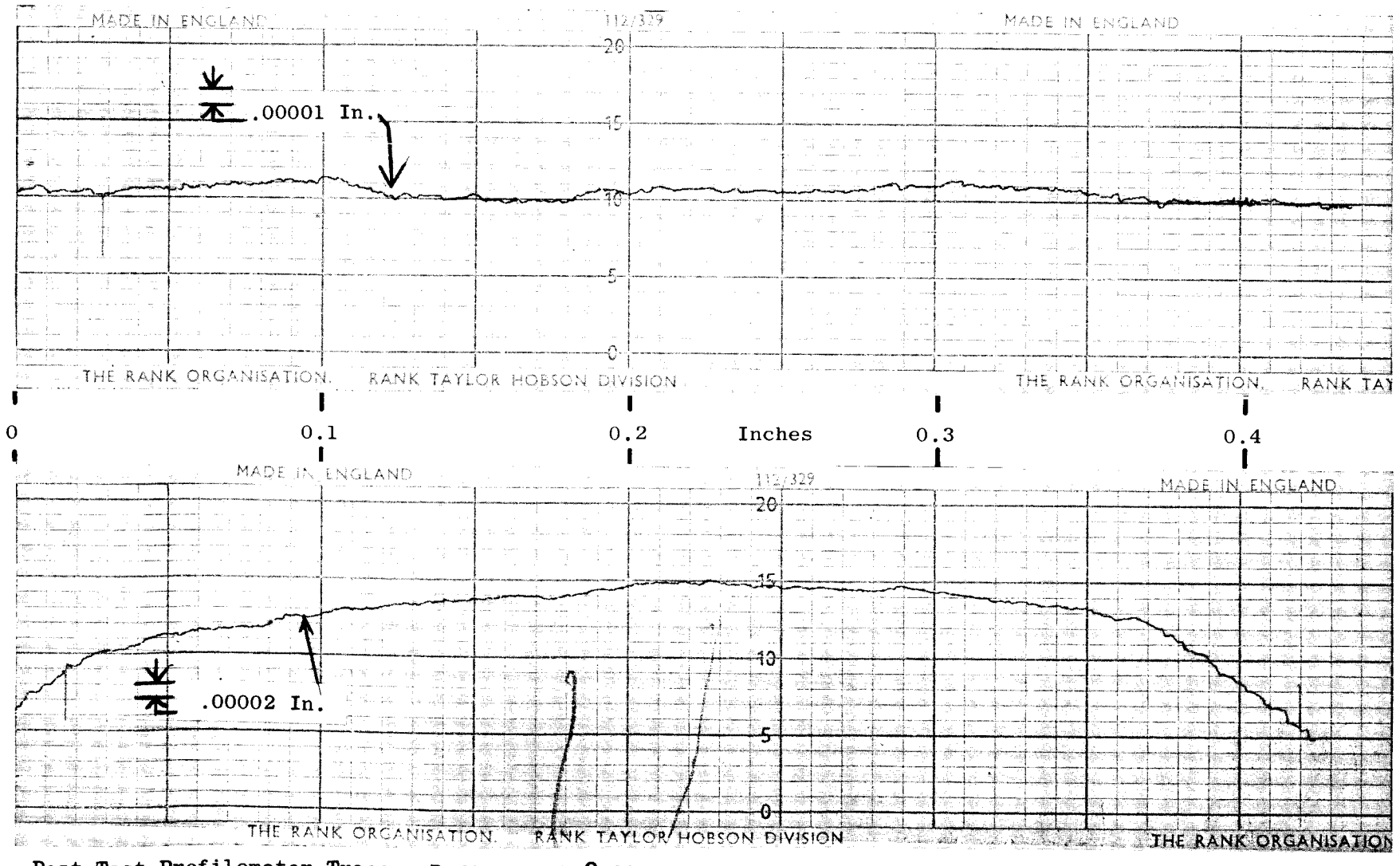

Post-Test Profilometer Trace - Radial at 90° CS from S/N

FRICTION AND WEAR TEST DATA FOR CARBOLOY 907 VS CARBOLOY 907 IN HIGH VACUUM

Test No. - 500705B

Assembly No. - IV

Loading Arm No. - 2

Test Date - 7/6/65

Rider
Material - Carboloy 907
Specimen No. - 1036-E-2

Disc
Material - Carboloy 907
Specimen No. - 1036-F-2A

Test Temperature, ^{o}F - RT

Max. ΔT of Rider, ^{o}F - 835

Speed, SFM - 500

Test Duration, Min. - 60.00

Compressive Load, Lbs - 6.90(P_7)

Compressive Stress, psi - 485,390

Load/Material UCS or 0.2%CYS -
Rider - 69
Disc - 69

Average Coefficient of Friction - 0.35

Chamber Pressure, Torr -
Start - 3.2×10^{-10}
Max. - 8.5×10^{-9}

Remarks -

Change in Coefficient of Friction with Time -

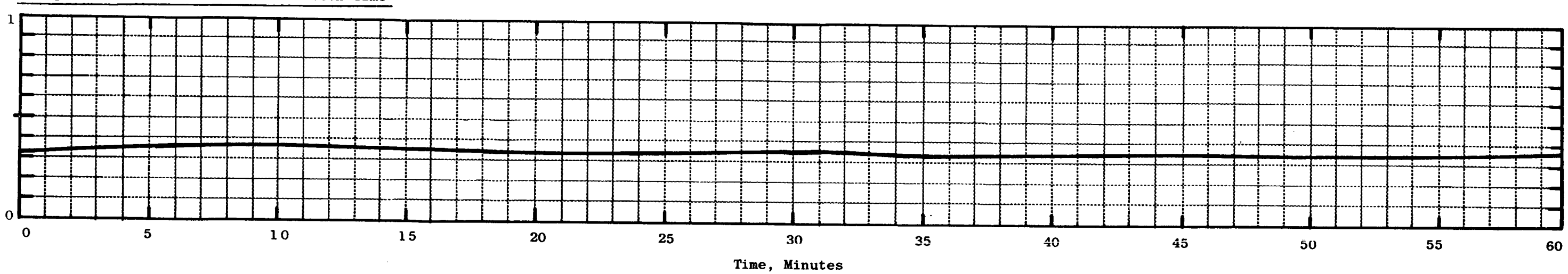

WEAR - RIDER

Initial Surface Finish - Not measured, <6

Wear Scar Dia., In. - 0.198

Weight, Gms -
Start - 3.4897
Finish - 3.3051
Change - -0.1846

Material Density, Gms/Cm^3 - 14.684

Volume Change, Mm^3 - -12.572

Wear Rate, $In^3/10^{10}ft$ - -257

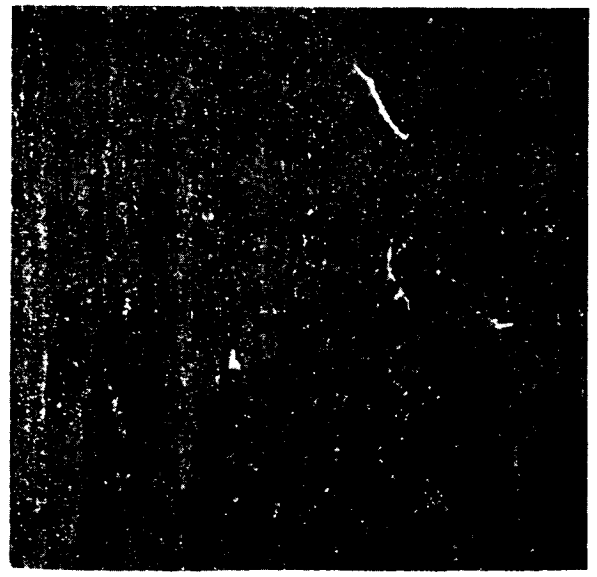

(C66081671) Mag.: 28.5X

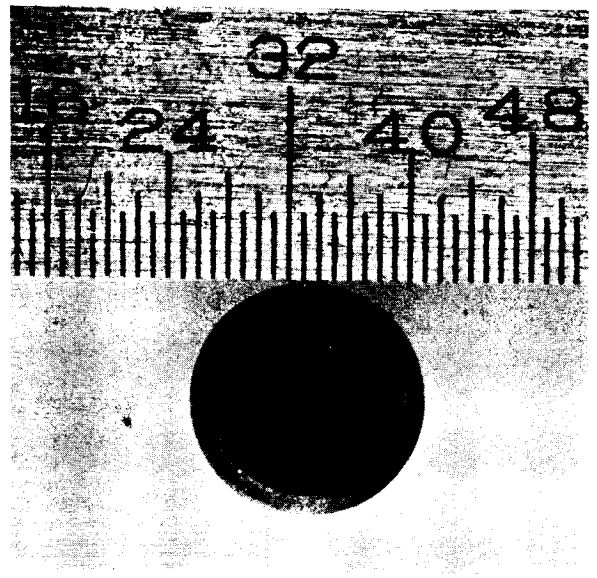

(C65081330) Mag.: 5X

WEAR - DISC

Test No. - 500705B

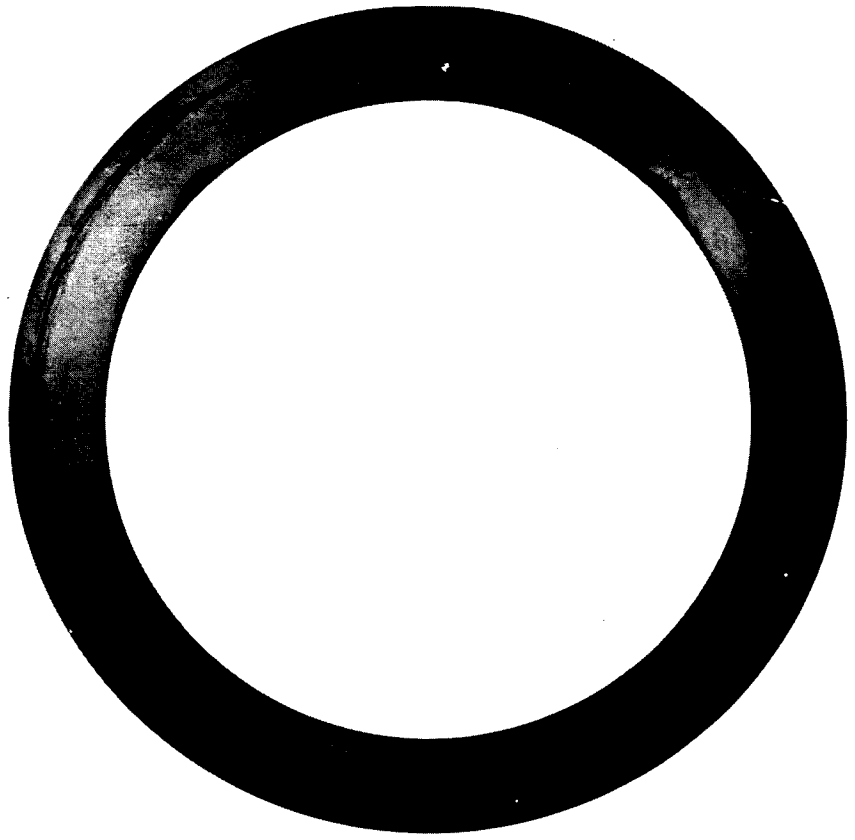

Mag.: 1X

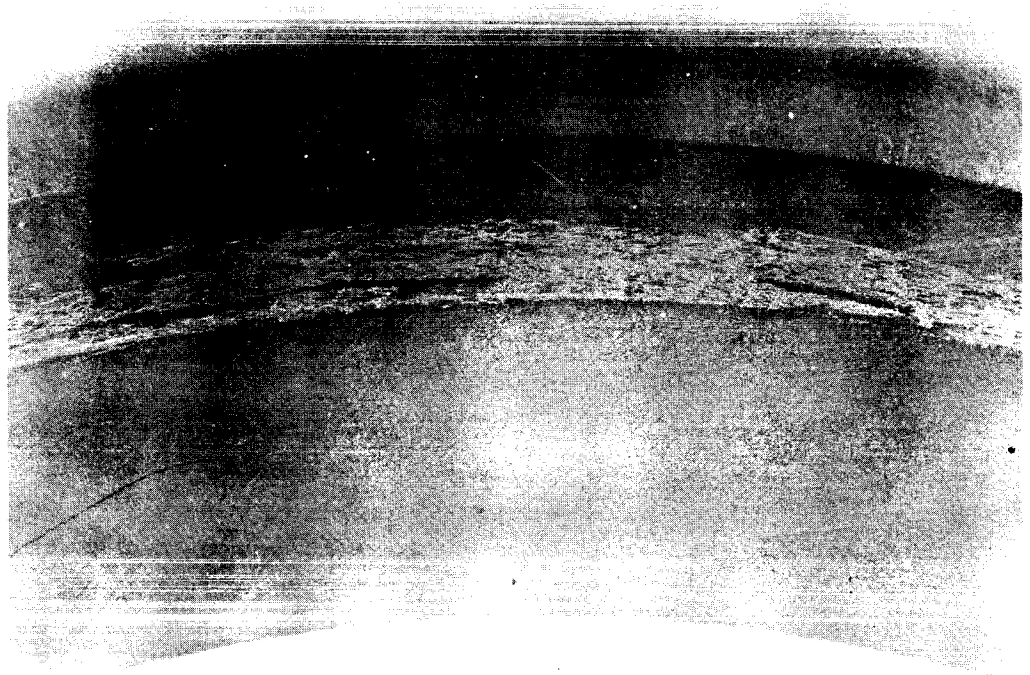

(C65081340)

Mag.: 5X

Initial Surface Finish, Avg. RMS - 3.5-5

Wear Scar Width, In. - 0.094

Weight, Gms /Cm^3 -
Start - 226.6406
Finish - 226.6508
Change - +0.0102

Material Density, Gms /Cm^3 - 14.684

Volume Change, Mm^3 - +0.695

Wear Rate, $In^3/10^{10}ft$ - +14.2

Post-Test Profilometer Trace - Circumferential at 90° CW from S/N

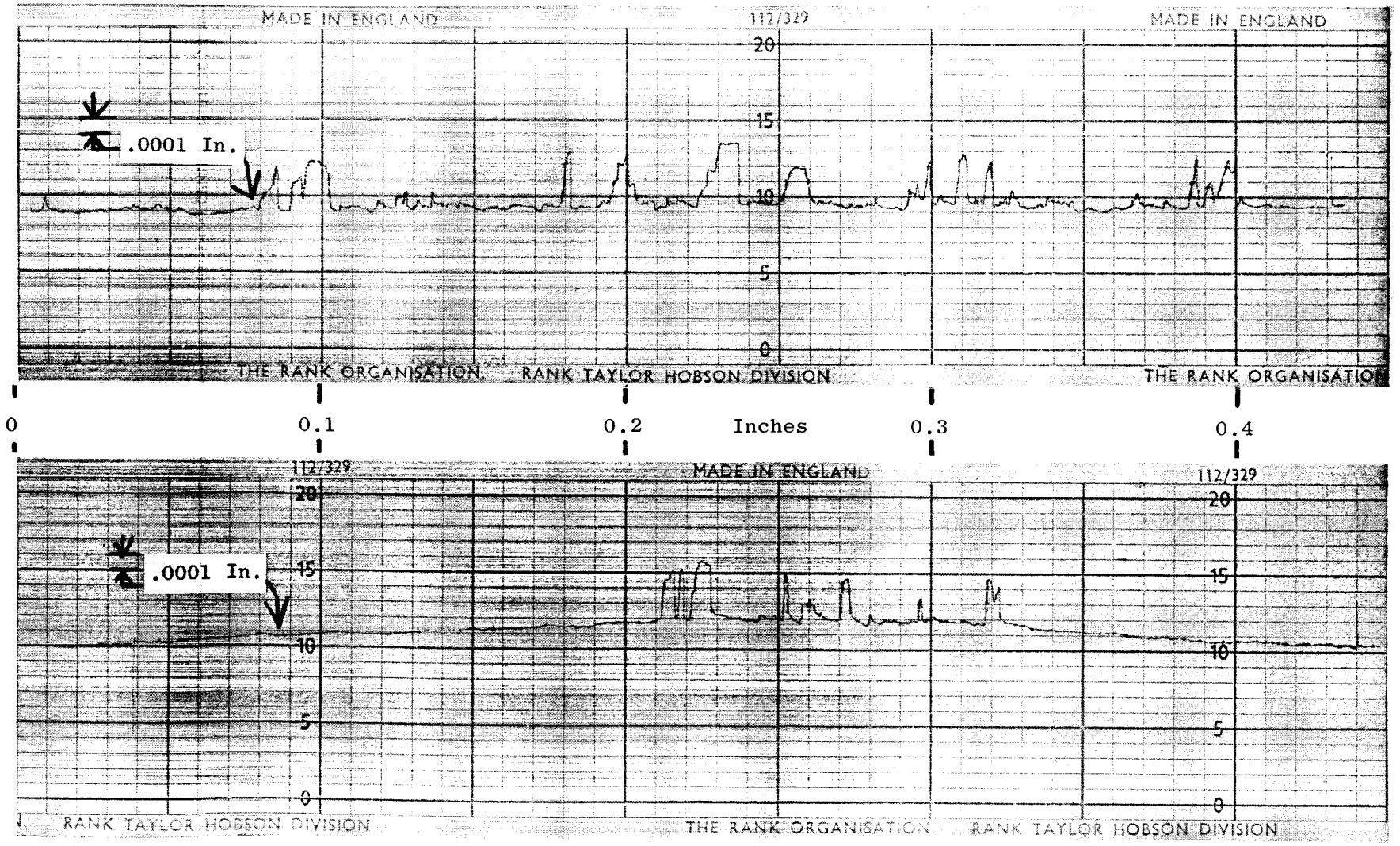

Post-Test Profilometer Trace - Radial at 90° CW from S/N

FRICTION AND WEAR TEST DATA FOR CARBOLOY 907 VS CARBOLOY 907 IN HIGH VACUUM

Test No. - 512705A

Assembly No. - V

Loading Arm No. - 1

Test Date - 8/7/65

Rider
Material - Carboloy 907
Specimen No. - 1036-E-6

Disc
Material - Carboloy 907
Specimen No. - 1036-F-10A

Test Temperature, ^{o}F - 1580

Max. ΔT of Rider, ^{o}F - 85

Speed, SFM - 500

Test Duration, Min. - 15.04

Compressive Load, Lbs - 2.58(P_7)

Compressive Stress, psi - 106,530

Load/Material UCS or 0.2%CYS -
Rider - 40
Disc - 40

Average Coefficient of Friction - 0.78

Chamber Pressure, Torr -
Start - 5.9×10^{-9}
Max. - 8.8×10^{-9}

Remarks - Test terminated due to slippage of magnetic drive.

Change in Coefficient of Friction with Time -

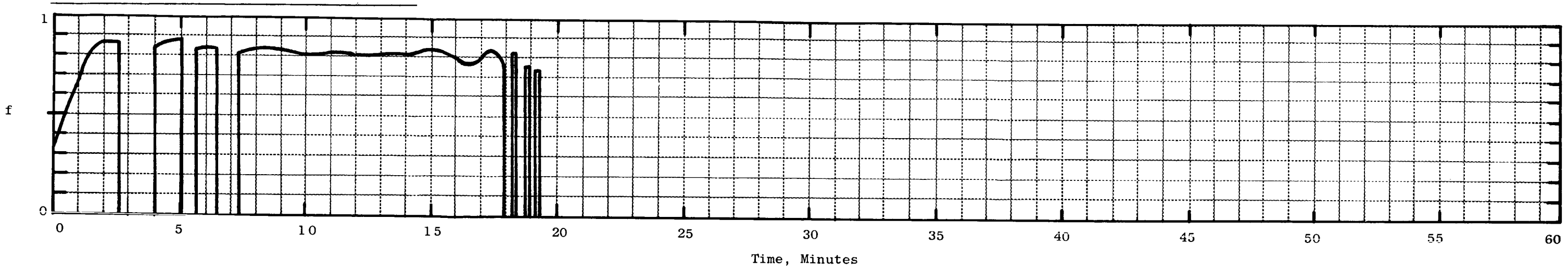

WEAR - RIDER

Initial Surface Finish -

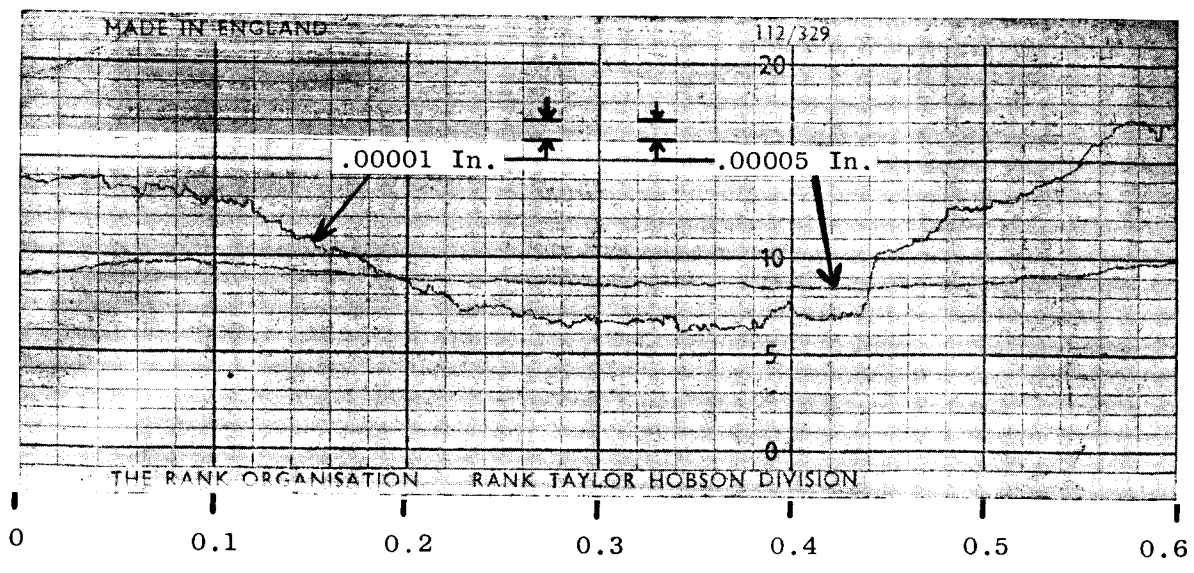

Wear Scar Dia., In. - 0.021

Weight, Gms -
Start - 3.5067
Finish - 3.5065
Change - -0.0002

Material Density, Gms/Cm^3 -
14.684

Volume Change, Mm^3 -
-0.014

Wear Rate, $In^3/10^{10}ft$ -
-1.09

(C66081603) Mag.: 28.5X

(C65081326) Mag.: 5X

WEAR - DISC

Test No. - 512705A

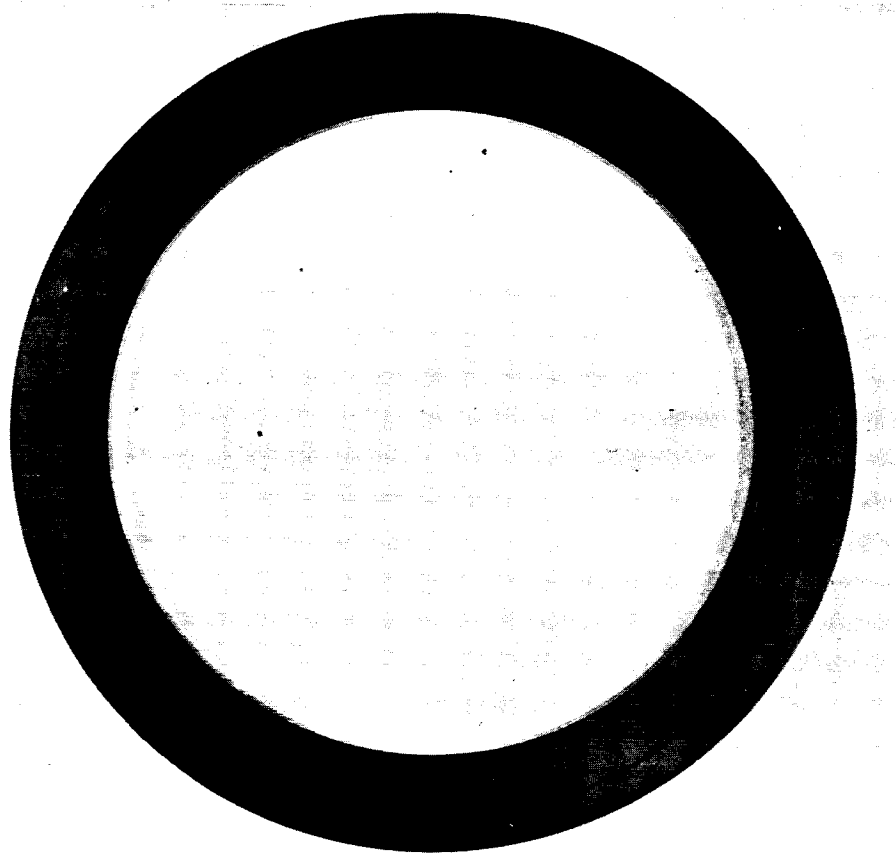

Mag.: 1X

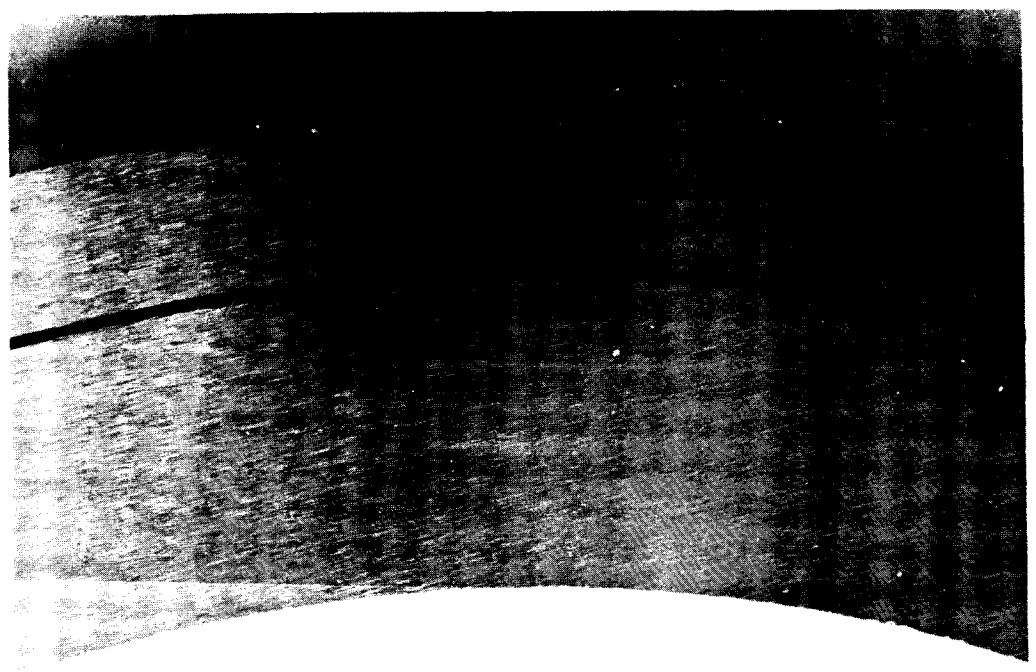

(C65081343)

Mag.: 5X

Initial Surface Finish, Avg. RMS - 4.5-5

Wear Scar Width, In. - 0.016

Weight, Gms /Cm^3 -
Start - 226.2255
Finish - 226.2254
Change - -0.0001

Material Density, Gms /Cm^3 - 14.684

Volume Change, Mm^3 - -0.007

Wear Rate, $In^3/10^{10}ft$ - -0.545

Post-Test Profilometer Trace - Circumferential at S/N

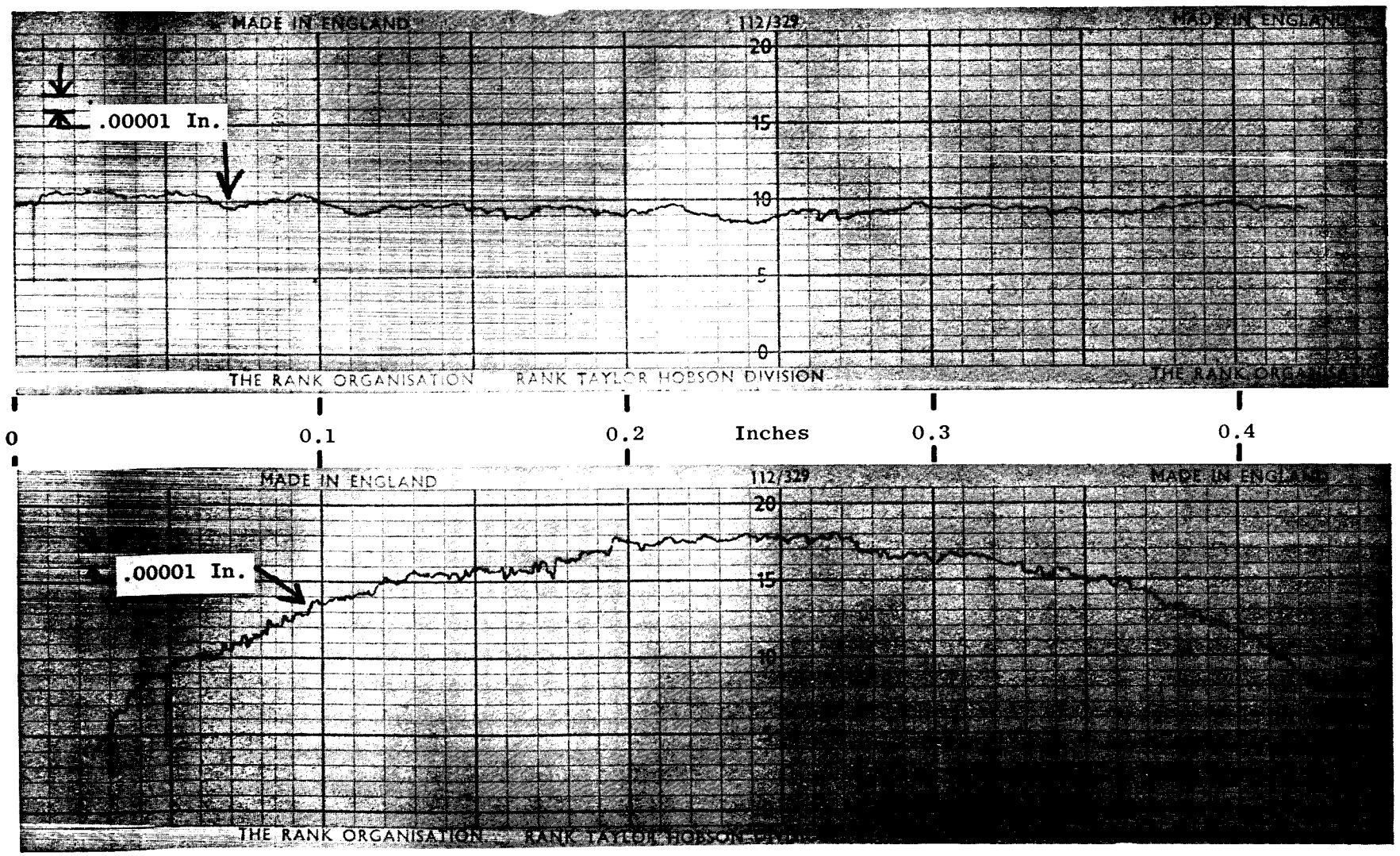

Post-Test Profilometer Trace - Radial at S/N

WEAR - DISC

Test No. - 512H05A

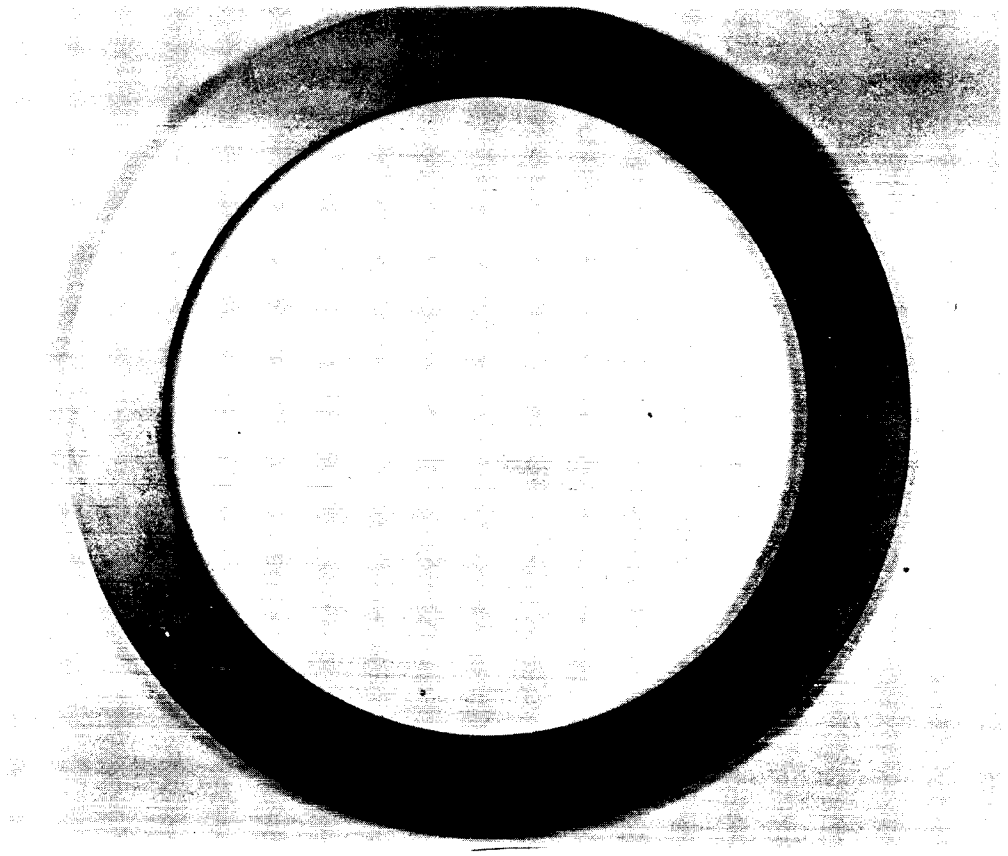

(C65081311) Mag.: 1X

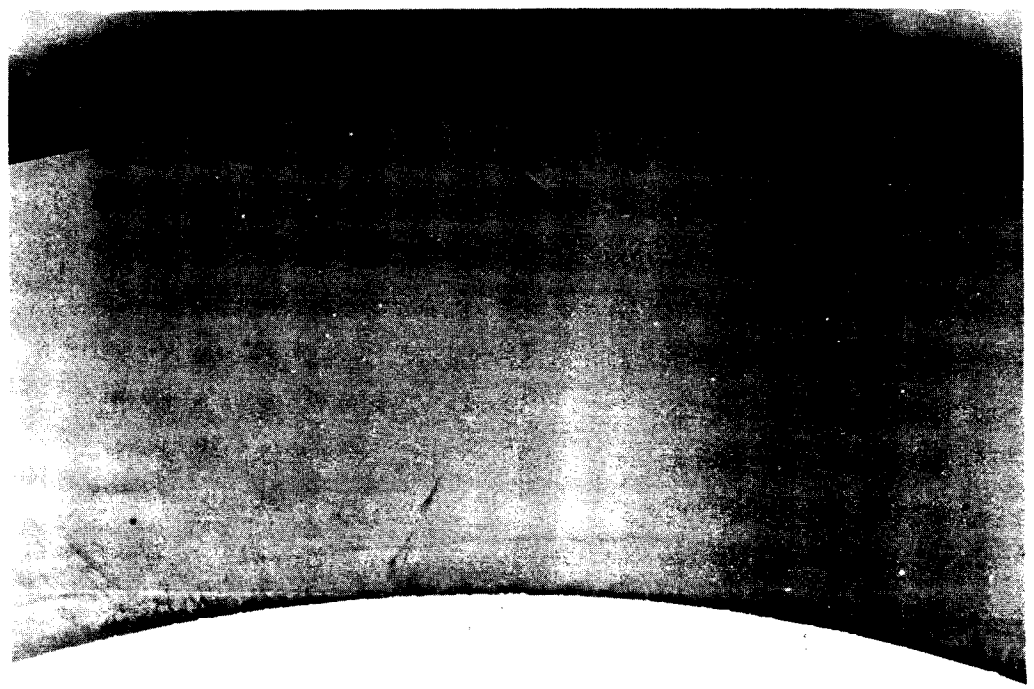

(C65081344) Mag.: 5X

Initial Surface Finish, Avg. RMS - 1.5-3

Wear Scar Width, In. - 0.016

Weight, Gms /Cm^3 -
Start - 226.8792
Finish - 226.8655
Change - -0.0137

Material Density, Gms /Cm^3 - 14.684

Volume Change, Mm^3 - -0.933

Wear Rate, $In^3/10^{10}ft$ - -16.0

Post-Test Profilometer Trace - Circumferential at 90° CW from S/N

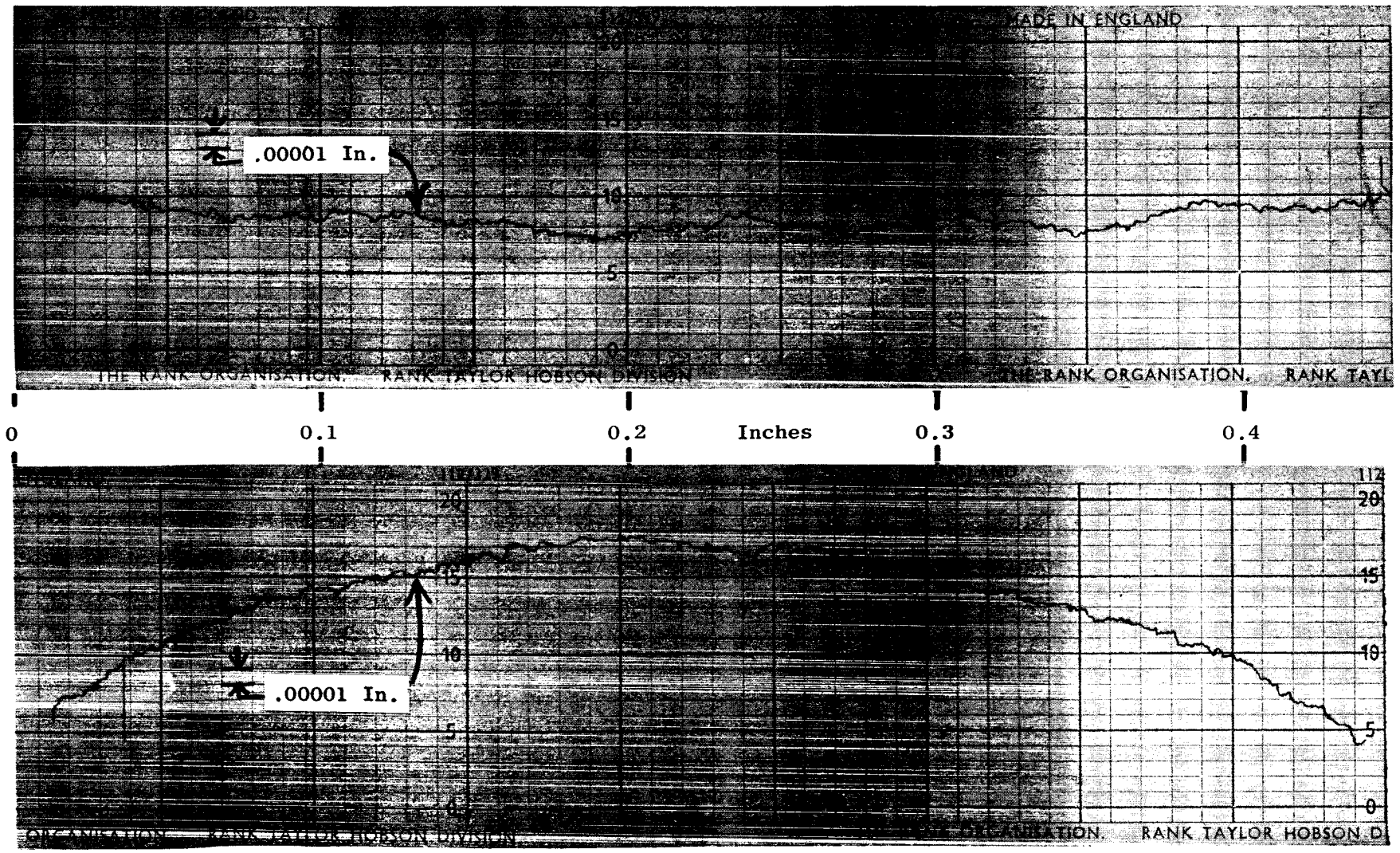

Post-Test Profilometer Trace - Radial at 90° CW from S/N

FRICTION AND WEAR TEST DATA FOR GRADE 7178 VS GRADE 7178 IN HIGH VACUUM

Test No. - 300705A

Assembly No. - VI

Loading Arm No. - 1

Test Date - 8/10/65

Rider
Material - Grade 7178
Specimen No. - 1046-E-3

Disc
Material - Grade 7178
Specimen No. - 1046-F-1A

Test Temperature, ^{o}F - RT

Max. ΔT of Rider, ^{o}F - 45

Speed, SFM - 500

Test Duration, Min. - 0.87

Compressive Load, Lbs - 6.12 (P_7)

Compressive Stress, psi - 484,800

Load/Material UCS or 0.2%CYS -
Rider - 69
Disc - 69

Average Coefficient of Friction - 0.56

Chamber Pressure, Torr -
Start - 1.0×10^{-9}
Max. - 1.0×10^{-9}

Remarks - Disc fractured upon application of load.

Change in Coefficient of Friction with Time -

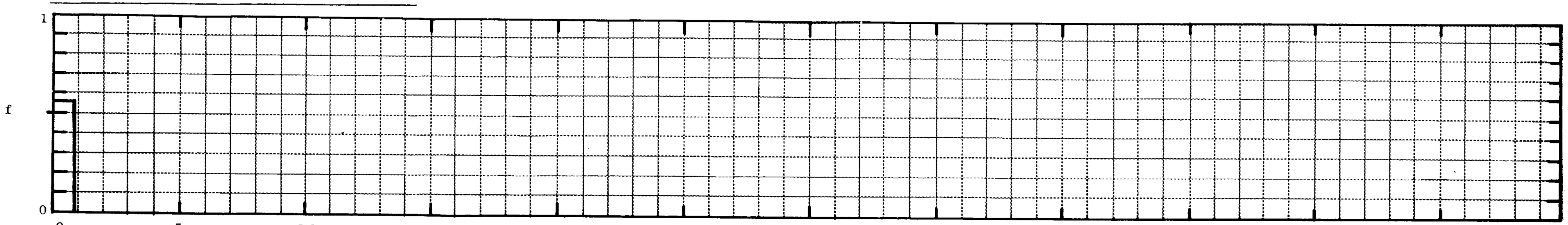

WEAR - RIDER

Initial Surface Finish -

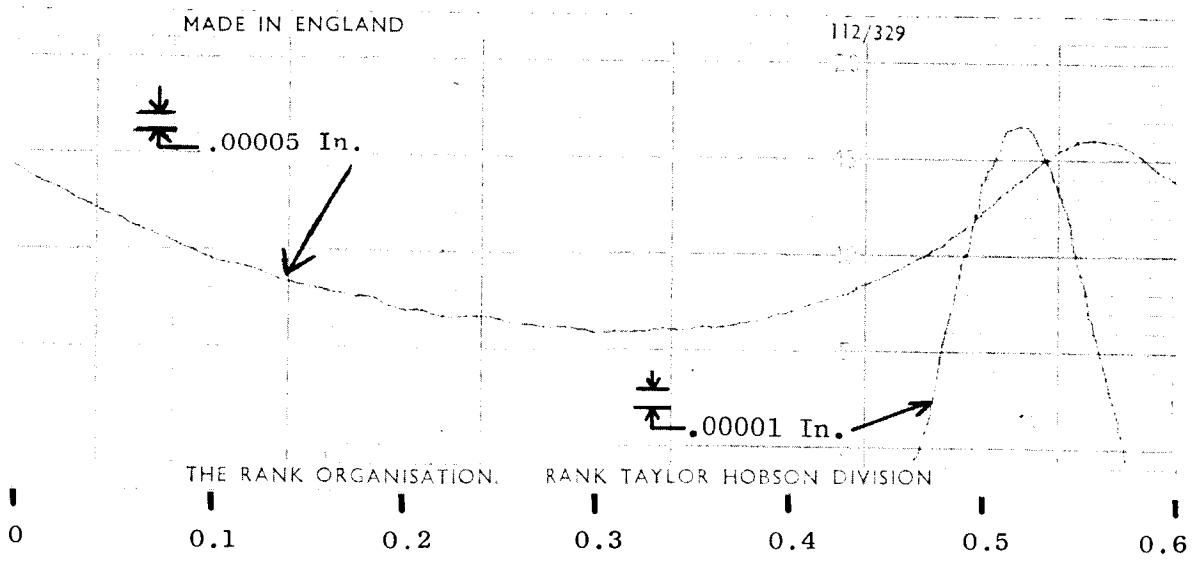

Wear Scar Dia., In. - 0.038

Weight, Gms -
Start - 3.1078
Finish - 3.1075
Change - -0.0003

Material Density, Gms/Cm^3 - 14.301

Volume Change, Mm^3 --0.021

Wear Rate, $In^3/10^{10}ft$ - -26.1

(C66081621) Mag.: 28.5X

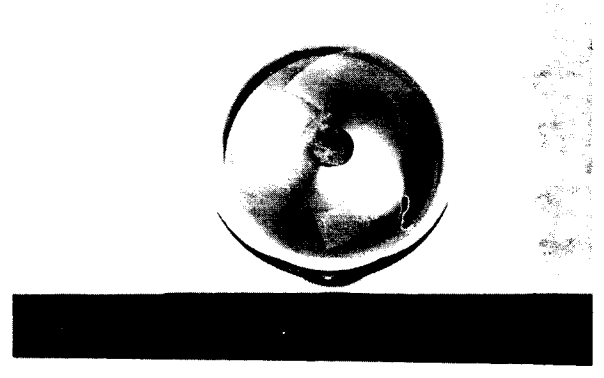

(C65121311) Mag.: 5X

WEAR - DISC

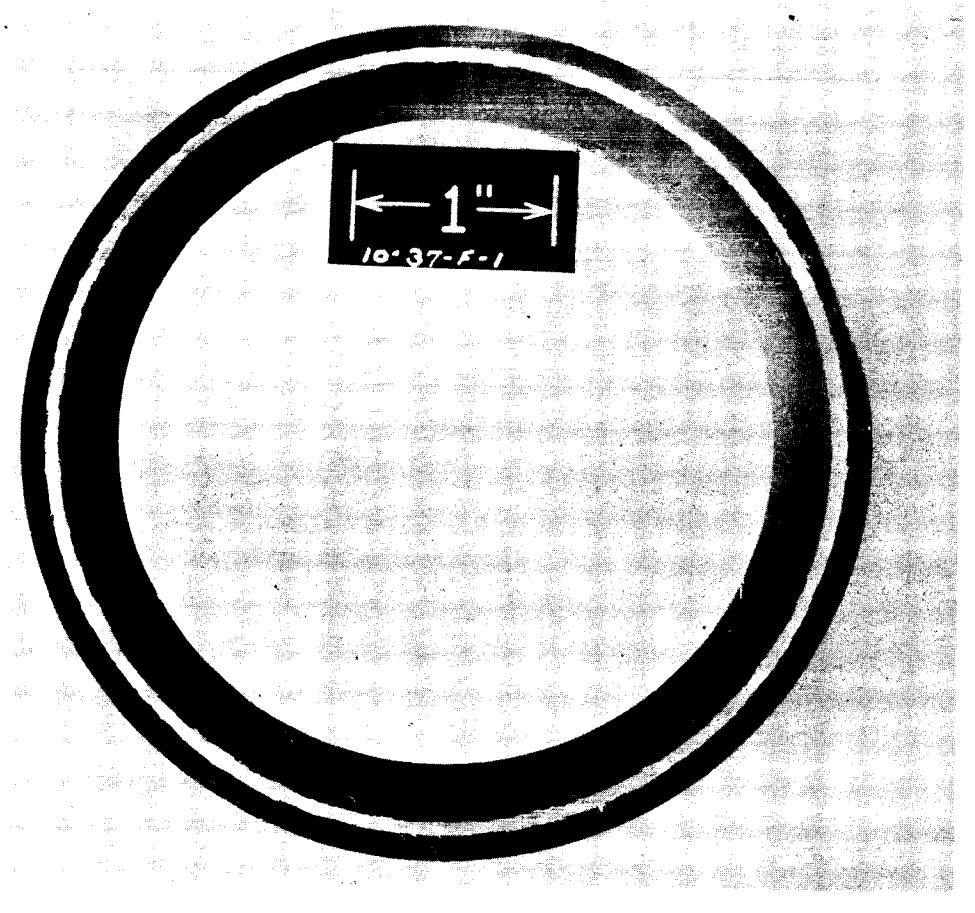

(C65121305) Mag.: 1X

(C65121307) Mag.: 5X

Initial

Wear Sc

Weight,
Start -
Finish
Change

Material

Volume C

Wear Rat

Post-Tes

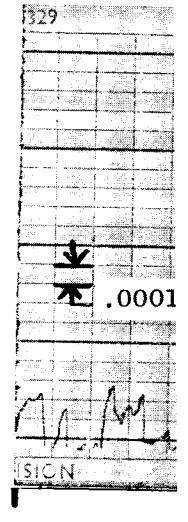

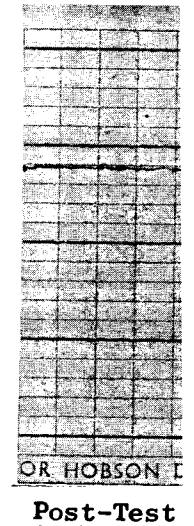

Post-Test

WEAR - DISC

Test No. - 300705A

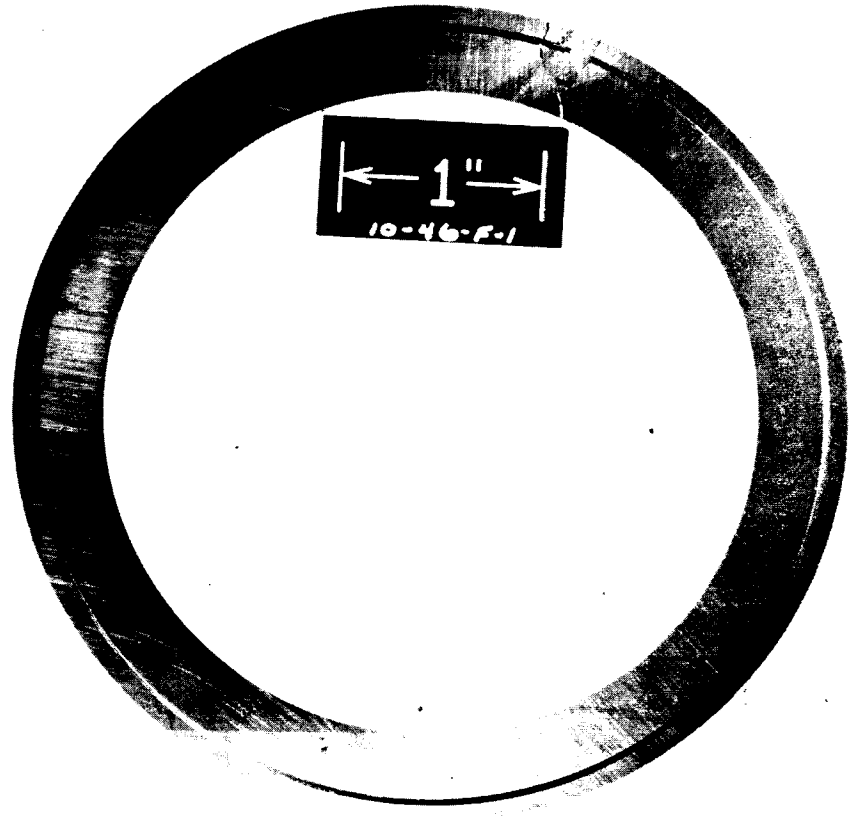

(C65121306) Mag.: 1X

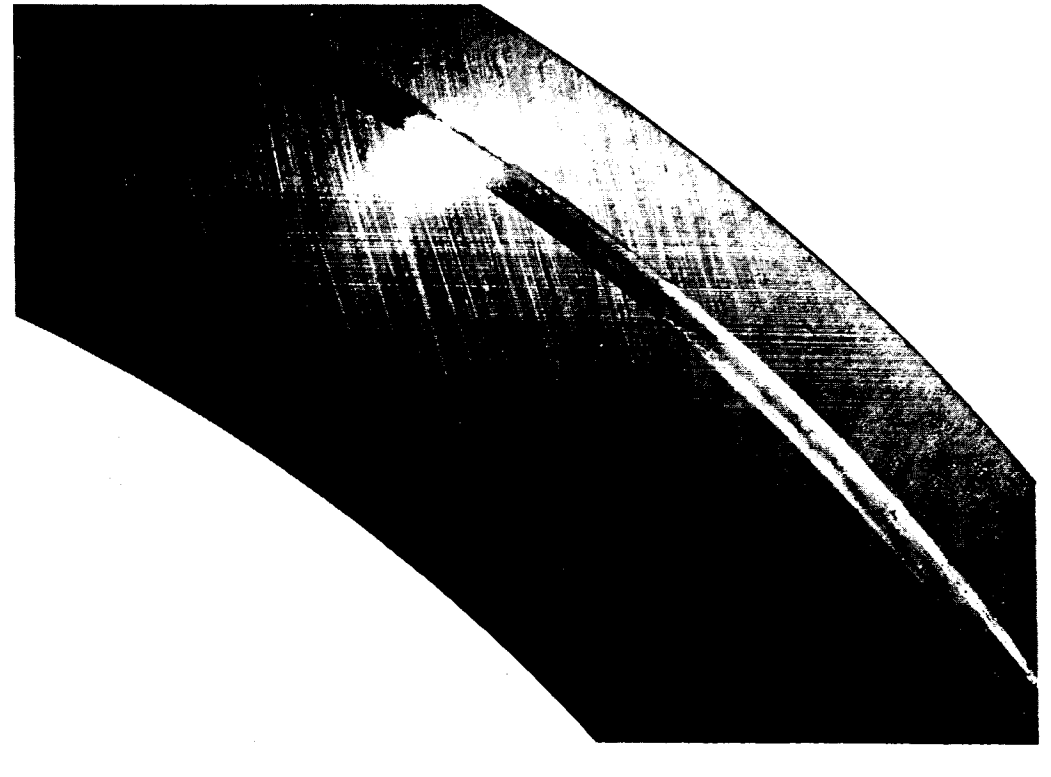

(C65121308) Mag.: 5X

Initial Surface Finish, Avg. RMS - 1.5

Wear Scar Width, In. - 0.031

Weight, Gms /Cm^3 -
Start - 207.3780
Finish - 207.2083
Change - -0.1697

Material Density, Gms /Cm^3 - 14.301

Volume Change, Mm^3 - 11.866

Wear Rate, $In^3/10^{10}ft$ - See remarks

Pre-Test Profilometer Trace (Typical)

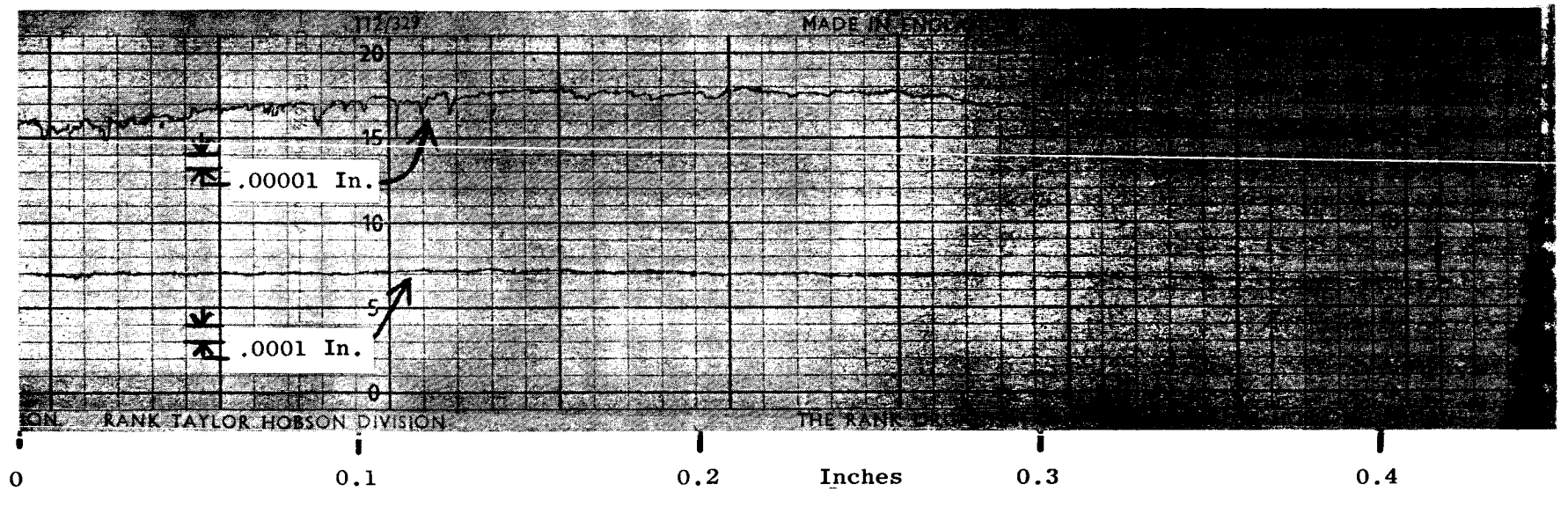

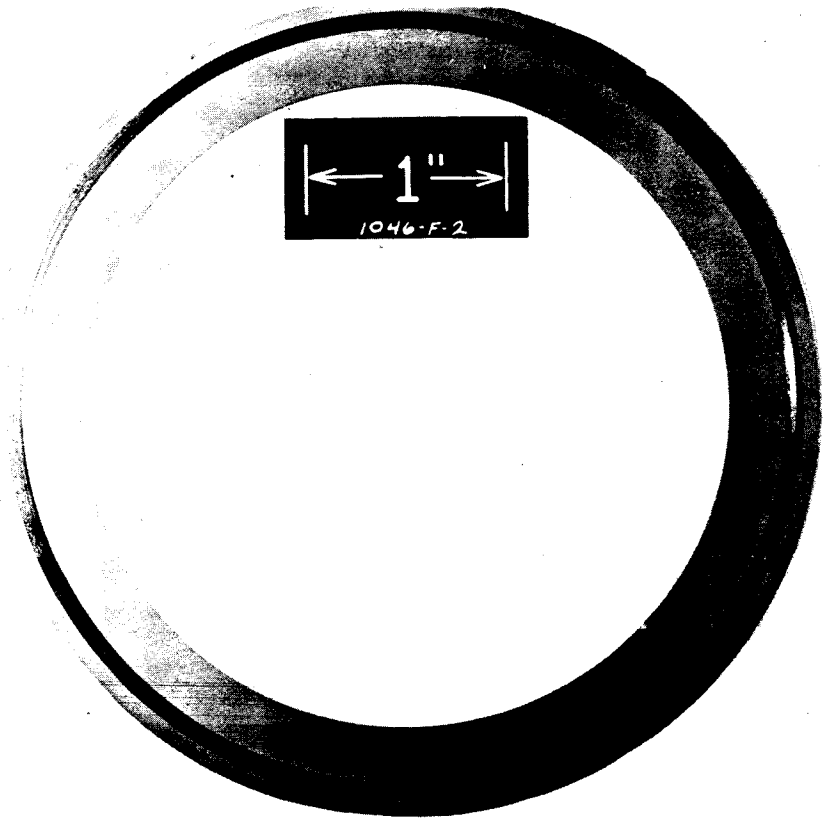

(C651223140) Mag.: 1X

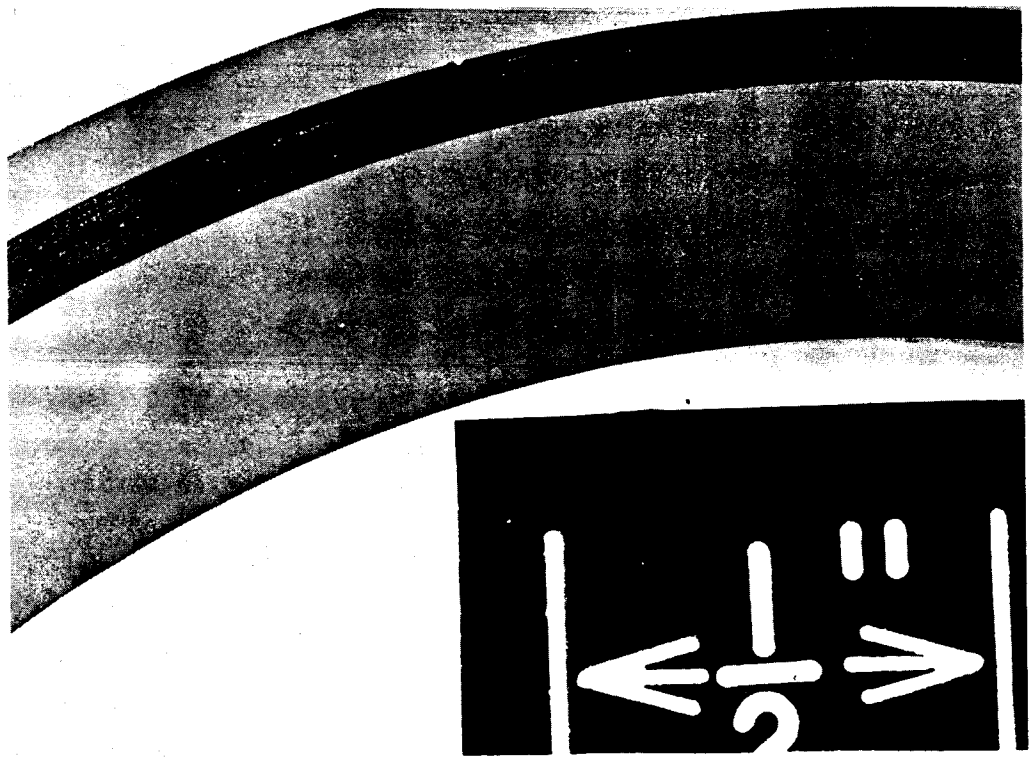

(C651223141) Mag.: 5X

Initial Surface Finish, Avg. RMS - 2.5

Wear Scar Width, In. - 0.078

Weight, Gms /Cm^3 -
Start - 207.6270
Finish - 207.5619
Change - -0.0651

Material Density, Gms /Cm^3 - 14.301

Volume Change, Mm^3 - -4.552

Wear Rate, $In^3/10^{10}ft$ - -347

Post-Test Profilometer Trace - Circumferential at S/N

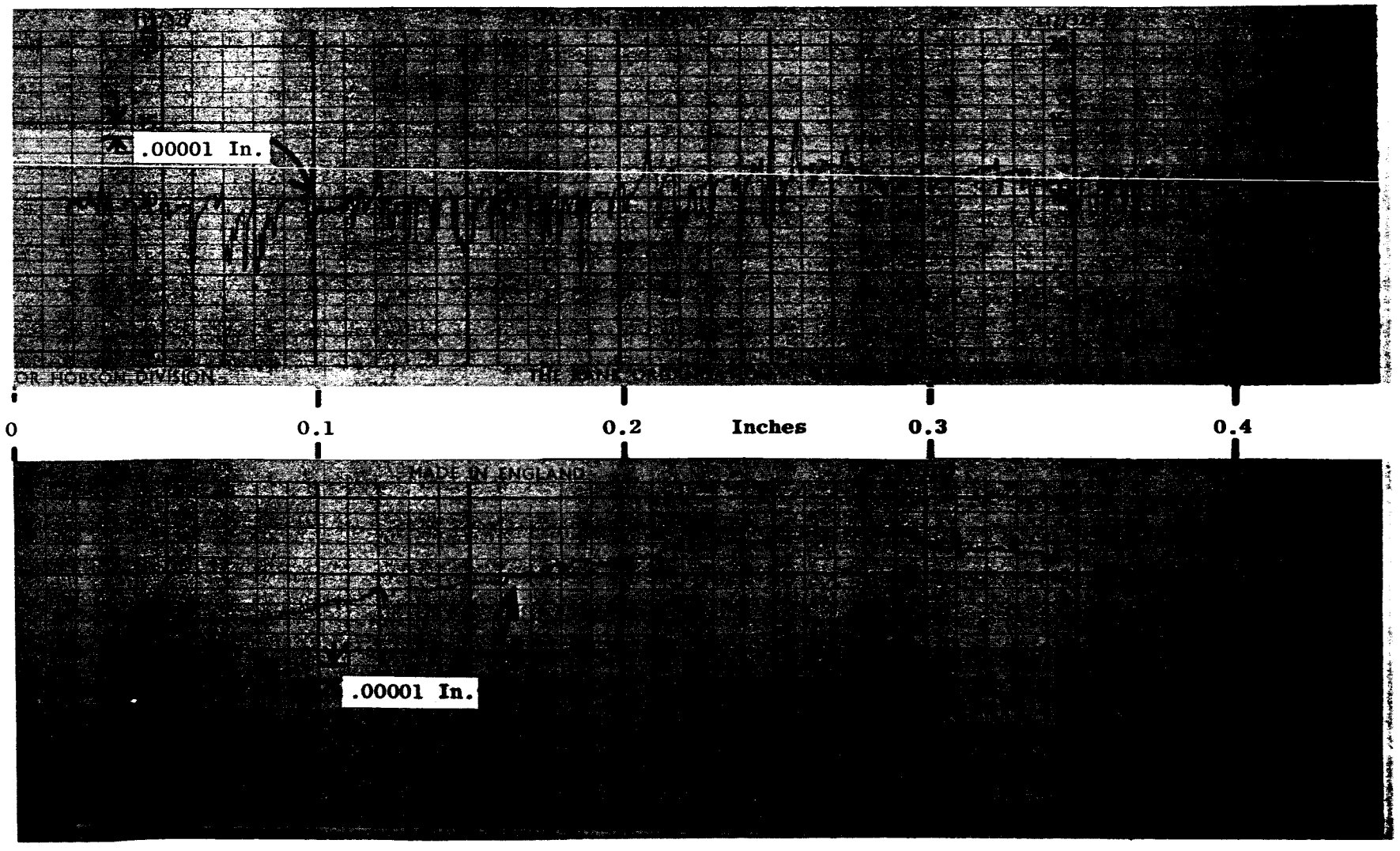

Post-Test Profilometer Trace - Radial at S/N

FRICTION AND WEAR TEST DATA FOR Mo-TZM ALLOY VS GRADE 7178 IN HIGH VACUUM

Test No. - 100K08A

Assembly No. - VII

Loading Arm No. - 2

Test Date - 10/15/65

Rider
Material - Mo-TZM
Specimen No. - 1037-E-2

Disc
Material - Grade 7178
Specimen No. - 1046-F-3A

Test Temperature, ^{o}F - RT

Max. ΔT of Rider, ^{o}F - 52

Speed, SFM - 800

Test Duration, Min. - 60.00

Compressive Load, Lbs - 0.080(K)

Compressive Stress, psi - 94,750

Load/Material UCS or 0.2%CYS -
Rider - 87
Disc - 13

Average Coefficient of Friction - 1.00

Chamber Pressure, Torr -
Start - 6.2×10^{-10}
Max. - 9.0×10^{-10}

Remarks -

Change in Coefficient of Friction with Time -

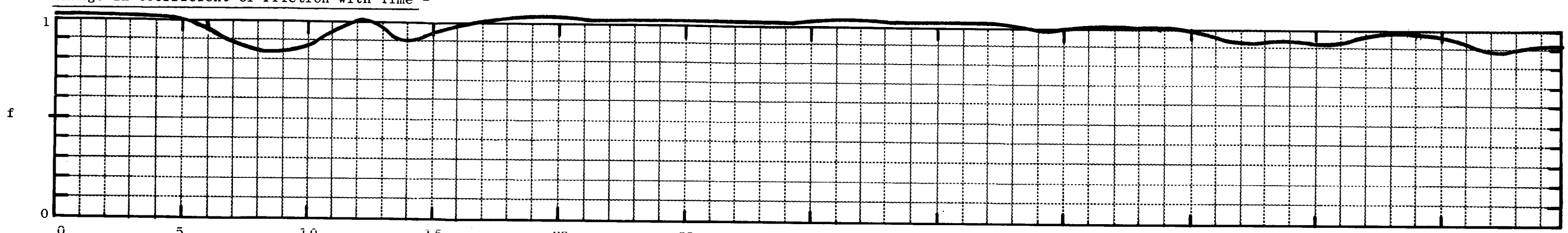

WEAR - RIDER

Initial Surface Finish -

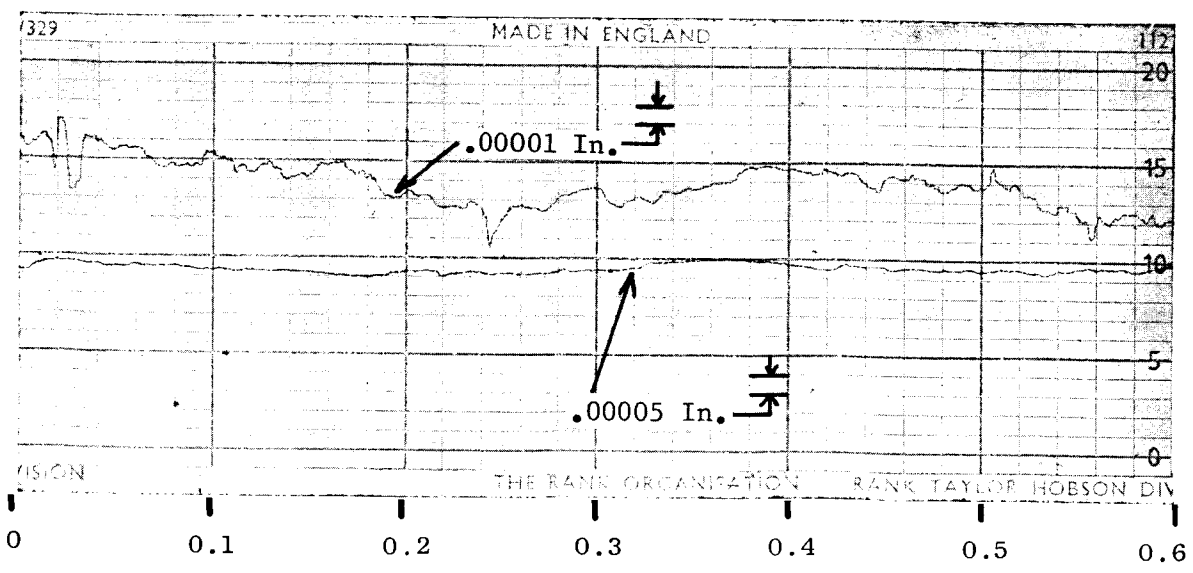

Wear Scar Dia., In. - 0.047

Weight, Gms -
Start - 2.3822
Finish - 2.3817
Change - -0.0005

Material Density, Gms/Cm^3 -
10.139

Volume Change, Mm^3 -
-0.049

Wear Rate, $In^3/10^{10}ft$ -
-0.537

(C66081661) Mag.: 28.5X

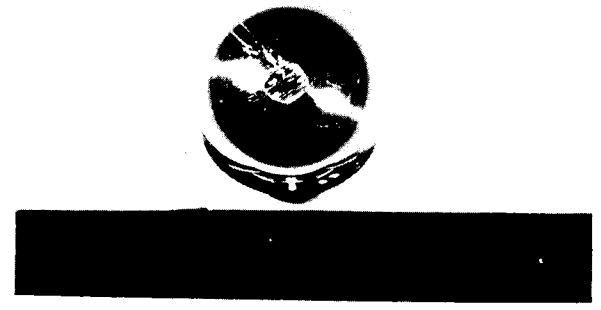

(C651223132) Mag.: 5X

WEAR - DISC

Test No. - 100K08A

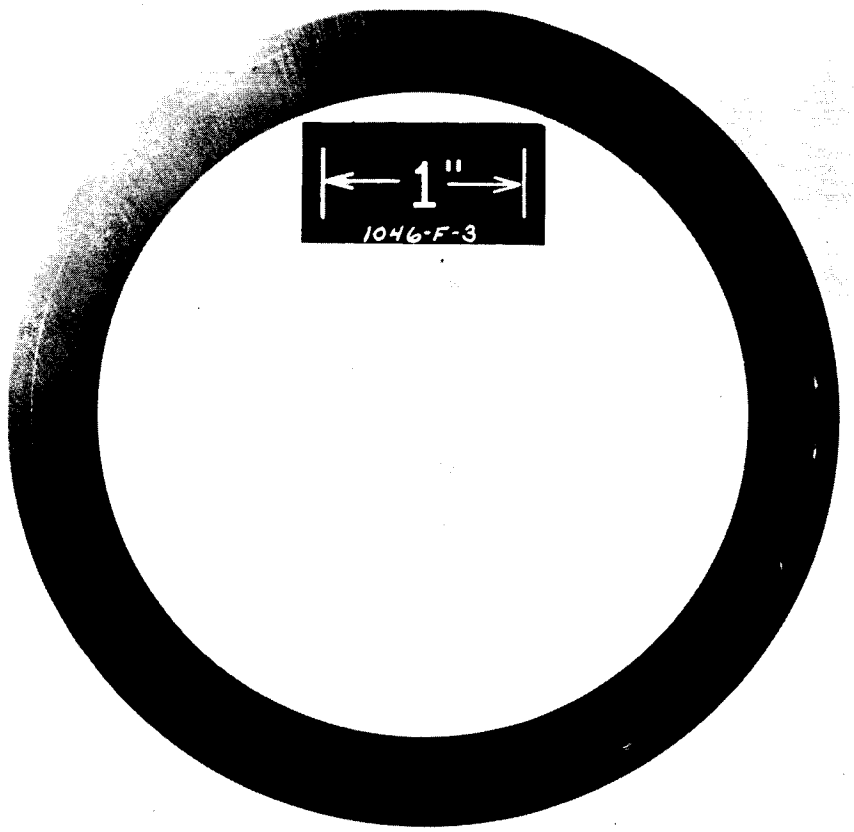

(C651223129) Mag.: 1X

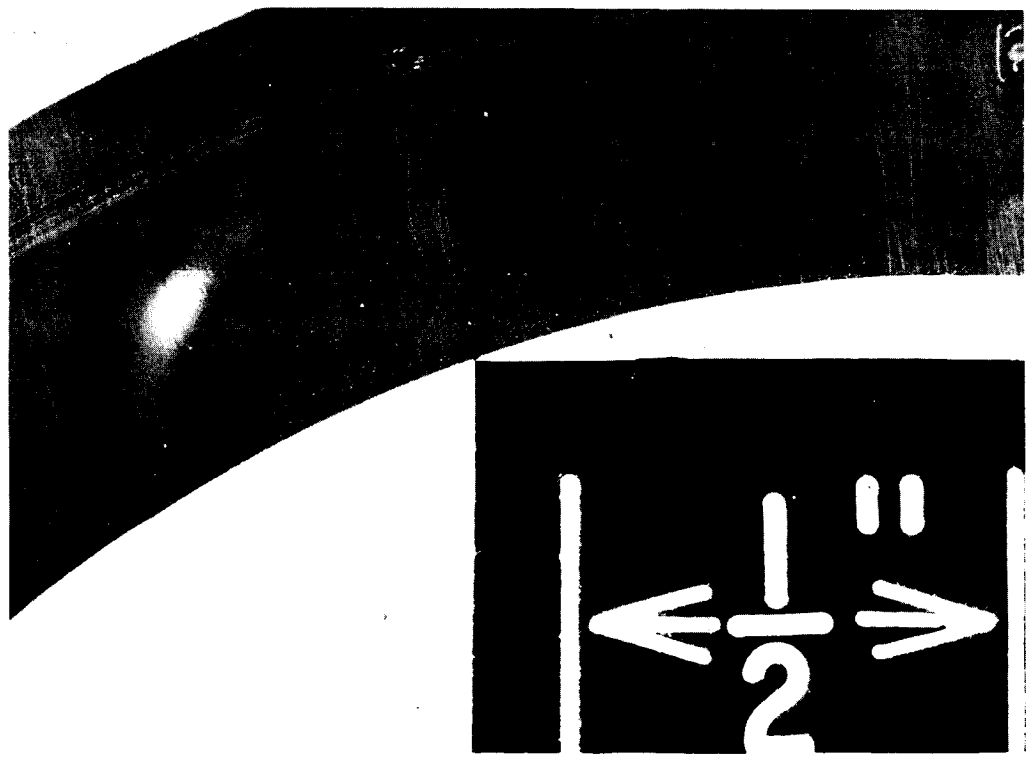

(C651223128) Mag.: 5X

Initial Surface Finish, Avg. RMS - 1-1.5

Wear Scar Width, In. - 0.031

Weight, Gms /Cm^3 -
Start - 207.0429
Finish - 207.0416
Change - -0.0013

Material Density, Gms /Cm^3 - 14.301

Volume Change, Mm^3 - -0.091

Wear Rate, $In^3/10^{10}ft$ - -0.989

Post-Test Profilometer Trace - Circumferential at S/N

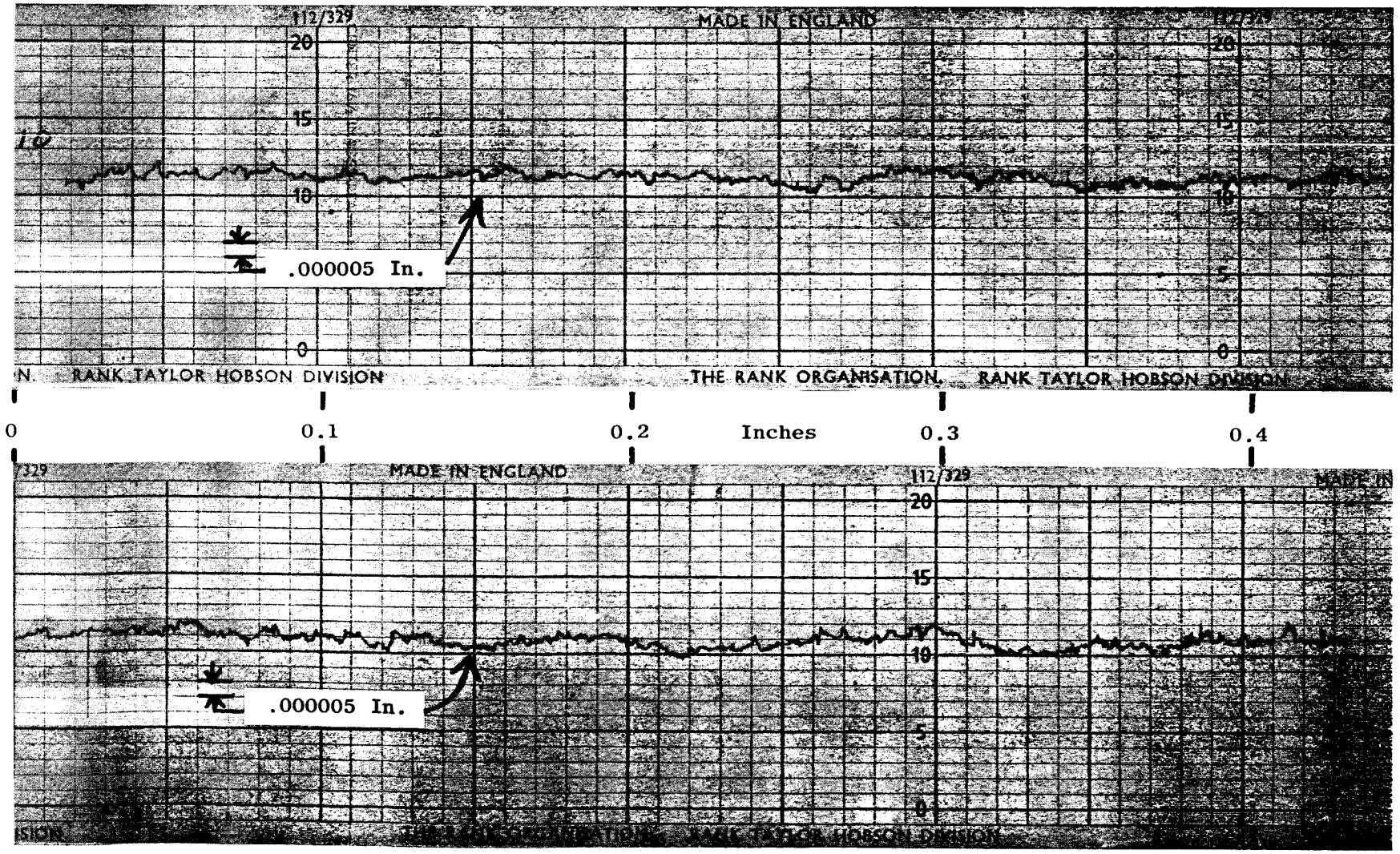

Post-Test Profilometer Trace - Radial at S/N

FRICTION AND WEAR TEST DATA FOR GRADE 7178 VS Mo-TZM ALLOY IN HIGH VACUUM

Test No. - 200K05B

Assembly No. - VII

Loading Arm No. - 4

Test Date - 10/13/65

Rider
Material - Grade 7178
Specimen No. - 1046-E-7

Disc
Material - Mo-TZM
Specimen No. - 1037-F-2A

Test Temperature, ^{o}F - RT

Max. ΔT of Rider, ^{o}F - 30

Speed, SFM - 500

Test Duration, Min. - 60.00

Compressive Load, Lbs - 0.082(K)

Compressive Stress, psi - 95,500

Load/Material UCS or 0.2%CYS -
Rider - 14
Disc - 87

Average Coefficient of Friction - 0.95

Chamber Pressure, Torr -
Start - 7.0×10^{-10}
Max. - 1.0×10^{-9}

Remarks -

Change in Coefficient of Friction with Time -

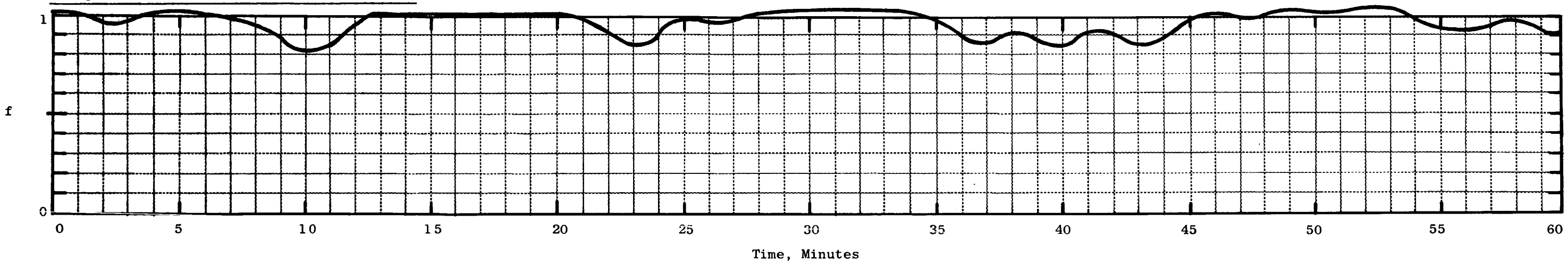

WEAR - RIDER

Initial Surface Finish -

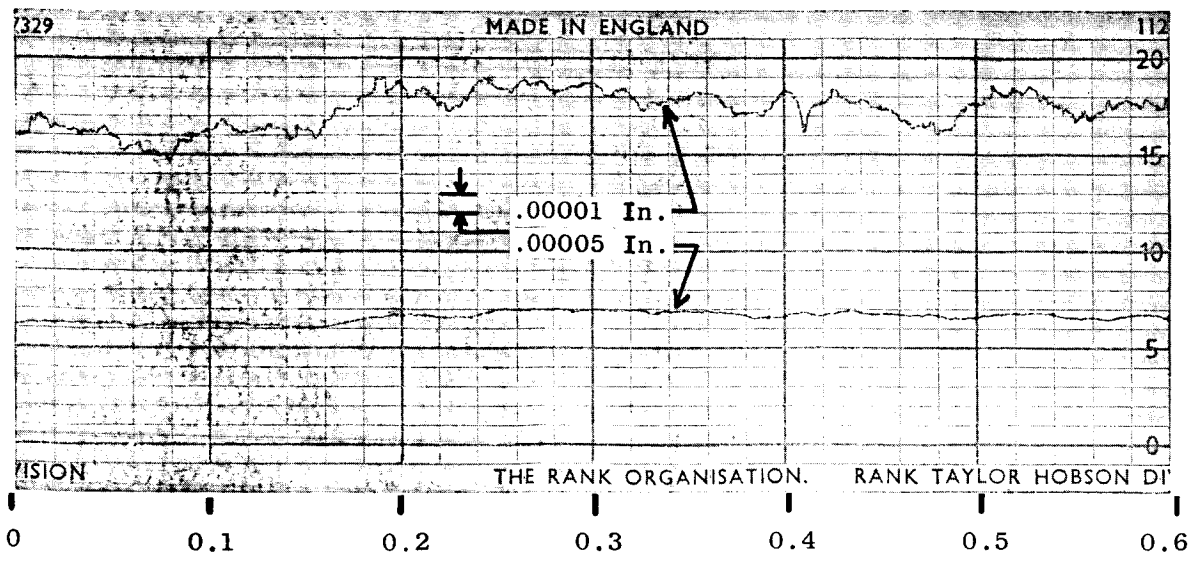

Wear Scar Dia., In. - 0.068

Weight, Gms -
Start - 3.0776
Finish - 3.0765
Change - -0.0011

Material Density, Gms/Cm^3 -
14.301

Volume Change, Mm^3 -
-0.077

Wear Rate, $In^3/10^{10}ft$ -
-1.35

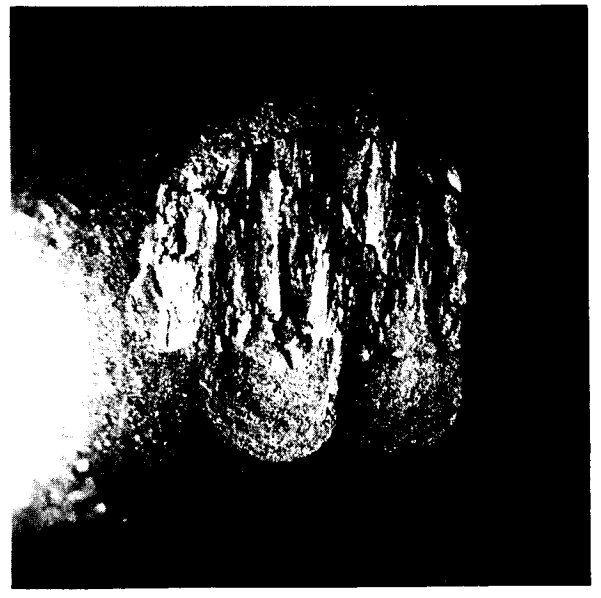

(C66081652) Mag.: 28.5X

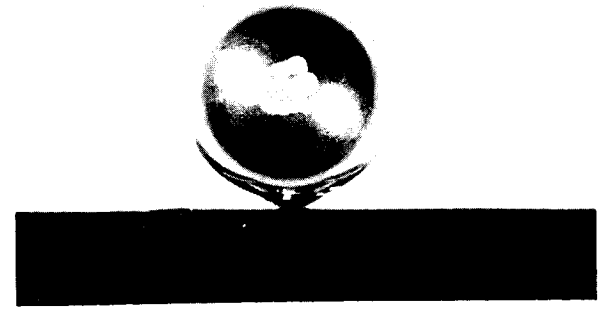

(C651223153) Mag.: 5X

WEAR - DISC

Test No. - 200K05B

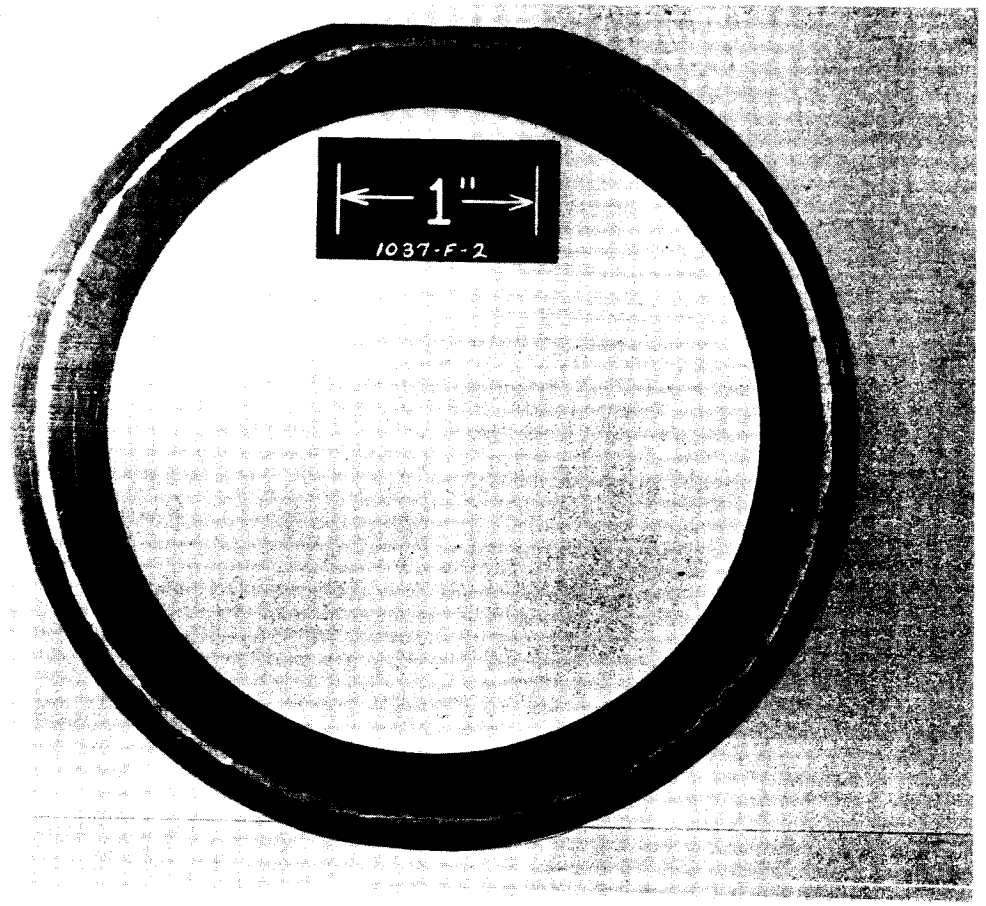

(C651223139) Mag.: 1X

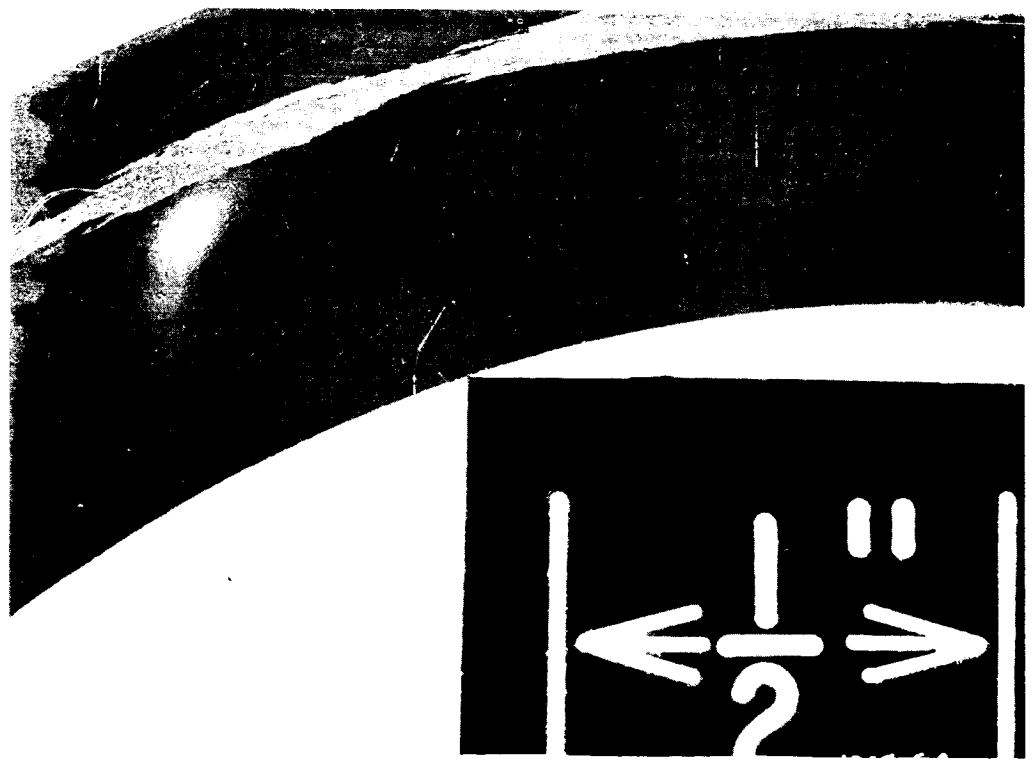

(C651223138) Mag.: 5X

Initial Surface Finish, Avg. RMS - 2.5-5

Wear Scar Width, In. - 0.047

Weight, Gms /Cm^3 -
Start - 155.4364
Finish - 155.3935
Change - -0.0429

Material Density, Gms /Cm^3 - 10.139

Volume Change, Mm^3 - -4.231

Wear Rate, $In^3/10^{10}ft$ - -74.2

Post-Test Profilometer Trace - Circumferential at S/N

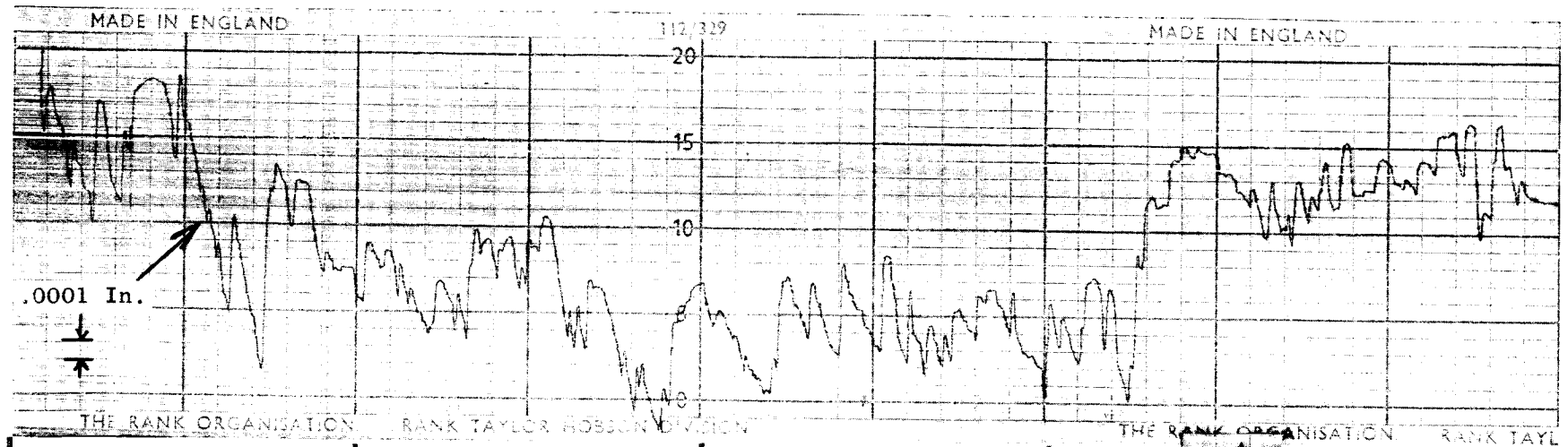

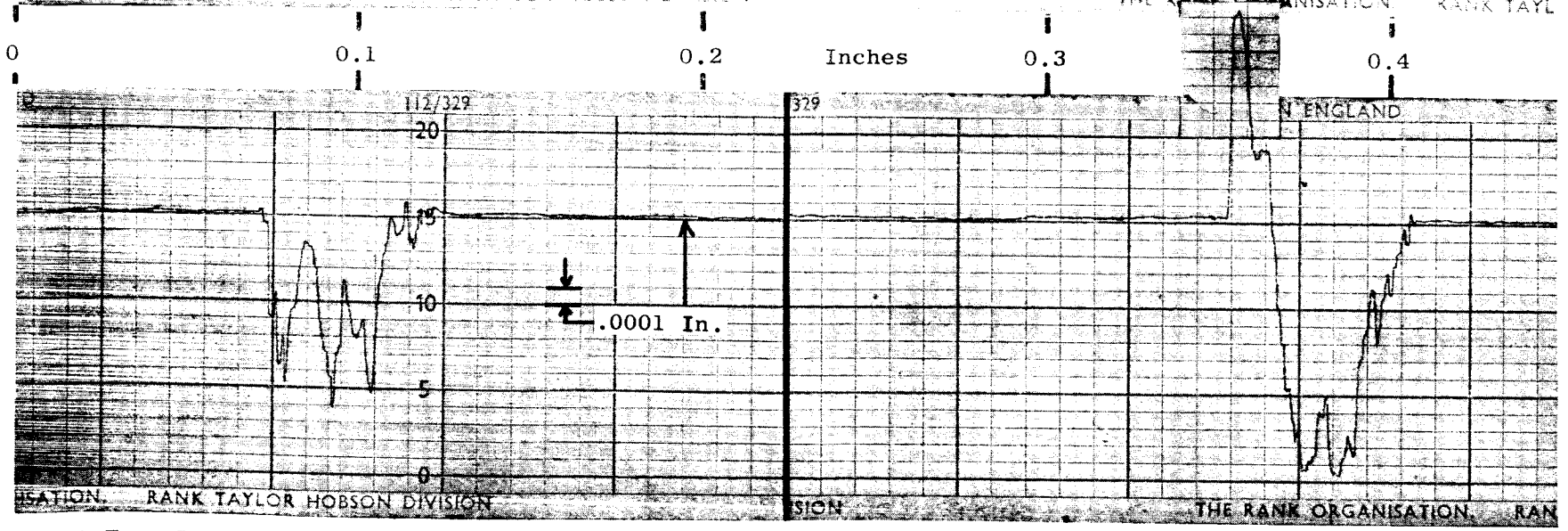

Post-Test Profilometer Trace - Radial at S/N

Radial at 90° CW of S/N

DISTRIBUTION LIST
QUARTERLY PROGRESS REPORTS
CONTRACT NAS 3-2534

NASA
Washington, D. C. 20546
ATTN: J.J. Lynch (RNP)

NASA
Washington, D. C. 20546
ATTN: George C. Deutsch (RR)

NASA
Scientific & Technical Information
Facility
Box 5700
Bethesda, Maryland 20014
ATTN: NASA Representative (2) + Repro.

NASA
Goddard Space Flight Center
Greenbelt, Maryland 20771
ATTN: Librarian

NASA
Langley Research Center
Hampton, Virginia 23365
ATTN: Librarian

NASA-Lewis Research Center
21000 Brookpark Road
Cleveland, Ohio 44135
ATTN: Librarian

NASA-Lewis Research Center
21000 Brookpark Road
Cleveland, Ohio 44135
ATTN: Report Control Office M.S. 5-5

NASA-Lewis Research Center
21000 Brookpark Road
Cleveland, Ohio 44135
ATTN: Dr. Bernard Lubarsky M.S. 500-201

NASA-Lewis Research Center
21000 Brookpark Road
Cleveland, Ohio 44135
ATTN: R.L. Cummings (500-201)

NASA-Lewis Research Center
21000 Brookpark Road
Cleveland, Ohio 44135
ATTN: G.M. Ault

NASA-Lewis Research Center
21000 Brookpark Road
Cleveland, Ohio 44135
ATTN: J.P. Joyce M.S. 500-201

NASA-Lewis Research Center
21000 Brookpark Road
Cleveland, Ohio 44135
ATTN: R.L. Davies M.S. 500-201

NASA-Lewis Research Center
21000 Brookpark Road
Cleveland, Ohio 44135
ATTN: J.E. Dilley M.S. 500-309

NASA-Lewis Research Center
21000 Brookpark Road
Cleveland, Ohio 44135
ATTN: J. J. Weber M.S. 3-19
Technology Utilization Office

NASA-Lewis Research Center
21000 Brookpark Road
Cleveland, Ohio 44135
ATTN: Thomas Strom

NASA-Lewis Research Center
21000 Brookpark Road
Cleveland, Ohio 44135
ATTN: T.A. Moss (NPTB) M.S. 500-201

NASA-Lewis Research Center
21000 Brookpark Road
Cleveland, Ohio 44135
ATTN: Dr. Louis Rosenblum M.S. 106-1

NASA
Manned Spacecraft Center
Houston, Texas 77001
ATTN: Librarian

NASA
George C. Marshall Space Flight Center
Huntsville, Alabama 38512
ATTN: Librarian

NASA
Jet Propulsion Laboratory
4800 Oak Grove Drive
Pasadena, California 99103
ATTN: Librarian

NASA
Western Operations Office
150 Pico Boulevard
Santa Monica, California 90400
ATTN: John Keeler

National Bureau of Standards
Washington, D. C. 20225
ATTN: Librarian

Flight Vehicle Power Branch
Air Force Aero Propulsion Laboratory
Wright Patterson AFB, Ohio
ATTN; Charles Armbruster ASRPP-10

Flight Vehicle Power Branch
Air Force Aero Propulsion Laboratory
Wright Patterson AFB, Ohio
ATTN: T. Cooper (MAMP)

Flight Vehicle Power Branch
Air Force Aero Propulsion Laboratory
Wright Patterson AFB, Ohio
ATTN: Librarian

Flight Vehicle Power Branch
Air Force Aero Propulsion Laboratory
Wright Patterson AFB, Ohio
ATTN: John L. Morris

Army Ordnance Frankford Arsenal
Bridesburg Station
Philadelphia, Pennsylvania 19137
ATTN: Librarian

Bureau of Ships
Department of the Navy
Washington, D. C. 20225
ATTN: Librarian

Bureau of Weapons
Research & Engineering
Material Division
Washington, D. C. 20225
ATTN: Librarian

U.S. Atomic Energy Commission
Technical Reports Library
Washington, D. C. 20545
ATTN: J.M. O'Leary

U.S. Atomic Energy Commission
Germantown, Maryland 20767
ATTN: Col. E.L. Douthett
SNAP 50/SPUR Project Office

National Aeronautics & Space Administration
Headquarters
Washington, D. C. 20546
ATTN: H. Rochen (RNP)

U.S. Atomic Energy Commission
Germantown, Maryland 20767
ATTN: Socrates Christopher

U.S. Atomic Energy Commission
Germantown, Maryland 20767
ATTN: Major Gordon Dicker
SNAP 50/SPUR Project Office

U.S. Atomic Energy Commission
Technical Information Service Extension
P.O. Box 62
Oak Ridge, Tennessee 37831 (3)

U.S. Atomic Energy Commission
Washington, D. C. 20545
ATTN: M.J. Whitman

Argonne National Laboratory
9700 South Cass Avenue
Library Service Department 203-CE125
Argonne, Illinois 60439
ATTN: Report Section

Brookhaven National Laboratory
Upton, Long Island, New York 11973
ATTN: Librarian

Oak Ridge National Laboratory
Oak Ridge, Tennessee 37831
ATTN: W.O. Harms

Oak Ridge National Laboratory
Oak Ridge, Tennessee 37831
ATTN: Dr. A.J. Miller

Oak Ridge National Laboratory
Oak Ridge, Tennessee 37831
ATTN: Librarian

Office of Naval Research
Power Division
Washington, D. C. 20225
ATTN: Librarian

U.S. Naval Research Laboratory
Washington, D. C. 20225
ATTN: Librarian

Aerojet-General Corporation
P.O. Box 296
Azusa, California
ATTN: Librarian

AiResearch Manufacturing Company
Sky Harbor Airport
402 South 36th Street
Phoenix, Arizona 85000
ATTN: Librarian

AiResearch Manufacturing Company
Sky Harbor Airport
402 South 36th Street
Phoenix, Arizona 85000
ATTN: E.A. Kovacevich

AiResearch Manufacturing Company
9851 - 9951 Sepulveda Boulevard
Los Angeles, California 90045
ATTN: Librarian

IIT Research Institute
10 West 35th Street
Chicago, Illinois 60616
ATTN: Librarian

Atomics International
8900 DeSoto Avenue
Canoga Park, California 91303
ATTN: Librarian

Avco
Research and Advanced Development
Department
201 Lowell Street
Wilmington, Massachusetts 01800
ATTN: Librarian

Babcock and Wilcox Company
Research Center
Alliance, Ohio 44601-2
ATTN: Librarian

Battelle Memorial Institute
505 King Avenue
Columbus, Ohio 43200
ATTN: C.M. Allen

Battelle Memorial Institute
505 King Avenue
Columbus, Ohio 43200
ATTN: Librarian

The Bendix Corporation
Research Laboratories Division
Southfield, Detroit, Michigan 48200
ATTN: Librarian

The Boeing Company
Seattle, Washington 98100
ATTN: Librarian

Climax Molybdenum Co. of Michigan
1600 Huron Parkway
Ann Arbor, Michigan 48105
ATTN: Librarian

Carborundum Company
Niagara Falls, New York 14300
ATTN: Librarian

Chance Vought Aircraft, Inc.
P.O. Box 5907
Dallas 22, Texas 75222
ATTN: Librarian

Clevite Corporation
Mechanical Research Division
540 East 105th Street
Cleveland, Ohio 44108
ATTN: Mr. N.C. Beerli
Project Administrator

Convair Astronautics
5001 Kerrny Villa Road
San Diego, California 92111
ATTN: Librarian

Crucible Steel Co. of America
Pittsburgh, Pennsylvania 15200
ATTN: Librarian

Curtiss-Wright Corporation
Wright Aero Division
Wood Ridge, New Jersey 07075
ATTN: Librarian

E.I. DuPont de Nemours and Co., Inc.
Wilmington, Delaware 19898
ATTN: Librarian

Electro-Optical Systems, Inc.
Advanced Power Systems Division
Pasadena, California 91100
ATTN: Librarian

Fansteel Metallurgical, Corporation
North Chicago, Illinois 60600
ATTN: Librarian

Firth Sterling, Incorporated
McKeesport, Pennsylvania
ATTN: Librarian

Aeronutronic Div. of Philco Corp.
Ford Road
Newport Beach, California
ATTN: Ferne M. Black/HDL
Acquisitions Librarian

General Atomic
John Jay Hopkins Laboratory
P.O. Box 608
San Diego, California 92112
ATTN: Librarian

General Electric Company
Atomic Power Equipment Division
P.O. Box 1131
San Jose, California

Norton Company
Worcester, Massachusetts 01600
ATTN: Librarian

General Electric Company
Missile & Space Vehicle Department
3198 Chestnut Street
Philadelphia, Pennsylvania 19104
ATTN: Librarian

General Electric Company
Vallecitos
Vallecitos Atomic Lab.
Pleasanton, California 94566
ATTN: Librarian

General Dynamics/Fort Worth
P.O. Box 748
Fort Worth, Texas 76100
ATTN: Librarian

General Motots Corporation
Allison Division
Indianapolis, Indiana 46206
ATTN: Librarian

Hamilton Standard
Div. of United Aircraft Corporation
Windsor Locks, Connecticut
ATTN: Librarian

Hughes Aircraft Company
Engineering Division
Culver City, California 90230-2
ATTN: Librarian

Kennametal, Incorporated
Latrobe, Pennsylvania
ATTN: Librarian

Latrobe Steel Company
Latrobe, Pennsylvania
ATTN: Librarian

Lockheed Missiles and Space Division
Lockheed Aircraft Corporation
Sunnyvale, California
ATTN: Librarian

Marquardt Aircraft Company
P.O. Box 2013
Van Nuys, California
ATTN: Librarian

The Martin Company
Baltimore, Maryland 21203
ATTN: Librarian

The Martin Company
Nuclear Division
P.O. Box 5042
Baltimore, Maryland 21220
ATTN: Librarian

Martin Marietta Corporation
Metals Technology Laboratory
Wheeling, Illinois

Massachusetts Institute of Technology
Cambridge, Massachusetts 02139
ATTN: Librarian

Materials Research and Development
Manlabs, Inc.
21 Erie Street
Cambridge, Massachusetts 02139

Materials Research Corporation
Orangeburg, New York
ATTN: Librarian

McDonnel Aircraft
St. Louis, Missouri 63100
ATTN: Librarian

MSA Research Corporation
Callery, Pennsylvania 16024
ATTN: Librarian

North American Aviation
Los Angeles Division
Los Angeles, California 90009
ATTN: Librarian

Pratt & Whitney Aircraft
400 Main Street
East Hartford, Connecticut 06108
ATTN: Librarian

Republic Aviation Corporation
Farmingdale, Long Island, New York
ATTN: Librarian

Rocketdyne
Canoga Park, California 91303
ATTN: Librarian

Sintercast Div. of Chromalloy Corp.
West Nyack, New York
ATTN: Librarian

S K F Industries, Inc.
Philadelphia, Pennsylvania 19100
ATTN: Librarian

Solar
2200 Pacific Highway
San Diego, California 92112
ATTN: Librarian

Southwest Research Institute
8500 Culebra Road
San Antonio, Texas 78206
ATTN: Librarian

Superior Tube Company
Norristown, Pennsylvania
ATTN: Mr. A. Bound

Sylvania Electrics Products, Inc.
Chem. & Metallurgical
Towanda, Pennsylvania
ATTN: Librarian

Oak Ridge National Laboratory
Oak Ridge, Tennessee
ATTN: W.H. Cook

Thompson-Ramo-Wooldridge, Inc.
Caldwell Res Center
23555 Euclid Avenue
Cleveland, Ohio 44117
ATTN: Librarian

Thompson-Ramo-Wooldridge, Inc.
Caldwell Res Center
23555 Euclid Avenue
Cleveland, Ohio 44117
ATTN: G.J. Guarnieri

Thompson-Ramo-Wooldridge, Inc.
New Devices Laboratories
7209 Platt Avenue
Cleveland, Ohio 44104
ATTN: Librarian

The Timken Roller Bearing Co.
Canton, Ohio 44706
ATTN: Librarian

Union Carbide Metals
Niagara Falls, New York 14300
ATTN: Librarian

Union Carbide Corp., Stellite Division
Komomo, Indiana
ATTN: Librarian

Union Carbide Nuclear Company
P.O. Box X
Oak Ridge, Tennessee 37831
ATTN: X-10 Laboratory
Records Department (2)

United Nuclear Corporation
5 New Street
White Plains, New York 10600-5
ATTN: Mr. Albert Weinstein
Senior Engineer

Universal Cyclops Steel Corporation
Refractomet Division
Bridgeville, Pennsylvania
ATTN: C.P. Mueller

University of Michigan
Department of Chemical & Metallurgical Engineering
Ann Arbor, Michigan 48103
ATTN: Librarian

Vanadium Alloys Steel Company
Latrobe, Pennsylvania
ATTN: Librarian

Vought Astronautics
P.O. Box 5907
Dallas, Texas 75222
ATTN: Librarian

Wah Chang Corporation
Albany, Oregon
ATTN: Librarian

Westinghouse Electric Corporation
Astronuclear Laboratory
P.O. Box 10864
Pittsburgh, Pennsylvania 15236
ATTN: Librarian

Westinghouse Electric Corp.
Materials Mfg. Division
RD#2, Box 25
Blairsville, Pennsylvania
ATTN: Librarian

Westinghouse Electric Corp.
Materials Mfg. Division
RD#2, Box 25
Blairsville, Pennsylvania
ATTN: F.L. Orrell

Mr. Rudolph Rust - M.S. 138-214
Jet Propulsion Laboratory
4800 Oak Grove Drive
Pasadena, California 91103

Mr. W.H. Podolny
United Aircraft Corporation
Pratt & Whitney Division
400 West Main Street
Hartford 8, Connecticut

Zirconium Corporation of America
Solon, Ohio
ATTN: Librarian

Wyman-Gordon Company
North Grafton, Massachusetts
ATTN: Librarian

Westinghouse Electric Corporation
Astronuclear Laboratory
P.O. Box 10864
Pittsburgh, Pennsylvania 15236
ATTN: R.T. Begley

Union Carbide Corporation
Parma Research Center
P.O. Box 6115
Cleveland, Ohio 44101
ATTN: Technical Information Service

Westinghouse Electric Corporation
Research & Development Center
Pittsburgh, Pennsylvania 15235
ATTN: E.S. Bober

E.I. DuPont de Nemours & Co., Inc.
Wilmington, Delaware 19858
ATTN: E.M. Mahla

Westinghouse Electric Corporation
Aerospace Electrical Division
Lima, Ohio
ATTN: R.W. Briggs

Eitel McCullough, Incorporated
301 Industrial Way
San Carlos, California
ATTN: Leonard Reed

Mechanical Technology, Inc.
968 Albany-Shaker Road
Latham, New York
ATTN: Mr. Eli B. Arwas

Varian Associates
Vacuum Products Division
611 Hansen Way
Palo Alto, California
ATTN: J. Shields

Ultek Corporation
920 Commercial Street
Palo Alto, California
ATTN: Librarian

Dr. James Hadley
Head, Reactor Division
Lawrence Radiation Laboratory
Livermore, California

Sandia Corporation
Aerospace Nuclear Safety Division
Sandia Base
Albuquerque, New Mexico 87119
ATTN: A.J. Clark (3)

Aerojet-General Corporation
1100 West Hollyvale Street
Azusa, California 91703
ATTN: H. Derow, Dept. 4923

Atomics International
P.O. Box 309
Canoga Park, California 91304
ATTN: R.W. Dickinson

Flight Vehicle Power Branch
Air Force Aero - Propulsion Lab. APIP-1
Wright Patterson AFB, Ohio
ATTN: George Glenn